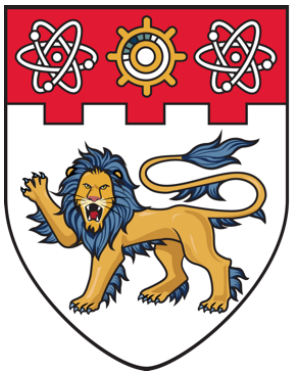

NANYANG TECHNOLOGICAL UNIVERSITY
SINGAPORE

Synthesis of Au@Pd Core/Shell Nanomaterials for High-Performance Ethanol Oxidation Reactions

XU WEICHANG

SCHOOL OF PHYSICAL AND MATHEMATICAL SCIENCES

2019

Synthesis of Au@Pd Core/Shell Nanomaterials for High-Performance Ethanol Oxidation Reactions

XU WEICHANG

SCHOOL OF PHYSICAL AND MATHEMATICAL SCIENCES

A thesis submitted to the Nanyang Technological University in partial fulfilment of the requirement for the degree of Doctor of Philosophy

2019

Statement of Originality

I hereby certify that the work embodied in this thesis is the result of original research done by me except where otherwise stated in this thesis. The thesis work has not been submitted for a degree or professional qualification to any other university or institution. I declare that this thesis is written by myself and is free of plagiarism and of sufficient grammatical clarity to be examined. I confirm that the investigations were conducted in accord with the ethics policies and integrity standards of Nanyang Technological University and that the research data are presented honestly and without prejudice.

22-8-2019 Xu Weichang 

. . . .

Date Name

Supervisor Declaration Statement

I have reviewed the content and presentation style of this thesis and declare it of sufficient grammatical clarity to be examined. To the best of my knowledge, the thesis is free of plagiarism and the research and writing are those of the candidate's except as acknowledged in the Author Attribution Statement. I confirm that the investigations were conducted in accord with the ethics policies and integrity standards of Nanyang Technological University and that the research data are presented honestly and without prejudice.

22-8-2019	Prof. ZHAO Yanli 
. . . . .	. . . . .
Date	Supervisor Name

Authorship Attribution Statement

This thesis contains material from 0 paper(s) published in the following peer-reviewed journal(s) where I was the first and/or corresponding author.

The contributions of the co-workers are as follows:

- The work in this thesis was mainly supervised by Professor Chen Hongyu.
- Professor Chen Hongyu provided the initial project direction and edited the manuscript drafts.
- Professor Liu Bin gave suggestions and proposed amendments of experimental details.
- I prepared the manuscript drafts. The manuscript was revised by Dr. Liu Teng and Dr. Song Xiaohui.
- I co-designed the experiments with Professor Chen Hongyu and Professor Liu Bin and performed all the laboratory work at the School of Physical and Mathematical Sciences.
- I performed all the materials synthesis, carried transmission electron microscopy, scanning electron microscopy, and electrochemical workstation and conducted data evaluation.
- Dr. Liu Teng and Dr. Zhang Liping assisted in the collection of the inductively coupled plasma optical emission spectrometry data.
- Dr. Lam Zhenhui, Mr. Zhang Junming and Ms. Cheng Xuejun assisted in the collection of the energy-dispersive X-ray spectroscopy data.

11-03-2019	Xu Weichang
. . . .	. . . .
Date	Name

Abstract

This thesis summarizes my postgraduate research on the studies of Pd-based electrocatalysts for ethanol oxidation reactions, mainly on two directions: (1) the fabrication of a high-surface-area electrode, Pd coated Au nanowire (AuNW) forest on porous nickel foam substrate, to enhance the catalytic activity of ethanol oxidation reactions, and (2) cyclic voltammetry (CV) guided deposition of sub-monolayer Pd on Au surface with fine-tuning Pd thickness and real-time monitoring of the electrochemical properties.

In Chapter Two, a modified procedure for the growth of AuNW forest on porous nickel foam substrate (previously only on oxide substrate), was proposed by changing the surface ligand from amino to cyano functionalized silane and applying the stirring condition. As a two-pronged strategy, the combination of AuNW and nickel foam could enhance the electrochemical active surface over 20 times, compared with Au nanoparticles decorated flat substrate. After the pulsed-current deposition of 1 nm Pd shell on Au, this flexible electrode showed significantly improved catalytic activity on the electro-oxidation of ethanol with high tolerance to hydroxyl and ethoxyl poisoning. The peak current density of as-prepared electrocatalyst was 3, 11 and 48 times higher than that of Pd coated bare nickel foam, Pd coated AuNW on fluorine doped tin oxide (FTO), and the state-of-the-art catalyst Pd on activated carbon (Pd/C), respectively.

In Chapter Three, one convenient and effective deposition method for the coating of

Pd overlayer on Au surface was realized by mimicking the primary cell in the 10 mM $PdCl_2$ deposition solution. The deposited amount of Pd can be tuned by the concentration of Pd precursor. When the concentration of $PdCl_2$ was reduced to 2.5 mM, the Au surface would be partially coated with Pd domains and the CV scan could facilitate the physical movement of Pd atoms to realize full coverage of the exposed Au surface. The mass-specific current of the Pd coated AuNW nickel foam electrode on ethanol oxidation can be enhanced to 6464 A/g, over two times higher than that of typical electrochemical deposited one. On the basis of a series of control experiments, the Pd movement mechanism was proposed that the Pd atoms may firstly get oxidized to free Pd ions in the electrolyte, which are then reduced back to cover the Au surface.

In Chapter Four, to solidify our proposed Pd movement mechanism, solution form of Pd precursor was added into the system, replacing previous solid state Pd. With potential cycling in the 16 μM $PdCl_2$, 1.0 M ethanol and 1.0 M NaOH electrolyte, sub-monolayer of Pd deposition on Au can be readily achieved. During CV scans, the onset potential and peak current density of backward peak reveals the binding affinity of –OH group and the catalytic activity, respectively. With such real-time monitoring, the thickness of the Pd overlayer can be continuously and precisely tuned by the number of CV cycles and directly correlates with the electrochemical properties.

Acknowledgments

My deepest and sincerest gratitude goes first to Professor Hongyu Chen, my supervisor, for his guidance and assistance. He has walked me through all five years of my academic life in Nanyang Technological University and torched me in my development of personality and thinking mode. Without his consistent and illuminating instruction, the competition of this thesis could be impossible.

Second, I would like to express my hearty gratitude to Professor Bin Liu (School of Chemical and Biomedical Engineering, Nanyang Technological University), who led me into the world of electrochemistry and provided me with inspiring advices. I am also greatly indebted to the professors and teachers, who have instructed and helped me a lot in the past five years.

Last my thanks would go to my family members for their loving considerations and great confidence in me all these years. I also owe my sincere gratitude to my lab mates and friends who gave me their help and time in helping me solve my problems during my difficulties.

Table of Contents

Abstract 1

Acknowledgments 3

Table of Contents 4

1. Introduction 6

1.1. Nanomaterials and Their Usage in Catalysis 6

1.2. Platforms for Nanomaterials Electrochemical Catalysis 18

1.3. Advantages of One Dimensional Nanostructures 24

1.4. Methods for Coating Ultrathin Layer 29

1.5. Major Issues and Possible Solutions 38

1.6. Summary 41

1.7. Reference 43

2. Pd Coated Au Nanowires on Nickel Foam as High-Performance Electrocatalyst for Ethanol Oxidation Reactions 49

2.1. Introduction 49

2.2. Materials and Methods 57

2.3. Results and Discussion 61

2.4. Conclusion 99

2.5. Reference 99

3. Enhancement in Catalytic Activities of Ethanol Oxidation Reactions by Primary Cell Deposition of Pd Shell and the Mechanism Study on the Movement of Pd 105

3.1. Introduction 105

3.2. Materials and Methods 109

3.3. Results and Discussion 114
3.4. Conclusion 147
3.5. Reference 148
4. Sub-atomic Layer Deposition of Pd with Real-time Monitoring 152
4.1. Introduction 152
4.2. Materials and Methods 154
4.3. Results and Discussion 158
4.4. Conclusion 183
4.5. Reference 183
5. Conclusion and Future Work 186
5.1. Conclusion 186
5.2. Future Work 189
5.3. Reference 192

1. Introduction

1.1. Nanomaterials and Their Usage in Catalysis

1.1.1. Advantages for Catalysis

Nowadays, nanomaterials have attracted much attention and interest, due to their unique chemical and physical properties. In principle, nanomaterials are materials of which at least one single unit is sized between 1 to 1000 nanometers (10^{-9} meter), and usually the size would be less than 100 nm.[1] Compared with the bulk material, the nanomaterial obtains various unique advantages, due to the smaller size, such as, quantum size effect,[2] nanosize dimension,[3] high surface area, high catalytic efficiency,[4] low cost,[4b, 5] etc. Based on these advantages, there are various applications generated from the nanomaterials with different composition, shape or size.[6] Here, some of the core strengths of nanomaterials and part of their basic applications are listed and introduced below.

From normal physical knowledge, it is well known that nanoparticles with diameter larger than 1 and smaller than 10 nm, which involved between the size of small molecules and the size of bulk materials, would display different electronic structures, because of the quantum mechanical rules.[2a] The resulting physical properties are very different from neither those of bulk materials nor those of molecular compounds, but it mainly depends on the chemical composition, the particle size, the shape of the nanomaterials, the lattice of the surface atoms, the inter particle distance, the property of the protecting shell, or some other factors.[2c] When the size of the nanoparticle is

comparable with the wavelength of the electron, the decrease in confining dimension makes the energy levels discrete, which would increase or decrease the band gap energy to ultimately alter the chemical or physical properties of the materials.[7] One typical example is the obvious different colors between the gold nugget (Figure 1-1-1a) and the Au nanoparticle solution (Figure 1-1-1b), all composing from Au atoms. Au nanoparticles in the size comparable with the visible light wavelength, exhibit strong absorption bands in the green or blue light regime that are not present in the bulk metal, showing red purple color.

Figure 1-1-1. The photos of (a) gold nugget and (b) 40 nm gold nanoparticles, showing different colors of gold materials.

When it comes to the different shapes or dimensions of nanomaterials, they are usually classified into three types, zero-, one- and two-dimensional nanomaterials (Figure 1-1-2), with different degrees of quantum size effect. For two dimensional materials,[8] thin films with nanoscale thickness are usually deposited on bulk substrate

or dispersed in the solution. The properties would be dominated by surface and interface effects or they may reflect the confinement of electrons in the direction perpendicular to the film. In two-dimensional nanomaterials, parallel to the film, the electrons behave like in the bulk material, since there was no space confinement parallel to the film. One-dimensional nanomaterials, with nanosized cross section, such as nanowires, nanobelts, nanorods and nanotubes, whose lateral dimensions fall anywhere in the range of 1 to 100 nm and the electrons are confined in one dimension.[9] Confinement effects for electrons may occur in the transverse direction while for the electrons along the wires they are free to move. For zero-dimensional materials, usually they are called as nanoparticles, clusters, colloids, nanocrystals, or some other names, depending on their different shapes or sizes.[10] They are composed of several tens to a few thousands of atoms inside each single nanoparticle. The electrons inside the nanoparticles are confined in all three directions. The confinement dimension of the electrons for different kinds of nanomaterials is different from each other, which would lead to different applications. For example, two-dimensional nanomaterials are usually used as the catalyst in various electrochemical reactions, due to their confinement of electrons in the transverse direction. The electrons can move along the wires more efficiently, which can effectively enhance the catalytic activity of the electrochemical reaction.

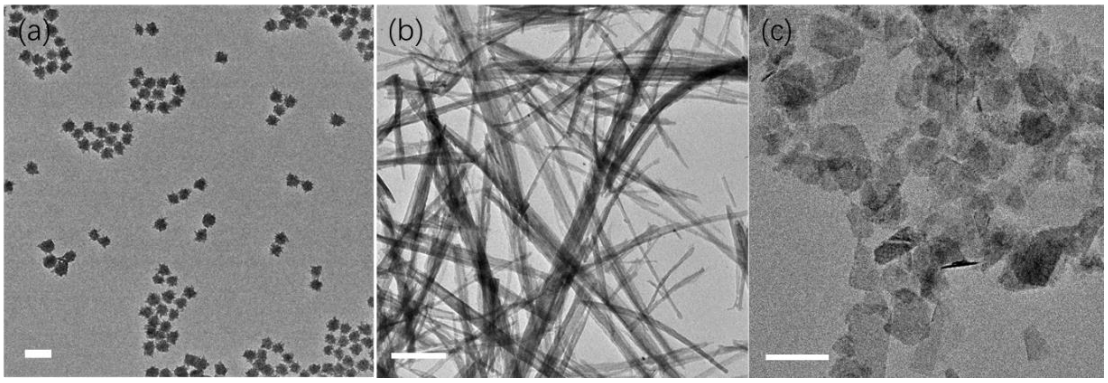

Figure 1-1-2. Transmission electron microscopy (TEM) images of zero-, one-, and two-dimensional nanomaterials for (a) cadmium sulfide nanoparticles, (b) cadmium hydroxide nanowires, and (c) rhenium selenide nanosheets (scale bar: 100 nm).

Another advantage, high catalytic efficiency, directly comes from the small size of the nanomaterials.[10a] It is well known that the nanomaterials are defined as materials with the size at least one dimensional between 1 to 1000 nm, which are at least hundreds or even over thousands of times smaller than micro materials or bulk materials. For catalysis, the most useful and efficient catalysts are the surface atoms of the materials exposed to the reactants.[11] To pursue higher catalytic efficiency, the most convenient and widely used method is to increase the surface/volume (S/V) ratio of the materials, utilizing more surface atoms for catalysis with the same amount of total atoms consumed. The smaller size can always lead to the higher S/V ratio (Figure 1-1-3). For nanomaterials, with the same amount of the materials, their S/V ratio dominates over the bulk materials, which would easily lead to serval times of increase of catalytic activity. In one simple chemical reaction, increased surface area usually means more chance to be attached with the starting materials as well as greater possibilities to make

the reaction taking place on the surface with the same reactant concentration. The nanomaterials, with various structures, morphologies or sizes, make full use of this advantage to an extreme level. Their increased surface area largely enhances the catalysis efficiency, compared with micro sized materials.

For the industrial production, one of the most critical issues is to gain more profits. By using nanomaterials as catalyst, not only the efficiency could be increased but also the cost could be decreased with the same catalytic activity. Using the nanomaterial as the catalyst in industrial production is one simple and easy method to cut the cost dramatically, since to reach the similar catalysis performance, the required amount of catalysis must be much smaller when the nanomaterial is used as the catalyst.[12] When it comes to some noble metal catalysts, such as, palladium, platinum, and gold, cutting the use of catalysts maintaining similar reactive activity could reduce large part of the production cost.

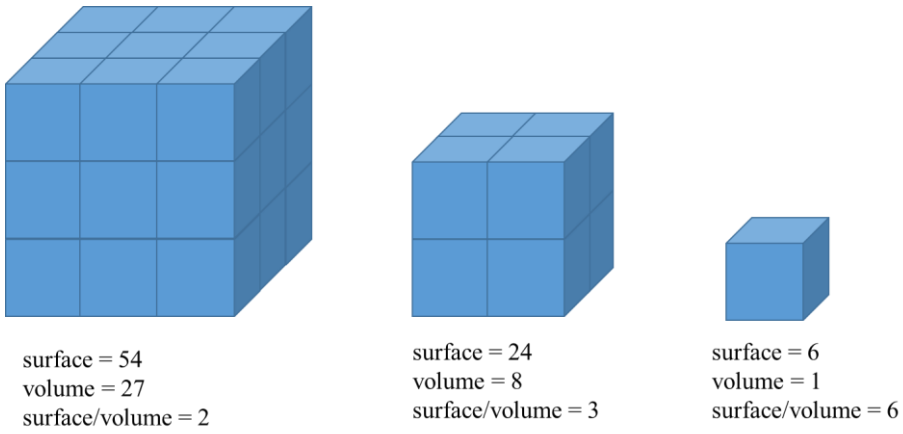

Figure 1-1-3. Illustration of the surface/volume ratio with different size of the particle to show that smaller size leads to higher surface/volume ratio.

1.1.2. Nano Catalysis in Solution Phase

The nanomaterial could increase the exposed surface area of the active component of the catalyst to a large degree, which dramatically enhances the possibilities of contacting between reactants and catalysts and mimicking the classic organic catalysts.[13] The activity and selectivity of nano catalyst could be manipulated by tailoring chemical or physical properties like size, shape, composition, structure, morphology, etc. Below are some of the examples for synthesized nanomaterials dissolving in solution phase as active catalysts.

Somorjai group[14] reported the successful synthesis of a nanosized platinum metal core coated with the mesoporous silica shell nano catalyst. The porous silica coating layer not only encaged the platinum cores up to an elevated temperature of 750 ℃ in air but also remained the same catalytic activity of platinum core as pure metal platinum nanoparticles without silica shell. This platinum core silica shell nano catalyst system showed us outstanding catalytic activity and stability compared with pure platinum metal, which also enabled their usage in high temperature catalytic reactions without being spoiled, such as ethylene hydrogenation and carbon monoxide oxidation.

Hutchings group[15] reported that Au nano catalysts could be used for the oxidation of primary alcohols, hydrocarbons and carbon monoxide which are all very important reactions for the synthesis of chemical intermediates in the industrial productions. Compared with bulk Au material, the Au nanomaterials showed unparalleled catalytic activity in all these different oxidation reactions.

Rothenberg group[16] synthesized a bimetallic core-shell nanomaterial with nickel core and Pd shell by using the combination of electrochemical method and solution chemical method. These bimetallic nanomaterials were then used as the catalyst for the Hiyama cross-coupling reaction between phenyltrimethoxysilane and different kinds of haloaryls. By using this core-shell nano catalyst, good product yield (over 86 %) was obtained with a variety of aromatic halides as substrates.

From all these previous examples, it is obvious that by using the nanomaterials as catalysts in solution phase, reaction rates and/or product yields could be enhanced to a large degree, compared with the bulk material. In addition, the selectivity and stability of nano catalysts remain at the similar or even better state after coated with protective shell, such as, mesoporous silica shell. The most important thing, in the nano catalyst system, the amount of catalyst is reduced while keeping the efficiency still the same or even better than traditional bulk catalyst.

1.1.3. Nano Catalysis on Substrate

Besides the great impact on nanomaterials dissolved in solution phase, it is very efficient for nanomaterial catalysts deposited on substrates as well. Besides the advantages showed in solution phase, the nanomaterials deposited on substrate still obtained some other advantages, such as, easy handling, convenient isolation, recycling and good stability. For most solution phase catalysts, the nanomaterials are usually used in the catalysis of organic reactions without supporting materials. While for some other

types of reactions, such as, the photocatalytic and electrochemical reactions, the nanomaterial catalysts must be deposited on some specific substrate, such as, glassy carbon, carbon cloth, etc., to realize the efficient catalysis.

When it comes to photocatalytic reactions, one of the major problems by semiconductor catalysts is the relatively low value of the overall quantum efficiency. The most critical catalytic source, electron–hole pairs, would easily and spontaneously recombine near the catalytic surface at high rate. To enhance the efficiency of photocatalysts, the nanomaterial has its own strength, quantum size effect, compared with the bulk material.[17] In order to match different demands and reaction conditions, the size, the shape, the lattice, the composition and the structure of nanomaterials are easier to be verified.

Ye group[18] reported the successful fabrication of two forms of Ag_3PO_4 single crystals, one for rhombic dodecahedron shape with exposed {110} facets, and the other one for cube shape with exposed {100} facets (Figure 1-1-4). With the exposure of visible light, the rhombic dodecahedron crystals exhibited higher photocatalytic activity for the degradation of methyl orange and Rhodamine B (RhB) dyes than the cubes. This result revealed that the {110} facet is more reactive than the {100} facet on catalyzing the degradation reaction of organic dyes.

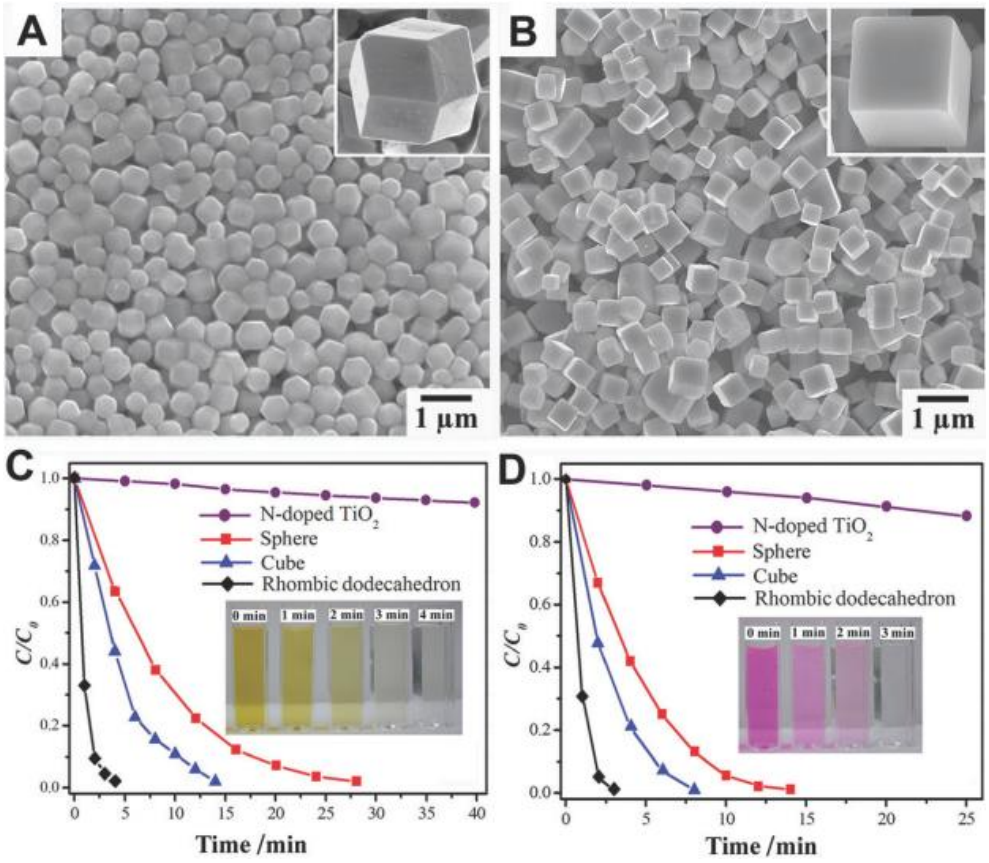

Figure 1-1-4. SEM (scanning electron microscopy) images of Ag_3PO_4 nano catalysts with different morphologies: (A) rhombic dodecahedrons and (B) cubes. The photocatalytic activities of Ag_3PO_4 rhombic dodecahedrons, cubes, spheres, and N-doped TiO_2 are shown for the degradation of (C) methyl orange and (D) RhB under visible light irradiation ($\lambda > 400$ nm). Reprinted with permission from Reference.[18] Copyright 2011 American Chemical Society.

Besides the decomposition of dyes, there are also some other photocatalysis applications for nano catalysts, such as water splitting[19] and 4-nitrophenol reduction.[20] For all these reactions, the nanomaterials are served as catalysts and could provide large active surface area for catalysis and high quantum efficiency to enhance the total

catalytic activity. The unique properties of nanomaterials, such as, high S/V ratio and confinement of electrons, play a key role in the enhancement of efficiency of photocatalysis reactions.

For another kind of heterogeneous reaction, the electrochemical reaction, there are lots of applications based on the combination of nanomaterials and electrochemical techniques, such as electrochemical sensor, energy storage, and electrochemical catalysis for various reactions. Since the nanomaterials obtain large surface area compared with bulk material, the electrochemical signal of the reaction would be dramatically enhanced. With quantum size effect, the nanomaterials would also show better activity or even better selectivity for some of the reactions.[21]

Sun group[22] reported the successful synthesis of tetrahexahedral (THH) Pd nanocrystals with vicinal high-index facets {730}, which provided the good catalytic performance towards ethanol oxidation. With the high density of the surface atomic steps, the THH Pd nanocrystals showed 6 times higher catalytic activity per surface area than the commercial used Pd black catalyst (Figure 1-1-5). This showed that with high-index-faceted metal nanocrystals, higher catalytic activity could be easily obtained, which was difficult to be realized by simply modifying or decorating bulk materials.

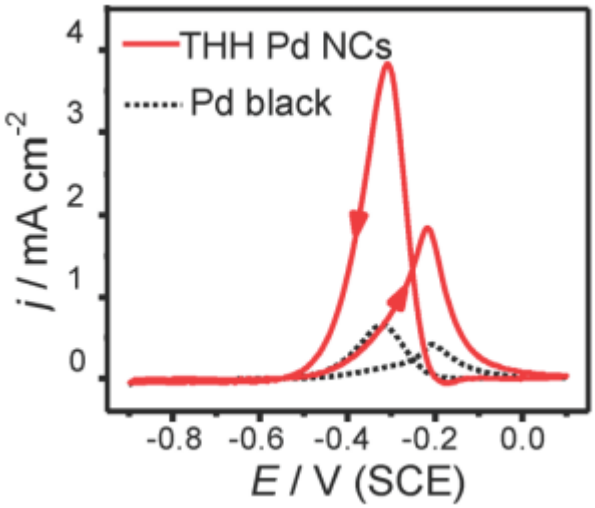

Figure 1-1-5. Cyclic voltammograms of THH palladium NCs (solid red line) and palladium black catalyst (dashed black line) at 10 mV/s in 0.1 M ethanol and 0.1 M NaOH aqueous solution. Reprinted with permission from Reference.[22] Copyright 2010 American Chemical Society.

Raj group[23] reported the successful preparation of Au nanoparticles (AuNP) self-assembling on a silicate network to efficiently catalyze the oxidation of glucose in the absence of any enzymes. From Figure 1-1-6, we can clearly see that with AuNP modified electrode, the current density was much higher than polycrystalline Au electrode, due to the higher surface area of AuNP dispersed on the electrode. The enhanced electrochemical signal could largely improve the sensitivity of sensing, when it comes to the extreme low concentration. Also, the error in testing could be relatively decreased to a large extent, compared with lower signal.

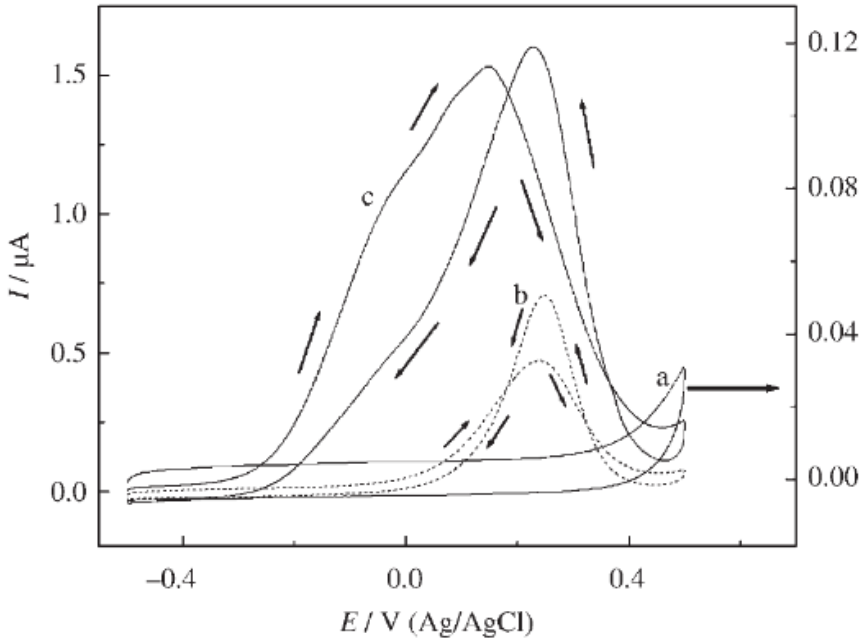

Figure 1-1-6. Cyclic voltammograms for the oxidation of glucose (1 mM) at: a) MPTS-modified polycrystalline Au electrode; b) MPTS-nAu electrode (gold nanoparticles); c) MPTS-nAuE electrode (gold nanoparticles decorated on enlarged silicate network) in 0.1 M phosphate buffer saline (PBS). Scan rate: 10 mV/s. Reprinted with permission from Reference.[23] Copyright 2006 Wiley-VCH.

In short summary, the advantages of nanomaterials for various catalysis applications are quantum size effect, nanosize dimension, high surface area, high catalytic efficiency and low cost. With these advantages, nanomaterials showed absolutely better catalytic abilities, higher product yield and better stability than bulk materials. For catalysis in solution phase and on substrate, with these listed but not limited advantages, the nanomaterial catalysts should be widely used and could be further studied and improved.

1.2. Platforms for Nanomaterials Electrochemical Catalysis

After understanding the importance of nanomaterials in electrochemical catalysis, another important factor for electrochemical reactions, the platform holding nanomaterials, should also be studied in detail. For most of the heterogeneous reactions, especially electrochemical catalysis reactions, the nanomaterials cannot be directly assembled into electrodes, but have to be attached onto some platforms, such as, glassy carbon, nickel foam and carbon cloth. The key function of the platform is to hold all the nano catalysts on its surface and to help catalyze the electrochemical reactions. So the choice of platform directly influences the catalytic activity and the stability of the electrode.

1.2.1. Widely Used Platforms

Conventional platforms for electrochemical catalysis are mainly divided into two categories according to different binding mode.[24] One kind is binder-free substrate, such as titanium sheet[25] and porous gold,[26] and the other kind usually needs binder to make catalyst attached on the substrate, such as indium tin oxide (ITO) substrate,[27] fluorine doped tin oxide (FTO) substrate[28] and glassy carbon.[29] Right now, for most of the research studies, the glassy carbon is the most widely used electrode substrate. The nanomaterial catalyst is firstly dropped on the glassy carbon electrode. If the nanomaterial was dissolved in solution, the solution should be dried enough and then the Nafion or other kind of binder solution is spread over the electrode surface to cover

the catalyst. For all these substrates, low flexibility is one of the major problems, which seriously hinder the further study to explore flexible electrode.

Also, the platform could be classified into non-flexible and flexible platform, due to the flexibility of the substrate. So recently, a growing number of new substrates have been reported as flexible substrate, such as, carbon cloth,[30] carbon paper,[31] graphene paper,[32] graphene foam,[33] and nickel foam.[34] The nano catalysts decorated on these substrates show equal or better catalytic properties than those on widely used non-flexible substrates. Also, it is obvious that these flexible substrates obtain better flexibility. These flexible substrates are widely worked as supercapacitors, batteries, fuel cells, and organic photovoltaics. When we bended or twisted these reported flexible electrodes, usually the electrochemical performances are almost not affected by the bending state and bending times.

1.2.2. Advantages of Flexible Platforms

Here, we mainly compare the non-flexible platforms and the flexible platforms. The advantages of non-flexible platforms are listed below. Firstly, most of the substrates, like glassy carbon or ITO have been widely studied for many years. All the procedures and benchmarking have established already and could be easily promoted. The field has already established the mature standard. Secondly, the non-flexible substrate is very strict and difficult to be damaged. The glassy carbon, ITO, and FTO is based on solid substrate and the shape cannot be easily changed. Thirdly, for most of these substrates,

they are silica based or metal based, which are quite hydrophilic. For most electrochemical reactions, the hydrophilic substrate can be better adsorbed and reacted with the starting materials in solution, since most of the electrochemical reactions are tested in the aqueous solution.

The non-flexible platforms showed high generality, good stability and hydrophilicity, while the flexible platforms owned some other advantages, different from the non-flexible ones. Firstly, the good flexibility results in the possibility to prepare flexible electrode. When the electrode is bended or twisted, the catalytic performance would keep the same or only decrease a little (usually less than 5 %). Secondly, the flexible electrode usually obtains high surface area due to its pores or gaps inside the electrodes. The electrode cannot be very solid or strict, and empty room is needed for the bending or twisting of the electrode. So it must have much surface area to release its strain. The high surface area is one of the important targets for electrochemical scientists to chase. Thirdly, there is an exception for flexible platform, nickel foam (Figure 1-2-1), the solid platform. For most of other flexible platforms, like carbon foam, carbon paper, they are not as solid as normal non-flexible electrode, such as FTO. This would easily result in the peeling off some part of the electrode. But for the nickel foam substrate, the property of metal, which is rigid and solid, is different from carbon based substrate. The nickel foam can remain both the flexibility and the hardness, all very critical properties in electrochemical catalysis. It is interesting to find out that the nickel foam substrate obtains both the advantages of non-flexible and flexible platforms.[34-35]

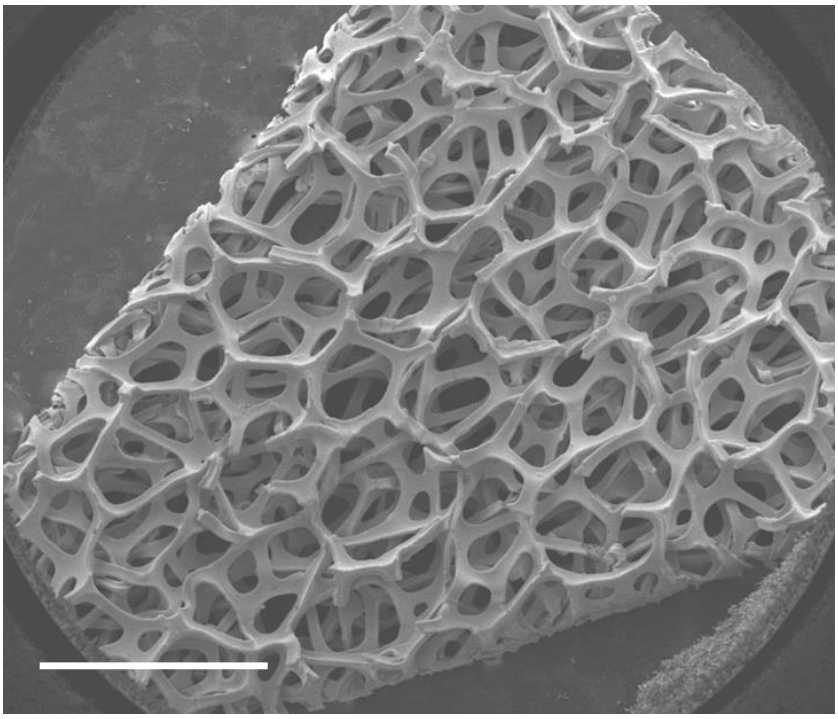

Figure 1-2-1. SEM images of flexible platform, nickel foam without any decoration with pores inside (scale bar: 1 mm).

1.2.3. Connection Methods between Nanomaterials and Platforms

After the discussion of advantages of different kinds of platform, the connection method should also be under concern as one key factor of electrochemical catalysis. There are mainly two methods to connect the nanomaterials with different platforms, one for binder method, and the other one for direct growing method, also known as binder-free method. For binder method, it has been discussed previously on Section 1.2.1, that usually nano catalysis was dropped on the electrode first and then the layer of binder solution. After the solution was dried, the polymers in the binder solution could bind these nanomaterials on the substrate firmly. The disadvantage of binder method is very obvious that, the partial loss of the active surface, usually leading to the

minor decrease of catalytic activities. It is well known that most of the binders are conductive polymers and they will not affect the catalysts on the electrode. However, in reality, it is difficult for the binders not to cover any of the active surface of nano catalyst. More or less, the electrochemical catalytic activity would be affected and decreased more or less.

For binder-free method, there would be no such problem, because the catalyst is directly grown on the electrode surface with different binding forces without any binders. For growing metal catalysts on nickel foam or other metal foam surface, the metal-metal bond would help the catalyst strongly bind on the electrode surface. For catalysts growing on carbon based platforms, usually, the chemical bond is formed from the ligand on catalysts and the ligand modified on electrode substrate. With strong metal-metal bond or chemical bond, the catalyst could be bound strongly on the platform and would not lose any of its active surface area since there was no binder covering the surface.

1.2.4. Basic Requirements for Platforms

First, the platform should be easily scaled up or expanded. For most of the industrial applications, if the surface area of the substrate is similar with the size of glassy carbon that was usually used for research, the amount of catalysts loaded on the substrate for real applications was only milligram or even microgram level. Unlike the experiments in laboratory, the demand for industrial application is much larger than milligram scale

on glassy carbon. So the first quality of substrate carrying catalysts should be the feasibility to be scaled up.

Second, the platform should be firm but not fragile. In industrial applications, the frequent damage of the platform should not be occurred. The platform must be solid enough to endure vigorous stirring or vibration and sometimes even collision. Some loose substrates, like carbon paper, are not the suitable choice, due to the easily peeling off of little fragments during stirring condition. And some fragile platforms, such as, ITO and FTO substrates, are not suitable for industrial applications as well, since the glass substrate could be easily broken under collision.

Third, the platform should be porous with high surface area. For industrial catalysis, there would be high demands for production efficiency within certain surface area and time, since the increase of the efficiency could always bring out considerable profits. So the use of platform with high specific surface could simply enhance the active surface area per project area. What is more, for porous structure, it would gain more possibilities of reaching the surface for reactants and leaving from the active surface for products, compared with solid platform.

The last but not the least, it would be better to use the flexible platform. The enhanced flexibility of the substrate could bring about many possibilities in different applications, such as foldable screen, portable monitor, wearable device and so on. It is well known that one of the major problem for lithium batteries is the outbreak of the fire or even explosion after bended or collided. The use of flexible battery could easily solve this

safety problem. Interestingly, there are plenty of pores or gaps inside the flexible substrate, and this could easily result in higher surface area compared with solid substrate. So the applying of flexible platforms would be the ideal target for researchers to pursue.

1.3. Advantages of One Dimensional Nanostructures

After the platforms are fully discussed, the loaded nanomaterial is also one key impactor influencing the efficiency and application of different catalysis reactions. Recently, one dimensional (1D) nanostructures, such as nanowires,[36] nanobelts,[37] nanotubes[38] and nanorods,[39] have gained more interests from the researchers mainly in electrochemical catalysis field, due to their unique advantages compared with other shapes or structures of the nanomaterial. It is well known that 1D structure could provide a suitable research platform for the investigation of electron transportation in different electrochemical reactions and implying relatively good electrochemical properties in various applications due to the confinement of electrons.[40] Here, some advantages of 1D nanomaterials which mainly affect the catalytic activity in electrochemical reactions are listed below.[9c, 41]

1.3.1. High Surface Area

Compared with zero dimensional (0D) and two dimensional (2D) nanostructures on the same surface area, 1D nanostructure obviously obtains larger surface area within

certain packing area. For other nanomaterials, their maximum surface area would be the fully covered state on the target substrate. However, for 1D structure, it could be grown on the vertical direction and can easily enhance the surface area by many times. The active surface area is increased from the platform surface area to the extended surface. From Figure 1-3-1, we can clearly see the surface area difference of packing nanoparticles and vertically aligned 1D nanomaterials. The 1D nanomaterials highly utilizes the large area above the substrate, while for normal nanomaterials, the simple packing cannot enhance the surface area much, compared with the substrate. The increase could only come from the gaps between nanomaterials.

1.3.2. High Electron Transportation Rate

For 0D nanostructures, we can simply accumulate the nanoparticles to serval layers to increase its surface area. Obviously, the active surface area could be increased a little, but the gaps between 0D nanostructures are very difficult to be fully covered. From the dash circles in Figure1-3-1a, many large gaps between the substrate and the top layer of nanoparticles could be observed. And this is only from the planar graph, while for the three-dimensional space, the gaps would be much larger and difficult to be covered. For 1D structure, there is only one junction between the top layer and the substrate, which is the connection point at the bottom of the nanostructure with the substrate. So we can clearly see that the 1D nanostructure is a well-connected whole system with little gaps, while the packed 0D nanostructure is an unconnected system with many

gaps in between the materials. So for electrochemical reactions, the close connection and the high efficiency of electron transport is very crucial. And it is obvious that 1D nano structure could provide higher electron transportation efficiency, compared with the packing of 0D nanomaterials.

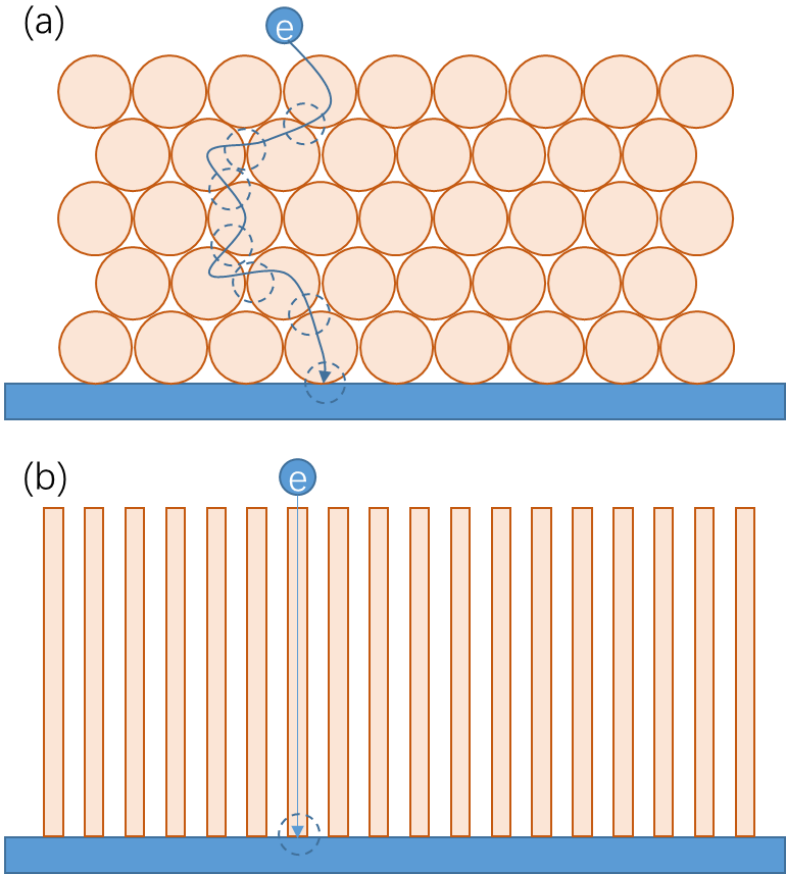

Figure 1-3-1. The illustration of the accumulation of packed 0D nanostructure (a) and growing 1D nanostructure (b) and the dash circles showed the connection point in the electron transportation pathway.

1.3.3. Facilitate Mass Transport

Besides the high efficient transportation of electrons, in electrochemical reactions, to increase the transportation rate of reactants and products is also a critical factor to enhance the electrochemical activity. Different from accumulated and packed nanoparticles, the gap between each aligned 1D nanostructure, such as nanowire forest (Figure 1-3-2), is quite uniform and lined. This could help the mass transport, since the nanowires in between creates the “material transfer pipe” from the top to the bottom of the nanomaterials. And also, if the nanowire is not restricted, it could swing in the solution under the help of stirring to further enhance the transportation ability of reactants near the electrode. If the 1D nano structure is hollow, like nanotube, the hollow part can further enhance the transportation amount. The reactants can move from both outside and inside the nanotubes to the electrode, while for hollow 0D structure, the pore inside can hardly help the transportation. Obviously, the vertically aligned 1D nanomaterials with good flexibility could help the mass transport.

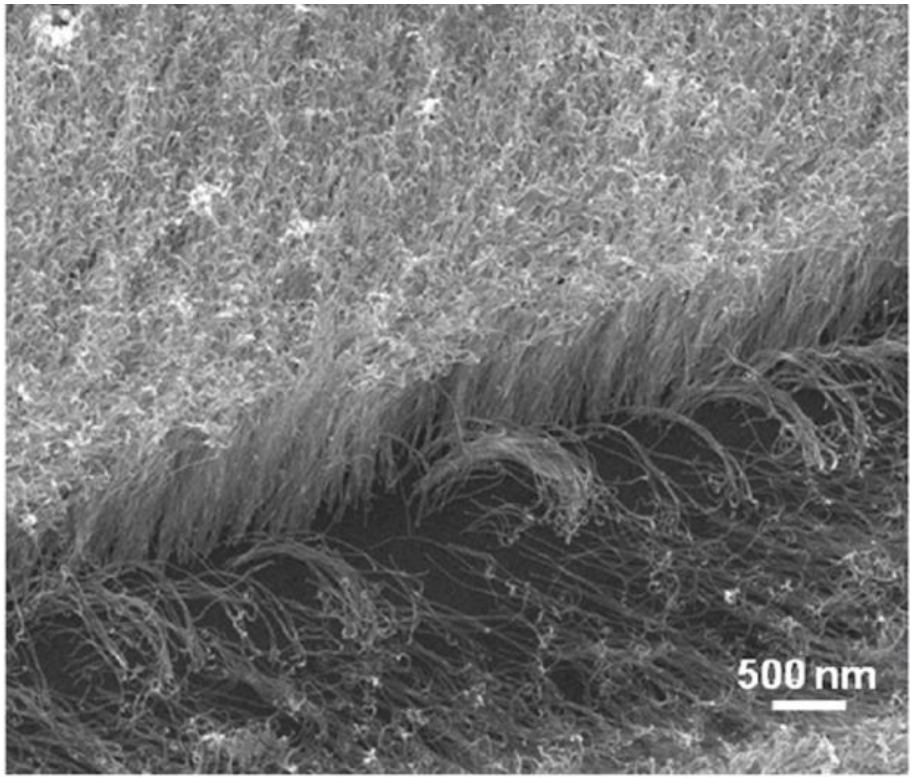

Figure 1-3-2. SEM image of vertically aligned 1D nanostructure gold nanowire forests on silicon wafer substrate. Reprinted with permission from Reference.[42] Copyright 2013 American Chemical Society.

1.3.4. Electron Confinement

For different dimensions of nanomaterials, electron confinement would take place when the size of the materials reaches the requirements of quantum size effect. However, the electron confinement of different nanomaterials could not always help increase the transferring rate of electrons onto the active points on catalysts. For example, for 2D nanomaterials, the structure could only confine the electrons in the cross section area and cannot help transfer the electrons approaching more active spots. For 0D nanomaterials, the confinement comes from everywhere, leading to the counteracting

effects from all directions and the confinement becomes meaningless. However, when it comes to 1D nanomaterials, the electron would be confined within the vertical direction, which is the exact electron pathway for more efficient electrochemical catalysis.[43] The shape of 1D nanomaterials is similar with that of electric wire, benefiting for the quick and effective transportation of electrons.

In short, with all these advantages, large surface area, high electron and mass transport rate, and electron confinement along the vertical line, the 1D nanostructure could be one of the best potential nanomaterials for different applications of electrochemical catalytic reactions.

1.4. Methods for Coating Ultrathin Layer

1.4.1. Reasons to Investigate the Coating Methods

From the previous two sections, it has been discussed that 1D nanostructure is one of the outstanding choices for electrochemical catalysis and different advantages as well as disadvantages of various platforms holding catalysts. The next key factor to figure out should be the suitable chemical composition catalyzing the electrochemical reactions. For various electrochemical reactions, different chemical composition could easily lead to totally different catalysis efficiency. Taking electro-oxidation ethanol in basic solution as an example, Pd catalyst could always show quite high catalytic activity, while for other noble metals, such as gold or silver alone, the catalytic efficiency is quite low. But the platform itself, composed of the substrate and the nano catalyst,

should be general to most of the reactions. So the quicker method to find out the efficient catalyst is to choose the suitable platform first, and then to search for the effective composition for desired reactions. In detail, one suitable platform system for different electrochemical reactions should be firstly designed and fabricated. Then different composition of the materials is coated or deposited on the surface of platform to realize different requirements for different electrochemical reactions. For example, for ethanol oxidation reaction, there is no doubt that the semiconductor zinc oxide could not be a good catalyst, but the author utilized the electrochemically deposited zinc oxide on the carbon paper as one good platform to create flexible and high surface area substrate for the ethanol oxidation reactions.[24] And for widely used commercial catalyst, Pd carbon (Pd/C), it is difficult to directly grow on the high surface area structure, such as, carbon fiber cloth (CFC). So the author used the zinc oxide nanoarrays as template to prepare the coating layer of PdCo on the surface. After coated with highly effective catalyst PdCo, the zinc oxide nanoarrays were then dissolved and the PdCo nanotube arrays became the high efficient catalyst for electrochemical oxidation of ethanol (Figure 1-4-1). From the previous example, it is clear to see that the large surface area for the catalyst comes from the platform (zinc oxide nanoarrays), and the catalytic property mainly comes from the coating layer (PdCo). After the platform is settled, different catalyst could be used to catalyze different reactions, such as, PdCo here for ethanol oxidation reaction.

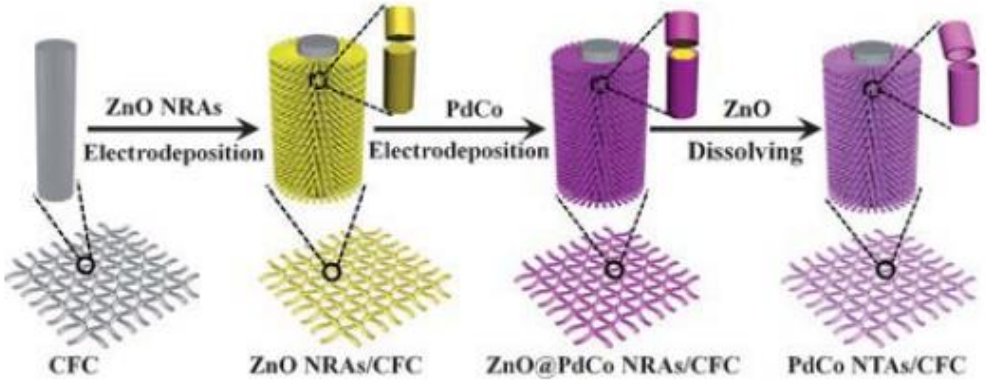

Figure 1-4-1. The example to deposit PdCo on zinc oxide surface to catalyze ethanol oxidation reactions. Reprinted with permission from Reference.[24] Copyright 2015 Wiley-VCH.

After the selection of platform, the next step is to choose one suitable coating method. Usually, the optimized coating method is to deposit ultrathin layer instead of thick layer. Because for most of the catalysis reactions, only the serval surface layers of atoms are involved in the catalysis steps, while the rest inner atoms would not help the catalysis much. But when it comes to counting the cost of the catalyst, all these atoms, including these outside catalytic and inner useless ones, would be calculated as the catalyst. So if only ultrathin layer of atoms is deposited over the substrate, the utilization rate of the materials as well as the catalysis efficiency could be dramatically enhanced and the cost would be largely cut down. This is similar with the principle using nanomaterials as catalyst, increasing the utilization ratio of the active atoms. Here, the ultrathin layer of catalyst could be viewed as one type of 2D nanomaterials.

Below are the introduction of three widely used methods for ultrathin layer coating, atomic layer deposition (ALD), underpotential deposition (UPD) and chemical bath deposition (CBD).

1.4.2. Atomic Layer Deposition

Atomic layer deposition (ALD) is a thin-film deposition method in which a film is grown on a substrate by exposing its surface to the gaseous species in the chamber. Figure 1-4-2 shows the typical ALD method under sequential, self-limiting surface reactions. The precursors are inserted as a series of sequential, non-overlapping pulses. In each of these pulses, the precursor molecules react with the surface molecules, so that the reaction terminates once all the reactive sites on the surface are consumed. Consequently, the maximum amount of material deposited on the surface after a single exposure to all of the precursors is determined by the number of active sites on the surface. By varying the number of deposition cycles, it is possible to grow materials uniformly and with high precision on arbitrarily complex and large substrates.[44]

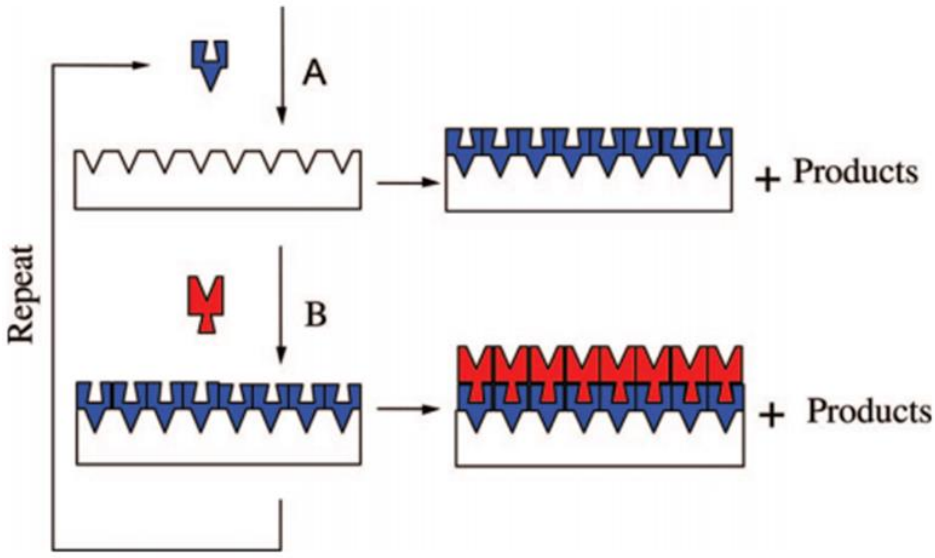

Figure 1-4-2. Schematic representation of ALD using self-limiting surface chemistry and an AB binary reaction sequence. Reprinted with permission from Reference.[44c] Copyright 1996 American Chemical Society.

The most significant advantage of ALD method is that the thin film can be precisely prepared to an atomically specified thickness. As for the growth of multilayer structures, the deposition shell can be controlled and realized by repeating all these processes. Another advantage for ALD method is that it can be run at relatively low temperature and this is benefit for some fragile substrates and materials, which are easily to be spoiled or decomposed at high temperature.[45]

The disadvantage of ALD method is also very obvious. First, the extremely harsh requirements for the substrate hinder the application of deposition layers for various types of nanomaterials. By using ALD, the demands for substrate include, high purity, confirmed chemistry composition and stable physical properties. Within the same deposition method, the substrate should be exactly the same as the previous times or

indication from the literature. Otherwise, the coating condition should and must be retested and tuned to the new substrate or starting materials. Second, the cost of applying ALD deposition is quite high, not only for the instruments, but also for the running for trials to find the suitable coating condition. Even after the condition has been fine-tuned, the cost for coating one time is still not low. Third, the ALD method is a quite time-consuming method. To coat different materials on different substrates, the condition should always be test first. And for the single layer, it takes quite long time to run for one cycle of the coating. The thickness of every single layer was atomic layer, which means that if you want to get a thicker layer, it would take much longer time, since the thickness is just the accumulation of atomic layers. The last but not the least, the requirements for precursors are quite harsh as well. The precursors must be volatile, but not that easy to be decomposed, since most of the precursors are very sensitive to oxygen and the purity of the precursors should be high enough.[44a, 44b, 45]

1.4.3. Underpotential Deposition

Underpotential deposition (UPD) is a coating method of electrodeposition of a species at a potential less negative than the equilibrium potential for the reduction of the species and usually the metal ions in the solution are reduced to pure metal onto the surface. The equilibrium potential for the reduction of the metal is the potential at which it will deposit by itself spontaneously.[46]

The advantage of UPD method is that the metal can be precisely deposited only one layer on the substrate by UPD method. And this coating process is carried out in aqueous solution, which is a quite general system and there are many choices of different metal ions. Compared with ALD method, the cost to run one cycle of UPD is much lower and there are much more choices of metal salts dissolved in electrolyte. Since the targeted deposition surface is under modification, by applying the potential less negative than equilibrium potential, the new layer can only be deposited on the targeted surface, not on the second or other layers.

Some of the disadvantages of UPD method are similar with the ALD method, such as harsh requirements for substrate, time-consuming and complicated steps to coat multilayers. What is more, there are some other disadvantages for UPD method. It is quite difficult to precisely control the multilayer coating. For the first layer, UPD could be a very powerful and useful method, but for the second and third layer, since the substrate has been changed, the coating accuracy is not as high as the first layer. For UPD method, the amount of electrons passed through the electric circuit is usually used to estimate the coating thickness, but sometimes, this estimation does not meet the real situation. Another disadvantage is that the UPD coated metal layer sometimes is not that stable as expected and is very easily spoiled while doing catalysis or simply after serval cyclic voltammetry (CV) tests. [47] The surface composition, the lattice or the morphology of the surface layer would occur during CV scans.[48]

1.4.4. Chemical Bath Deposition

Chemical bath deposition (CBD) method usually involves two steps, the nucleation of precursors and the particle growth deposition, forming a solid phase in the solution. The liquid precursor undergoes the chemical reaction and the deposition at targeted position.[49]

The advantages of CBD are obvious including the mild reaction condition and simple equipment requirements (only solution containers) under ambient conditions. Also, CBD method could produce relatively stable, uniform and hard films with quite good reproducibility through simple process. The deposition of the thin film mainly depends on the deposition conditions, the starting materials and the substrate. Changing the reaction temperature, duration of deposition, precursors in the solution and different targeted deposition substrate could easily alter the deposition results.

The disadvantages of CBD method are list below. First, the deposition solution is wasted after one cycle of deposition since the unreacted precursors are difficult to recycle. Second, usually the coating layer is uneven due to the non-uniformity distributed surface charge. The roughness of the surface could easily lead to the inhomogeneity of surface charge. Pointed part can accumulate more surface charge than flat part.[49] Third, the controllability of the thickness by CBD method is not that high compared with other two methods. The thickness mainly depends on the deposition duration and the temperature. Once the surface layer is formed, usually the thickness is

already up to serval nanometers. And the precise control is difficult to be realized under CBD method.

1.4.6. One Other Deposition Method

After comparisons with the advantages and disadvantages of different types of deposition methods, it seems that each deposition method owns its unique advantages, such as, precise control at atomic level, relatively mild deposition condition and simple steps for continuous multilayer deposition. For different target products, different deposition methods can be selected, according to their characteristics. However, the combination of simple operation under ambient condition and precise control at atomic level is relatively difficult to be realized.

More importantly, for electrochemical catalysis research, one of the most concerned targets is to establish accurate structure-property correlation. Right now, there are many reported works focusing on this target. Wang group[50] reported that the catalytic activity and selectivity of metal nanoparticles can be regularly tuned by size effect. The Faradaic efficiency for CO production can be enhanced from 5.8% to 91.2%, when the diameter of Pd nanoparticles decreased from 10.3 nm to 3.7 nm. Kibler group[51] reported that the chemical properties, such as, the adsorption of hydrogen or the electrooxidation of formic acid, of palladium monolayer would be altered, when it is compressed or dilated, depending on the lattice parameters of the substrate. There is a direct and clear correlation between the potential of hydrogen desorption peak and the d-band center

shift. Markovic group[52] reported that more oxophilic sites on nanomaterials, especially on Ir (defects) and PtRu (Ru atoms) electrodes would enhance the adsorption of OH species, to greatly increase the catalytic activity of hydrogen oxidation reaction.

For all these previously mentioned deposition methods, it is difficult to measure the catalysis property during the preparation process, which might bring about lots of uncertainties. The samples might already be changed or spoiled before the property measuring step, especially for ultrathin deposition layers (thickness less than 1 nm), or alloy small nanomaterials (diameter less than 5 nm). So if measuring the properties during the deposition steps could be realized, it would be much more accurate and convenient to establish structure-property correlation.

In short summary, the basic characteristics for one ideal deposition method should include listed properties: precise control of the layer thickness at atomic level, continuously fine-tuning layer thickness, relative mild reaction environment and real-time detection of property during deposition process.

1.5. Major Issues and Possible Solutions

In recent years, the global energy demand keeps growing, due to the industrial development and population growth. The energy shortage has become one of the most critical problems in the world right now. The increasing trend of world primary energy consumption stays almost unchanged from 1990 to 2015 (Figure 1-5-1).[53] Over 85 % of the world consumption still comes from non-renewable energies, including coal,

natural gas and oil and this percentage did not change much over the last two decades. Using non-renewable could also bring about lots of environment problems, global warming, sea level rise, extinction of species and so on.

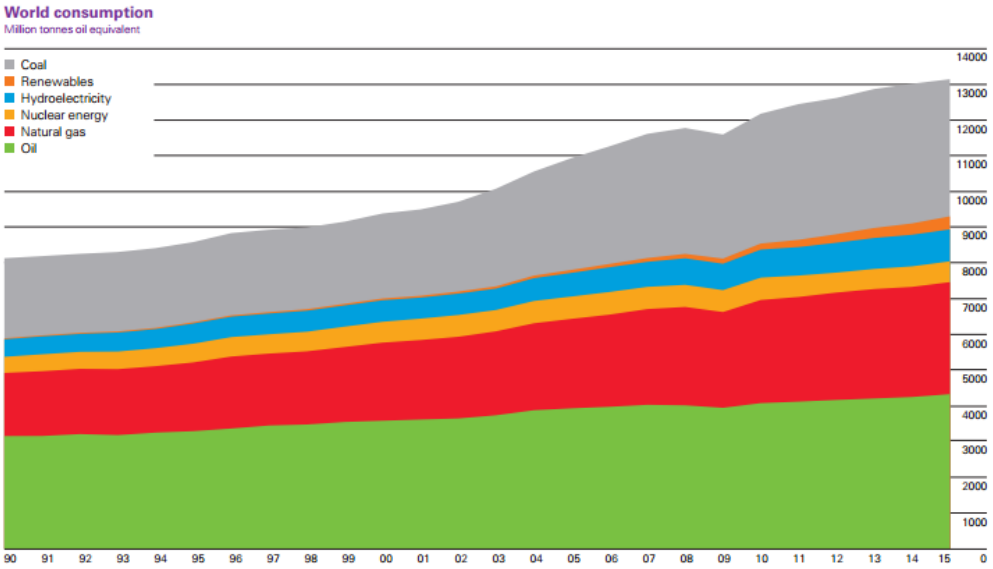

Figure 1-5-1. The trend of global primary energy consumption of different energy sources from 1990 to 2015.[53]

There are mainly two ways to solve this problem. One is to use more renewable energies, and the other is to enhance the energy conversion efficiency. Right now, the percentage of renewable energy of global energy consumption is less than 3% and there could be much more improvement for higher percentage. Most renewable energy comes either directly or indirectly from the sun, such as, solar energy, bioenergy, and wind energy. In addition, increasing the reaction efficiency could directly reduce the energy consumption, maintaining the same power output. It is well known that chemical reactions occur faster and more efficiently in the presence of a catalyst and over 90%

of the world commercially produced chemical products involve catalysis steps at some stage within their manufacture process. So using more renewable energies and enhancing catalytic efficiency could reduce the increasing trend of global non-renewable energy consumption.

However, there are still some challenges before the extensive use of renewable energy, especially the relatively low efficiency. Taking direct ethanol fuel cell (DEFC) as an example, Shell Eco Marathon team reported to use DEFC for their vehicles with maximum power density of 2 kW.[54] While for our daily used vehicles, the maximum power density is usually over 100 kW. The gap between the demonstration and the practical application is difficult to bridge. So more efforts is needed to enhance the efficiency of DEFCs and applying the nanomaterial as electrode is one practical and simple method. High surface area of the nanomaterial as well as the substrate could dramatically enhance the catalytic activity of ethanol electro-oxidation reaction. Previous discussion (Section 1.3) has proved that simply packing nanomaterials on substrate could not help enhance the efficiency much. Precise design and control the growing process of the nanomaterial could be the better option.

It is well known that the catalytic property of the nanomaterial is larger than that of the same amount bulk material. Except the size, other correlations, such as, structure, shape, composition and lattice, are difficult to establish. There is little method to quickly set up the structure-property correlation, since the property measurement and morphology characterization is always after the preparation step. The sample used for

property and morphology test sometimes is not the same one. It would be much easier to establish quick and clear correlations, if the growing step is combined with the property test step.

In short, right now, there must be some interferences in the continuous increasing of non-renewable energy consumption. Applying more renewable energy and increase catalytic efficiency could be two possible solutions. More effects should be spent on designing the nanomaterial and establishing structure-property correlation.

1.6. Summary

Comparing nanomaterials and bulk materials for catalysis, the advantages of nanomaterials are quite clear, such as, quantum size effect, large surface area and high catalytic activities due to the high surface/volume ratio for various catalysis applications. To increase the catalytic activity, the nanomaterial would be the much better than the bulk material. For platforms carrying catalysts in electrochemical reactions, usually the non-flexible substrate is widely used as the working electrode, due to its good stability, good hydrophilic and its well-studied system. While right now more and more effects are focusing on flexible substrates, although sometimes they are easier to be damaged and not that hydrophilic than widely used glassy carbon or FTO. They still show great potential to become the next generation platform for electrochemical reactions, because of their good flexibility and high surface area. For the selection of detailed kind of nanomaterials, 1D nanostructure is better than normal

0D and 2D nanostructures, due to the high surface area, high electron transport rate, relatively high mass transport and electron confinement along the vertical electric circuit. When different chemical composition of the materials is used to catalyze different electrochemical reactions, coating the surface layer of the materials would be applied onto the platform. For coating ultrathin layers in gas phase, ALD is a good choice to precisely deposit atomic layers and for solution phase, UPD is usually used to deposit metal monolayer. By using CBD method, simple and quick coating layers in solution could be easily realized. However, for all these deposition, key defects still exists and the preparation step could not simultaneously take place with the property measurement step. This hinders the establishments of accurate structure-property correlation. One better deposition or preparation method, containing various advantages of these methods, should be applied to build the correlation and enhance the catalytic ability more conveniently.

To inhibit the fast growth of global non-renewable energy consumption, more renewable and sustainable energies should be applied, such as, solar energy, biomass energy and hydrogen energy, although their efficiency is not high enough for practical applications nowadays. More and more efforts should be focused on designing and preparation of high surface area nanomaterials. Also, by enhancing the catalytic abilities, the energy consumption could be effectively reduced maintain the same power output.

1.7. Reference

1. (a) Buzea, C.; Pacheco, I. I.; Robbie, K., Nanomaterials and nanoparticles: Sources and toxicity. Biointerphases, 2(4), MR17-MR71. *Biointerphases* **2007,** *2* (4), MR17-71; (b) Mccance, D. J., Human papillomaviruses and cervical cancer. *Advances in Cancer Research* **1997,** *71* (Suppl 1), 321-341.

2. (a) Alivisatos, A. P., Semiconductor Clusters, Nanocrystals, and Quantum Dots. *Science* **1996,** *271* (5251), 933-937; (b) Andres, R. P.; Bein, T.; Dorogi, M.; Feng, S.; Henderson, J. I.; Kubiak, C. P.; Mahoney, W.; Osifchin, R. G.; Reifenberger, R., "Coulomb Staircase" at Room Temperature in a Self-Assembled Molecular Nanostructure. *Science* **1996,** *272* (5266), 1323-1325; (c) Brust, M.; Kiely, C. J., Some recent advances in nanostructure preparation from gold and silver particles: a short topical review. *Colloids & Surfaces A Physicochemical & Engineering Aspects* **2002,** *202* (2), 175-186.

3. (a) Moon, R. J.; Martini, A.; Nairn, J.; Simonsen, J.; Youngblood, J., ChemInform Abstract: Cellulose Nanomaterials Review: Structure, Properties and Nanocomposites. *Chemical Society Reviews* **2011,** *40* (7), 3941-3994; (b) Marambiojones, C.; Hoek, E. M. V., A review of the antibacterial effects of silver nanomaterials and potential implications for human health and the environment. *Journal of Nanoparticle Research* **2010,** *12* (5), 1531-1551; (c) Grieger, K. D.; Linkov, I.; Hansen, S. F.; Baun, A., Environmental risk analysis for nanomaterials: Review and evaluation of frameworks. *Nanotoxicology* **2012,** *6* (2), 196-212.

4. (a) Qian, F.; Gradecak, S.; Li, Y.; Wen, C. Y.; Lieber, C. M., Core/multishell nanowire heterostructures as multicolor, high-efficiency light-emitting diodes. *Nano Letters* **2005,** *5* (11), 2287-91; (b) Wen, B.; Cao, M.; Lu, M.; Cao, W.; Shi, H.; Liu, J.; Wang, X.; Jin, H.; Fang, X.; Wang, W., Reduced graphene oxides: light-weight and high-efficiency electromagnetic interference shielding at elevated temperatures. *Advanced Materials* **2014,** *26* (21), 3484–3489; (c) Zhou, M.; Wang, H.-L.; Guo, S., Towards high-efficiency nanoelectrocatalysts for oxygen reduction through engineering advanced carbon nanomaterials. *Chemical Society Reviews* **2016,** *45* (5), 1273-1307.

5. (a) Palomares, V.; Serras, P.; Villaluenga, I.; Hueso, K. B.; Carreterogonzález, J.; Rojo, T., Na-ion batteries, recent advances and present challenges to become low cost energy storage systems. *Energy & Environmental Science* **2012,** *5* (3), 5884-5901; (b) Yi, L.; Liu, Y.; Yang, N.; Tang, Z.; Zhao, H.; Ma, G.; Su, Z.; Wang, D., One dimensional CuInS2–ZnS heterostructured nanomaterials as low-cost and high-performance counter electrodes of dye-sensitized solar cells. *Energy & Environmental Science* **2013,** *6* (3), 835-840.

6. Ryckman, J. D.; Liscidini, M.; Sipe, J. E.; Weiss, S. M., Direct imprinting of porous substrates: a rapid and low-cost approach for patterning porous nanomaterials. *Nano Letters* **2011,** *11* (5), 1857.

7. (a) And, M. C. D.; Astruc, D., Gold Nanoparticles: Assembly, Supramolecular

Chemistry, Quantum-Size-Related Properties, and Applications toward Biology, Catalysis, and Nanotechnology. *Chemical Reviews* **2004,** *35* (16), 293-346; (b) Weller, H., Quantized semiconductor particles: a novel state of matter for materials science. *Advanced Materials* **1993,** *5* (2), 88-95; (c) Hines, M. A.; Scholes, G. D., Colloidal PbS Nanocrystals with Size‐Tunable Near‐Infrared Emission: Observation of Post‐Synthesis Self‐Narrowing of the Particle Size Distribution. *Advanced Materials* **2003,** *15* (21), 1844‐1849; (d) Anpo, M.; Shima, T.; Kodama, S.; Kubokawa, Y., Photocatalytic hydrogenation of propyne with water on small-particle titania: size quantization effects and reaction intermediates. *Cheminform* **1987,** *18* (43), 4305-4310.

8. (a) Spear, J. C.; Ewers, B. W.; Batteas, J. D., 2D-nanomaterials for controlling friction and wear at interfaces. *Nano Today* **2015,** *10* (3), 301-314; (b) Narayanan, T. N.; Gupta, B. K.; Vithayathil, S. A.; Aburto, R. R.; Mani, S. A.; Taha-Tijerina, J.; Xie, B.; Kaipparettu, B. A.; Torti, S. V.; Ajayan, P. M., Hybrid 2D Nanomaterials as Dual‐Mode Contrast Agents in Cellular Imaging. *Advanced Materials* **2012,** *24* (22), 2992-2998.

9. (a) Qiu, T.; Chu, P. K., Self-selective electroless plating: An approach for fabrication of functional 1D nanomaterials. *Materials Science & Engineering R* **2008,** *61* (1–6), 59-77; (b) Koenigsmann, C.; Wong, S. S., One-dimensional noble metal electrocatalysts: a promising structural paradigm for direct methanol fuel cells. *Energy & Environmental Science* **2011,** *4* (4), 1161-1176; (c) Xia, Y.; Yang, P.; Sun, Y.; Wu, Y.; Mayers, B.; Gates, B.; Yin, Y.; Kim, F.; Yan, H., One‐Dimensional Nanostructures: Synthesis, Characterization, and Applications. *Advanced Materials* **2003,** *15* (5), 353-389.

10. (a) Tiwari, J. N.; Tiwari, R. N.; Kim, K. S., Zero-dimensional, one-dimensional, two-dimensional and three-dimensional nanostructured materials for advanced electrochemical energy devices. *Progress in Materials Science* **2012,** *57* (4), 724-803; (b) Reed, M. A.; Randall, J. N.; Aggarwal, R. J.; Matyi, R. J.; Moore, T. M.; Wetsel, A. E., Observation of discrete electronic states in a zero-dimensional semiconductor nanostructure. *Phys.rev.lett* **1988,** *60* (6), 535.

11. Barth, J. V.; Costantini, G.; Kern, K., Engineering atomic and molecular nanostructures at surfaces. *Nature* **2005,** *437* (7059), 671-679.

12. (a) Haruta, M., Catalysis of Gold Nanoparticles Deposited on Metal Oxides. *Cattech* **2002,** *6* (3), 102-115; (b) Itoh, H.; Naka, K.; Chujo, Y., Synthesis of gold nanoparticles modified with ionic liquid based on the imidazolium cation. *Journal of the American Chemical Society* **2004,** *126* (10), 3026-3027.

13. (a) Corma, A.; Garcia, H., Supported gold nanoparticles as catalysts for organic reactions. *Chemical Society Reviews* **2008,** *39* (50), 2096-2126; (b) Polshettiwar, V.; Varma, R. S., Green chemistry by nano-catalysis. *Green Chemistry* **2010,** *12* (5), 743-754.

14. Joo, S. H.; Park, J. Y.; Tsung, C. K.; Yamada, Y.; Yang, P.; Somorjai, G. A., Thermally stable Pt/mesoporous silica core-shell nanocatalysts for high-temperature reactions. *Nature Materials* **2009,** *8* (2), 126-31.

15. (a) Dan, I. E.; Knight, D. W.; Hutchings, G. J., Solvent-free Oxidation of Primary Alcohols to Aldehydes using Supported Gold Catalysts. *Science* **2005,** *103* (1-2), 362-365; (b) Hughes, M. D.; Xu, Y. J.; Jenkins, P.; Mcmorn, P.; Landon, P.; Dan, I. E.; Carley, A. F.; Attard, G. A.; Hutchings, G. J.; King, F., Tunable gold catalysts for selective hydrocarbon oxidation under mild conditions. *Nature* **2005,** *437* (7062), 1132; (c) Herzing, A. A.; Kiely, C. J.; Carley, A. F.; Landon, P.; Hutchings, G. J., Identification of active gold nanoclusters on iron oxide supports for CO oxidation. *Science* **2008,** *321* (5894), 1331-1335.
16. (a) Durán, P. L.; Thathagar, M. B.; Hartl, F.; Rothenberg, G., Palladium-coated nickel nanoclusters: new Hiyama cross-coupling catalysts. *Physical Chemistry Chemical Physics* **2006,** *8* (1), 151; (b) Pachón, L. D.; Rothenberg, G., Transition-metal nanoparticles: synthesis, stability and the leaching issue. *Applied Organometallic Chemistry* **2010,** *22* (6), 288-299.
17. (a) Jing, L.; Sun, X.; Shang, J.; Cai, W.; Xu, Z.; Du, Y.; Fu, H., Review of surface photovoltage spectra of nano-sized semiconductor and its applications in heterogeneous photocatalysis. *Solar Energy Materials & Solar Cells* **2003,** *79* (2), 133-151; (b) Chen, D.; Ray, A. K., Photocatalytic kinetics of phenol and its derivatives over UV irradiated TiO 2. *Applied Catalysis B Environmental* **1999,** *23* (2–3), 143-157; (c) Ishibashi, K. I.; Fujishima, A.; Watanabe, T.; Hashimoto, K., Detection of active oxidative species in TiO 2 photocatalysis using the fluorescence technique. *Electrochemistry Communications* **2000,** *2* (3), 207-210; (d) Hoffmann, M. R.; Choi, W.; Bahnemann, D. W., Environmental Applications of Semiconductor Photocatalysis. *Chemical Reviews* **1995,** *95* (1), 69-96; (e) Litter, M. I., Heterogeneous photocatalysis : Transition metal ions in photocatalytic systems. *Applied Catalysis B* **1999,** *23* (2–3), 89-114; (f) Li, X. Z.; Li, F. B.; Yang, C. L.; Ge, W. K., Photocatalytic activity of WO x -TiO 2 under visible light irradiation. *Journal of Photochemistry & Photobiology A Chemistry* **2001,** *141* (2), 209-217.
18. Bi, Y.; Ouyang, S.; Umezawa, N.; Cao, J.; Ye, J., Facet effect of single-crystalline Ag3PO4 sub-microcrystals on photocatalytic properties. *Journal of the American Chemical Society* **2011,** *133* (17), 6490-6492.
19. (a) Al-Shahry, M.; Ingler, W. B., Efficient Photochemical Water Splitting by a Chemically Modified$n-TiO_2$. *Science* **2003,** *34* (2), 2243-2245; (b) Park, J. H.; Sungwook Kim, A.; Bard, A. J., Novel Carbon-Doped TiO2 Nanotube Arrays with High Aspect Ratios for Efficient Solar Water Splitting. *Nano Letters* **2006,** *6* (1), 24-28; (c) Wang, G.; Wang, H.; Ling, Y.; Tang, Y.; Yang, X.; Fitzmorris, R. C.; Wang, C.; Zhang, J. Z.; Li, Y., Hydrogen-treated TiO2 nanowire arrays for photoelectrochemical water splitting. *Nano Letters* **2011,** *11* (7), 3026.
20. (a) Taddei, C.; Gambino, R.; Metafora, S.; Monroy, A., Preparation of Polycrystalline TiO 2 Photocatalysts Impregnated with Various Transition Metal Ions: Characterization and Photocatalytic Activity for the Degradation of 4-Nitrophenol. *Electrochimica Acta* **2002,** *54* (11), 3199-3205; (b) Dieckmann, M. S.; Gray, K. A., A comparison of the degradation of 4-nitrophenol via direct and sensitized photocatalysis

in TiO 2 slurries. *Water Research* **1996,** *30* (5), 1169-1183.
21. Lim, B.; Jiang, M.; Camargo, P. H.; Cho, E. C.; Tao, J.; Lu, X.; Zhu, Y.; Xia, Y., Pd-Pt bimetallic nanodendrites with high activity for oxygen reduction. *Cheminform* **2009,** *40* (33), 1302-1305.
22. Tian, N.; Zhou, Z. Y.; Yu, N. F.; Wang, L. Y.; Sun, S. G., Direct electrodeposition of tetrahexahedral Pd nanocrystals with high-index facets and high catalytic activity for ethanol electrooxidation. *Journal of the American Chemical Society* **2010,** *132* (22), 7580-1.
23. Jena, B. K.; Raj, C. R., Enzyme-free amperometric sensing of glucose by using gold nanoparticles. *Chemistry - A European Journal* **2006,** *12* (10), 2702–2708.
24. Wang, A. L.; He, X. J.; Lu, X. F.; Xu, H.; Tong, Y. X.; Li, G. R., Palladium-cobalt nanotube arrays supported on carbon fiber cloth as high-performance flexible electrocatalysts for ethanol oxidation. *Angewandte Chemie* **2015,** *127* (12), 3740-3744.
25. Guo, Y.; Feng, X.; Han, T.; Wang, S.; Lin, Z.; Dong, Y.; Wang, B., Tuning the luminescence of metal-organic frameworks for detection of energetic heterocyclic compounds. *Journal of the American Chemical Society* **2014,** *136* (44), 15485-8.
26. Wang, R.; Wang, C.; Cai, W. B.; Ding, Y., Ultralow-platinum-loading high-performance nanoporous electrocatalysts with nanoengineered surface structures. *Advanced Materials* **2010,** *22* (16), 1845.
27. Choi, B. S.; Lee, Y. W.; Kang, S. W.; Hong, J. W.; Kim, J.; Park, I.; Han, S. W., Multimetallic alloy nanotubes with nanoporous framework. *Acs Nano* **2012,** *6* (6), 5659-5667.
28. Daniel, Q.; Ambre, R. B.; Zhang, B.; Philippe, B.; Chen, H.; Li, F.; Fan, K.; Ahmadi, S.; Rensmo, H.; Sun, L., Re-Investigation of Cobalt Porphyrin for Electrochemical Water Oxidation on FTO Surface: Formation of CoOx as Active Species. *Acs Catalysis* **2017,** *7* (2), 1143-1149.
29. (a) Liu, M.; Lu, Y.; Chen, W., Electrocatalysts: PdAg Nanorings Supported on Graphene Nanosheets: Highly Methanol-Tolerant Cathode Electrocatalyst for Alkaline Fuel Cells (Adv. Funct. Mater. 10/2013). *Advanced Functional Materials* **2013,** *23* (10), 1348-1348; (b) Ruan, L.; Zhu, E.; Chen, Y.; Lin, Z.; Huang, X.; Duan, X.; Huang, Y., Biomimetic synthesis of an ultrathin platinum nanowire network with a high twin density for enhanced electrocatalytic activity and durability. *Angewandte Chemie International Edition* **2013,** *52* (48), 12577; (c) Li, H. H.; Cui, C. H.; Zhao, S.; Yao, H. B.; Gao, M. R.; Fan, F. J.; Yu, S. H., Catalysts: Mixed‐PtPd‐Shell PtPdCu Nanoparticle Nanotubes Templated from Copper Nanowires as Efficient and Highly Durable Electrocatalysts (Adv. Energy Mater. 10/2012). *Advanced Energy Materials* **2012,** *2* (10), 1182-1187; (d) Iyyamperumal, R.; Zhang, L.; Henkelman, G.; Crooks, R. M., Efficient electrocatalytic oxidation of formic acid using Au@Pt dendrimer-encapsulated nanoparticles. *Journal of the American Chemical Society* **2013,** *135* (15), 5521-4.
30. Liu, B.; Zhang, J.; Wang, X.; Chen, G.; Chen, D.; Zhou, C.; Shen, G., Hierarchical Three-Dimensional ZnCo2O4 Nanowire Arrays/Carbon Cloth Anodes for a Novel

Class of High-Performance Flexible Lithium-Ion Batteries. *Nano Letters* **2012,** *12* (6), 3005.
31. Kadirgan, F.; Beyhan, S.; Atilan, T., Preparation and characterization of nano-sized Pt–Pd/C catalysts and comparison of their electro-activity toward methanol and ethanol oxidation. *International Journal of Hydrogen Energy* **2009,** *34* (10), 4312-4320.
32. Liu, F.; Song, S.; Xue, D.; Zhang, H., Folded structured graphene paper for high performance electrode materials. *Advanced Materials* **2012,** *24* (8), 1089-1094.
33. Luo, J.; Liu, J.; Zeng, Z.; Chi, F. N.; Ma, L.; Zhang, H.; Lin, J.; Shen, Z.; Fan, H. J., Three-Dimensional Graphene Foam Supported Fe3O4 Lithium Battery Anodes with Long Cycle Life and High Rate Capability. *Nano Letters* **2013,** *13* (12), 6136-6143.
34. Guan, C.; Liu, J.; Cheng, C.; Li, H.; Li, X.; Zhou, W.; Zhang, H.; Fan, H. J., Hybrid structure of cobalt monoxide nanowire@ nickel hydroxidenitrate nanoflake aligned on nickel foam for high-rate supercapacitor. *Energy & Environmental Science* **2011,** *4* (11), 4496-4499.
35. Xia, X.; Tu, J.; Zhang, Y.; Wang, X.; Gu, C.; Zhao, X.; Fan, H. J., High-Quality Metal Oxide Core/Shell Nanowire Arrays on Conductive Substrates for Electrochemical Energy Storage. *Acs Nano* **2012,** *6* (6), 5531-5538.
36. Wu, Z. S.; Ren, W.; Wang, D. W.; Li, F.; Liu, B.; Cheng, H. M., High-Energy MnO2 Nanowire/Graphene and Graphene Asymmetric Electrochemical Capacitors. *Acs Nano* **2010,** *4* (10), 5835-5842.
37. Zheng, Y. R.; Gao, M. R.; Gao, Q.; Li, H. H.; Xu, J.; Wu, Z. Y.; Yu, S. H., Water Oxidation: An Efficient CeO2/CoSe2 Nanobelt Composite for Electrochemical Water Oxidation (Small 2/2015). *Small* **2015,** *11* (2), 182-188.
38. Li, X.; Rong, J.; Wei, B., Electrochemical behavior of single-walled carbon nanotube supercapacitors under compressive stress. *Acs Nano* **2016,** *4* (10), 6039-6049.
39. Xiong, D.; Wang, X.; Li, W.; Liu, L., Facile synthesis of iron phosphide nanorods for efficient and durable electrochemical oxygen evolution. *Chemical Communications* **2016,** *52* (56), 8711.
40. Wang, H. Q.; Batentschuk, M.; Osvet, A.; Pinna, L.; Brabec, C. J., Rare‐Earth Ion Doped Up‐Conversion Materials for Photovoltaic Applications. *Advanced Materials* **2011,** *23* (22‐23), 2675-2680.
41. (a) Hu, J.; Odom, T. W.; Lieber, C. M., Chemistry and Physics in One Dimension: Synthesis and Properties of Nanowires and Nanotubes. *Cheminform* **1999,** *32* (5), no-no; (b) Wang, Z. L., Characterizing the Structure and Properties of Individual Wire-Like Nanoentities. *Advanced Materials* **2010,** *12* (17), 1295-1298.
42. He, J.; Wang, Y.; Feng, Y.; Qi, X.; Zeng, Z.; Liu, Q.; Teo, W. S.; Gan, C. L.; Zhang, H.; Chen, H., Forest of Gold Nanowires: A New Type of Nanocrystal Growth. *Acs Nano* **2013,** *7* (3), 2733-40.
43. Zhou, H.; Zhou, W.; Adzic, R. R.; Wong, S. S., Enhanced Electrocatalytic Performance of One-Dimensional Metal Nanowires and Arrays Generated via an Ambient, Surfactantless Synthesis. *J.phys.chem.c* **2009,** *113* (14), 5460-5466.
44. (a) Puurunen, R. L., Surface chemistry of atomic layer deposition: A case study for

the trimethylaluminum/water process. *Journal of Applied Physics* **2005,** *97* (12), 121301-121301-52; (b) Miikkulainen, V.; Leskelä, M.; Ritala, M.; Puurunen, R. L., Crystallinity of inorganic films grown by atomic layer deposition: Overview and general trends. *Journal of Applied Physics* **2013,** *113* (2), 021301-021301-101; (c) Ott, A. W.; Mccarley, K. C.; Klaus, J. W.; Way, J. D.; George, S. M., Atomic layer controlled deposition of Al 2 O 3 films using binary reaction sequence chemistry. *Applied Surface Science* **1996,** *107* (107), 128–136.

45. George, S. M., Atomic layer deposition: an overview. *Chemical Reviews* **2010,** *110* (1), 111-131.

46. Kolb, D. M.; Przasnyski, M.; Gerischer, H., Underpotential deposition of metals and work function differences. *Journal of Electroanalytical Chemistry* **1974,** *54* (1), 25-38.

47. Duncan, H.; Lasia, A., Mechanism of hydrogen adsorption/absorption at thin Pd layers on Au(1 1 1). *Electrochimica Acta* **2007,** *52* (21), 6195-6205.

48. Alvarez, B.; Feliu, J. M.; Clavilier, J., Long-range effects on palladium deposited on Pt (1 1 1). *Electrochemistry communications* **2002,** *4* (5), 379-383.

49. Wang, Y.; He, J.; Liu, C.; Chong, W. H.; Chen, H., Thermodynamics versus Kinetics in Nanosynthesis. *Angewandte Chemie International Edition* **2015,** *54* (7), 2022-2051.

50. Dunfeng, G.; Hu, Z.; Jing, W.; Shu, M.; Fan, Y.; Guoxiong, W.; Jianguo, W.; Xinhe, B., Size-dependent electrocatalytic reduction of CO2 over Pd nanoparticles. *Journal of the American Chemical Society* **2015,** *137* (13), 4288.

51. Kibler, L. A.; El-Aziz, A. M.; Rüdiger, H.; Kolb, D. M., Tuning reaction rates by lateral strain in a palladium monolayer. *Angewandte Chemie International Edition* **2010,** *44* (14), 2080-2084.

52. Strmcnik, D.; Uchimura, M.; Wang, C.; Subbaraman, R.; Danilovic, N.; Vliet, D. V. D.; Paulikas, A. P.; Stamenkovic, V. R.; Markovic, N. M., Improving the hydrogen oxidation reaction rate by promotion of hydroxyl adsorption. *Nature Chemistry* **2013,** *5* (4), 300-306.

53. BP Statistical Review of World Energy. 2016.

54. Kamarudin, M. Z. F.; Kamarudin, S. K.; Masdar, M. S.; Daud, W. R. W., Review: Direct ethanol fuel cells. *International Journal of Hydrogen Energy* **2013,** *38* (22), 9438-9453.

2. Pd Coated Au Nanowires on Nickel Foam as High-Performance Electrocatalyst for Ethanol Oxidation Reactions

2.1. Introduction

Recently, direct alcohol fuel cells (DAFCs) are attracting more and more interests as a new kind of portable power sources, due to their unquestionable advantages comparing with another clean energies, like the hydrogen fuel cell and the solid oxide fuel cell.[1] Alcohols, such as methanol, ethanol, ethylene glycol, and glycerol, exhibit relatively high volumetric energy density compared with hydrogen gas. In addition, the storage and the transportation of alcohols are much easier than hydrogen gas. Therefore, increasing research efforts are being carried out on designing and developing more efficient anode electrocatalysts for DAFCs.

Among various kinds of alcohols, the ethanol showed some unique properties. First, the ethanol is the least toxic alcohols, compared with other widely produced alcohols. The drinking of ethanol aqueous solution fermented from grains or fruits, has been served as popular beverage for thousands of years around the world. Second, the ethanol is the renewable energy, which meets the requirements for sustainable development.[2] Large amount of the sugar can be refined from the crops, like corn and then the ethanol can be easily distilled from the sugar. Next, the produced ethanol could be utilized as the fuel in mobile vehicles. After the combustion, the release of carbon dioxide could be reabsorbed by crops again (Figure 2-1-1). All these steps fulfill the complete carbon

cycle (from the crop, to the sugar, to the ethanol, to the carbon dioxide and back to the crop). Thirdly, the energy density of the ethanol is comparable with the gasoline. The energy density of methanol is only 6.1 kWh/kg, while that of ethanol increases to 8.0 kWh/kg, which is more consistent with the gasoline, around 10 kWh/kg. In general, the ethanol could be one of the most promising cases in further scientific research and in the industrial productions for DAFCs.[3]

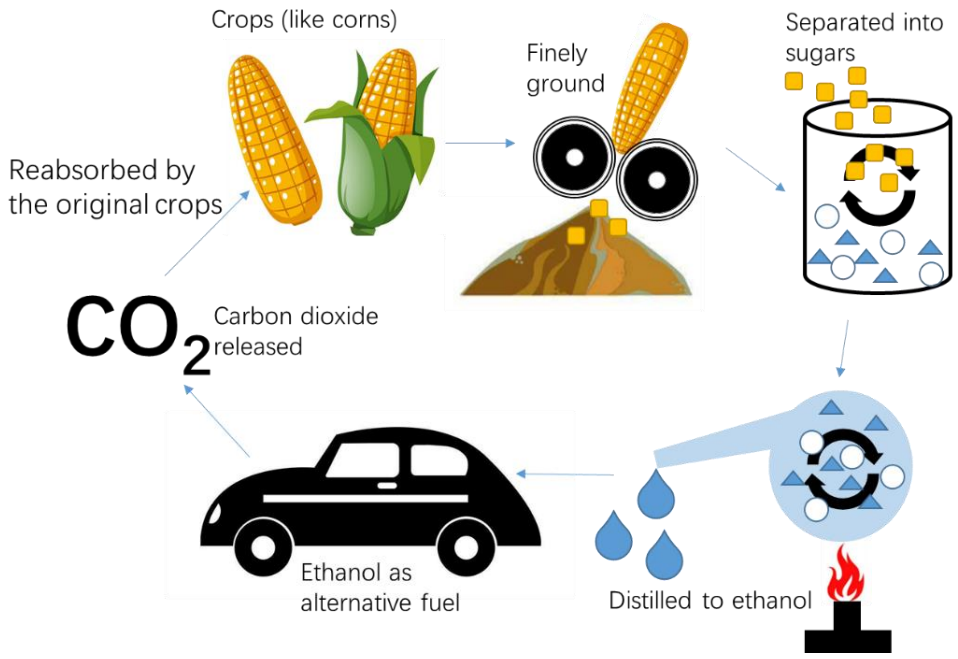

Figure 2-1-1. Illustration of the carbon recycling of the renewable energy, ethanol.

To enhance the efficiency of DAFCs, the most fatal short slab has to be firstly solved. Usually, the low efficiency of the anode electrode, which is used to catalyze the alcohol oxidation reactions, restricts the development of DAFCs. Right now, many researchers are mainly focusing on improving the performance of the anode part. When it comes to the anode in DAFCs, the electrodes are usually divided into two kinds, based on

different connection conditions between the nano catalyst and the electrode. One is called the supported electrode and the other is the unsupported one.[1c]

For supported electrode, the nanomaterials are firstly deposited on some conductive medium materials, such as carbon nanotubes (Figure 2-1-2),[4] carbon nanospheres,[5] and active carbon fibers,[6] rather than the direct attachment onto the electrode surface. One of the most significant advantages of this supported electrode is that serval new functions of the catalyst could be easily involved into the system, not only from the nanomaterial itself, but also from the supported medium materials. When it comes to different types of the support materials, the new functions or advantages could be provided, such as, high surface area without aggregation, good electrical conductivity with packed nanomaterials, suitable porosity for better flowing efficiency of reactants/products, and better stability for long time usage. Most of the problems occurred in this packing system without supporters could be solved by choosing one suitable supporter system.[1b]

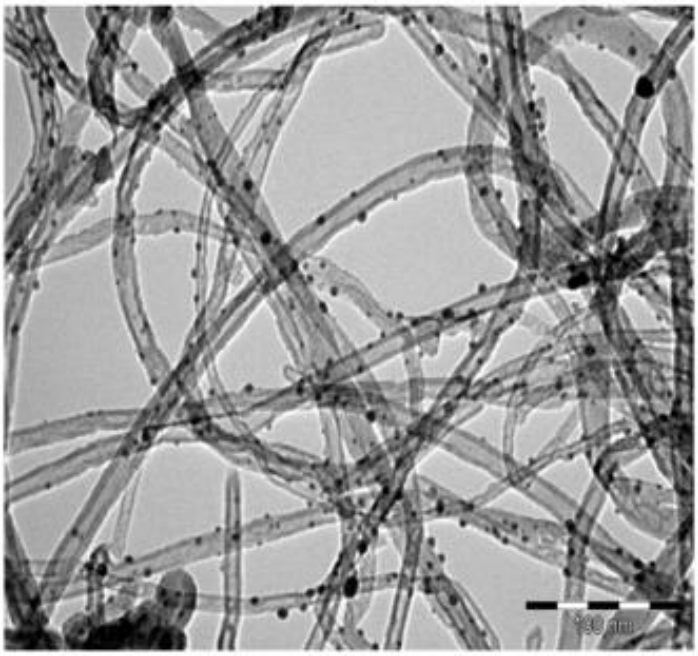

Figure 2-1-2. TEM image of one example of supported electrode, palladium nanoparticles grown on medium material multiwall carbon nanotubes (scale bar: 100 nm). Reprinted with permission from Reference.[4] Copyright 2009 Elsevier.

For unsupported electrode, the catalyst is usually directly deposited or grown onto the substrate or platform.[7] After the direct deposition, the unsupported electrode obtains the similar advantages as the supported one, but the reaction efficiency is usually much higher, due to the less interference from the support materials. Firstly, the electrochemical active surface area of unsupported electrode is significantly larger than that of the supported one, since most of the active surface area of unsupported electrode could be utilized to do the catalysis without any interference from the supporters or the substrate. While, some of the active surface of supported one would be covered by the support materials, leading to the loss of active surface, as well as the catalytic activity.

Secondly, the conductivity of the unsupported electrode can be largely enhanced, since the unsupported electrode could be regarded as the continuous system with much less junction between the catalyst and the substrate. While for the supported electrode, there would be much more intervals in between each nanomaterial. So the conductivity of unsupported electrode is usually higher than that of supported one, due to the large distance caused by the supporters. Thirdly, the flowing efficiency of the reactants/products of the unsupported electrode was higher than that of the supported one, since there are lots of naturally formed gaps in between each nanomaterial, which can help mass transport in large degree (Figure 2-1-3). The medium in the supported electrode with packed nanomaterials usually hinders the flowing of reactants to some degree. Fourthly, the mechanical stability of the unsupported electrode would dominate over the supported one, because the chemical bonds between catalyst and electrode in unsupported electrode are strong and solid. Relatively extreme conditions, such as, stirring, shaking or vibration cannot easily break the chemical bonds.[1c, 8] In short, the unsupported electrode usually has more advantages over the supported ones in the active surface area, the conductivity, the flowing efficiency, and the mechanical stability.

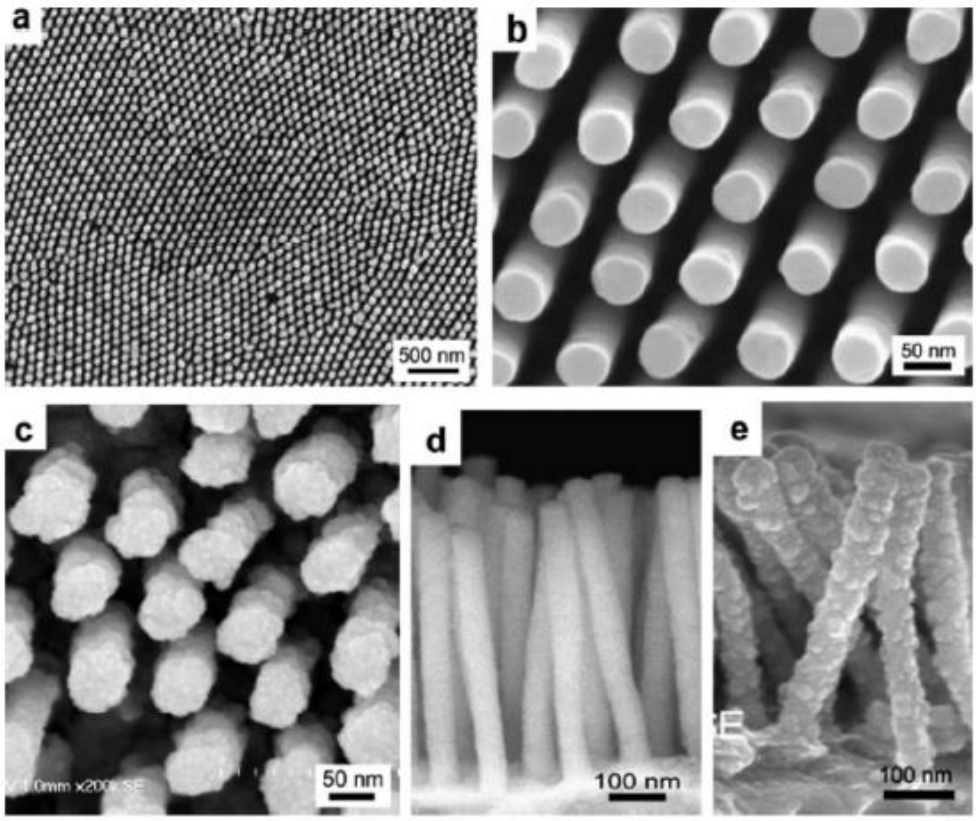

Figure 2-1-3. SEM images of (a) and (b) Pd nanowire arrays, (c) Pd core-Pt shell nanowire arrays, (d) cross-section of Pd nanowire arrays, and (e) cross-section of Pd core-Pt shell nanowire arrays. Reprinted with permission from Reference.[1c] Copyright 2009 American Chemical Society.

From the previous comparisons with the supported and unsupported electrode, obviously, the unsupported electrode would be a better choice for the anode of ethanol oxidation reactions. However, right now, limited methods have been mastered to prepare this kind of electrode and these methods usually own some drawbacks. To grow unsupported catalyst on electrode, there are mainly two methods, the anodic aluminum oxide (AAO) template method and the electrochemical deposition template method.

Since the direct growth of nanowires on substrate is quite difficult, researchers right now usually first use either AAO or electrochemical deposited zinc oxide nanoarrays as template and then deposit the targeted nanomaterials in the pores of AAO or on the surface of zinc oxide nanoarrays (Figure 2-1-3 c-e). The last step is to remove the template.[9] The main disadvantage of this method is the low controllability of the thickness of the nanomaterial. The diameters of AAO template and the zinc oxide nanoarrays. The diameters of these materials are usually larger than 50 nm, which are difficult to be further declined. This would easily lead to the dramatically loss of the active surface area.

Chen group recently reported the successful fabrication of a new kind of ultrathin Au nanowire (AuNW) forest on the silicon wafer with diameter less than 5 nm.[10] As shown in Figure 2-1-4, the thickness of the nanowire mainly depends on the concentration of the strong ligand on the Au surface. This vertically aligned ultrathin AuNW could be considered as one of the suitable and effective catalyst platforms for various electrochemical reactions, including the ethanol oxidation reaction. However, the AuNW forest could be only grown on some hydrophilic oxide substrate, such as, glass and silicon wafer. It is well known that the growth of nanomaterials on silicon wafer could only be used as the demonstration and this hinders the further practical electrochemical applications.

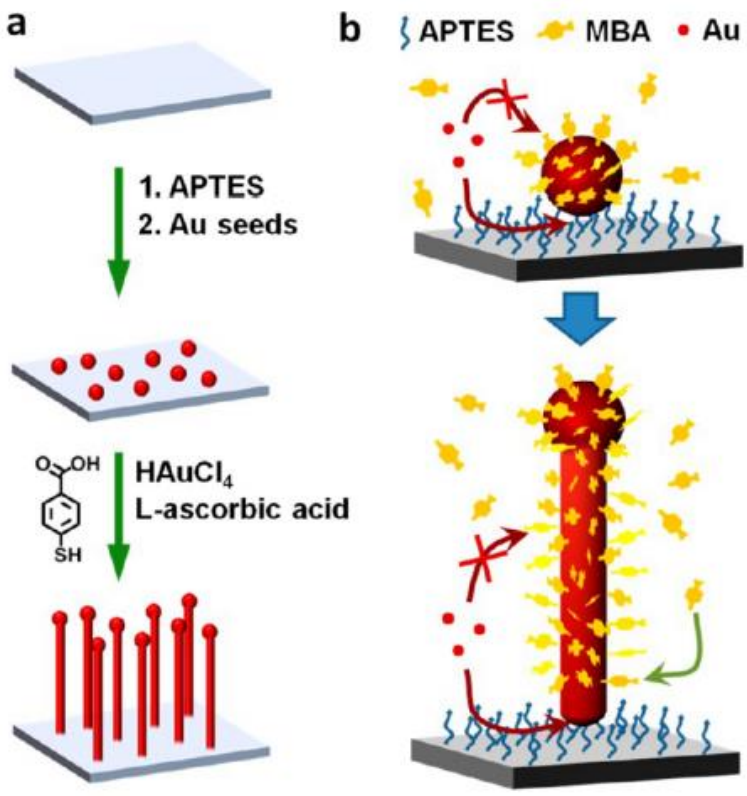

Figure 2-1-4. Illustration of the synthesis method to grow ultrathin gold nanowire forest on silicon wafer. Reprinted with permission from Reference.[11] Copyright 2013 American Chemical Society.

To overcome these drawbacks of the unsupported electrode and restricted growth substrate of the AuNW forest, here we reported the modified fabrication method of the successful growth of 5 nm AuNW forest on the porous nickel foam substrate with over 20 times larger active surface area than AuNW on flat substrate. The electrochemically coated 1 nm Pd overlayer on the AuNW surface would to greatly enhance the catalytic activity on ethanol oxidation reactions. As a two-pronged strategy to increase the active surface area, both the catalytic activities and the stabilities of the Pd coated AuNW nickel foam electrode could be largely enhanced. The pores inside the nickel foam also

results in the good flexibility of the electrode. Over 90 % of the current density can be retained after bended for 50 times. The largely increased surface area and good flexibility makes the Pd deposited AuNW on nickel foam electrode more promising as the anode in ethanol fuel cells and some other practical industrial applications.

2.2. Materials and Methods

2.2.1. Materials

All the aqueous solutions used in the experiments were prepared with deionized water (resistivity > 18 $M\Omega \cdot cm^{-1}$). Hydrogen tetrachloroaurate(III) ($HAuCl_4$, 99.9%, Au 49% on metals basis, Alfa Aesar), palladium chloride ($PdCl_2$, 98%, Sigma Aldrich), 4-mercaptobenzoic acid (4-MBA, 90%, Sigma Aldrich), (3-aminopropyl)triethoxysilane (APTES, Sigma Aldrich), (3-mercaptopropyl)triethoxysilane (MPTES, Sigma Aldrich), (3-cyanopropyl)triethoxysilane (CPTES, Sigma Aldrich), sodium citrate tribasic dihydrate (99.0%, Sigma Aldrich), L-ascorbic acid (Sigma Aldrich), sodium borohydride ($NaBH_4$, 98%, Sigma Aldrich), sodium hydroxide (98%, Sigma Aldrich), palladium on activated charcoal (Pd/C, Sigma Aldrich), ethanol for electrochemistry test (analytical grade, Merck) and ethanol for the growth of AuNW (99.86% technical grade) were used as received. Copper specimen grids (200 meshes) with carbon support film were purchased from Beijing XXBR Technology Co. Nickel foams with different thickness (0.5 mm, 1.0 mm, 2.0 mm and 5.0 mm) were purchased from Suzhou JSD Co and cut into 1*2 cm^2 to use. Fluorine doped tin oxide (FTO) glasses were purchased

from Sigma Aldrich.

2.2.2. Methods

Characterization methods. All transmission electron microscopy (TEM) images were collected on a JEM-1400 (JEOL) operated at 100 kV. All scanning electron microscopy (SEM) images were collected on a JSM-6700F (JEOL). All electrochemistry data were collected on a CHI-760e electrochemical workstation.

Preparation of TEM samples. TEM copper grids were treated with oxygen plasma in a Harrick plasma cleaner/sterilizer for 30 s to improve the surface hydrophilicity. Then the sample solution was dropped onto the hydrophilic face of TEM copper grids placed on the filter paper in less than 30 min. The filter paper below TEM copper grids was used to wick off the excess sample solution around the TEM grid, which was then dried in air for 1 h.

Synthesis of 3-5 nm gold nanoseed (AuNS). A 50 mL round bottom flask was filled with 20 mL deionized water. Then 160 μL sodium citrate (10 mg/mL) aqueous solution and 100 μL $HAuCl_4$ (50 mM) aqueous solution was added into the flask and kept stirring for 1 min. Then 620 μL ice-cold $NaBH_4$ (0.1 M) aqueous solution was added in one shot with continuous vigorous stirring. The solution turned from light yellow to reddish orange, indicating the formation of AuNS. The solution was kept stirring for 10 min and collected to use after overnight for the complete consumption of unreacted $NaBH_4$.

Synthesis of AuNW on nickel foam substrate by APTES. Before the growth of AuNW forest on nickel foam, the purchased nickel foam was first sonicated in ethanol/acetone 1:1 solution for 15 min for three times to remove some organic residual. After that, the nickel foam was continuously sonicated in deionized water for 15 min for three times. Then dried on filter paper to use. The nickel foam was firstly functionalized with amino group by reacting with APTES water/ethanol 1:1 solution (1 μL/mL) for 30 min. Then the nickel foam was washed with ethanol twice and then with water twice. After each washing or soaking step, the excess ethanol or water in nickel foam was removed by filter paper. After APTES was functionalized, the nickel foam was soaked in excess citrate-stabilized AuNS (3-5 nm) aqueous solution for 1 h to ensure the adsorption of AuNS. Then the nickel foam was washed with water twice to remove the excess and unabsorbed AuNS. The AuNS-adsorbed nickel foam was then immersed in a reaction solution containing the solvent ethanol 2 mL, the ligand 4-MBA (10 mM) in 400 μL ethanol, the gold source $HAuCl_4$ (50 mM) in 100 μL water and the reducing agent L-ascorbic acid (20 mM) in 600 μL water for 30 min. Finally, the nickel foam was rinsed with ethanol and dried on filter paper.[10]

Synthesis of AuNW on nickel foam substrate with stirring. To grow AuNW on nickel foam with stirring, all reaction conditions were unchanged except that within the APTES functionalized step, the AuNS adsorption step and the AuNW growth step, the solution was kept stirring.

Synthesis of AuNW on nickel foam substrate with different silanes. To grow

AuNW on nickel foam with different silanes, all reaction conditions were unchanged except the replacement of APTES with CPTES or MPTES.

Synthesis of AuNW on nickel foam substrate without AuNS. After the nickel foam was functionalized with APTES or some other silanes, the nickel foam was directly dropped into the Au growth solution and kept for 30 min. After that, the nickel foam was washed with ethanol twice to remove residual solution on the surface.

Electrochemical coating Pd on AuNW nickel foam. The electrochemical method by CHI-760e electrochemical workstation was used to deposit Pd overlayer on AuNW nickel foam and FTO substrates. The graphite and the saturated calomel electrode (SCE) was served as the counter electrode and the reference electrode, respectively. The working electrode we used was AuNW decorated nickel foam or FTO substrate in the electrolyte containing 1.0 mM $PdCl_2$, 0.5 mM pH = 6 phosphate aqueous buffer solution. The stirring speed during the coating step was 250 rpm all the time. During the coating step, the -2.5 mA current was applied on the working electrode for 20 s, then kept stirring with 0 mA for another 20 s for the Pd precursors to flow inside the nickel foam. Usually the pulsed current was applied for 12 min.

Electrochemical tests for ethanol oxidation reaction. The electrochemical properties of different catalysts were studied in the standard three-electrode cell. The cyclic voltammetry tests, stability tests, and some other electrochemical tests were carried out by the CHI-760e electrochemical workstation. The counter electrode was platinum foil (1*2 cm^2). The reference electrode in all electrochemical tests was

saturated calomel electrode (SCE). The working electrode was nickel foam or FTO with Pd coated AuNW. The electrolyte was 1.0 M sodium hydroxide, 1.0 M ethanol aqueous solution saturated with nitrogen gas. The stirring speed during the purging nitrogen gas process and electrochemical test was 250 rpm all the time. The scan rate of cyclic voltammetry test was 50 mV/s. The stability test was carried out at -0.2 V vs. SCE. All the electrochemical tests were carried out at 25 ℃.

2.3. Results and Discussion

Growth of AuNW on nickel foam by standard method. The growth method and the mechanism of ultrathin AuNW forest on oxide substrate has been fully studied by Chen group.[10] The vertically aligned AuNW was synthesized mainly in three steps, the decoration of silane, the adsorption of AuNS, and the growth of AuNW. The oxide substrate, such as, Si/SiO_2 wafer, was firstly functionalized with amino group by soaking into the (3-aminopropyl) triethoxysilane (APTES) aqueous/ethanol solution. Then the APTES functionalized substrate was decorated with 3-5 nm Au nanoseeds (AuNS). Finally, with most of the Au surface strongly covered by thiol ligands 4-mercaptobenzoic acid (4-MBA), the Au precursor was forced to be selectively deposited at the ligand-deficient interface between the AuNS and substrate. With the increasing amount of Au deposition, the ultrathin vertically aligned AuNW forest can be successfully obtained on the substrate (Figure 2-1-4). However, the most serious confinement of this method for wilder practical applications is that the AuNW forest

can only be grown on the hydrophilic oxide substrate, which seriously limits the usage in many electrochemical applications. Most oxide substrates cannot be worked as suitable conductive substrates for electrochemical catalysis, due to their bad conductivity. So some modifications should be applied on this growth method, making it possible for the successful growth of AuNW on some widely used high surface area conductive substrates, like the nickel foam here.

Firstly, the growth condition on nickel foam substrate was simply followed the same method as the growth on Si wafer.[10] The nickel foam was treated with APTES solution in the first step, and then soaked in the AuNS stock solution. Finally, the AuNS decorated nickel foam was soaked in the Au growth solution, containing the reducing agent ascorbic acid, the ligand 4-mercaptobenzoic acid (4-MBA) and the Au source $HAuCl_4$. Since the targeted surface area of nickel foam was roughly 20 times larger than that of silicon wafer, the growth time was increased from 15 to 30 min accordingly, in order to make sure that there was enough time for the growth of AuNW.

As shown in the Figure 2-3-1, relatively long AuNW (longer than 500 nm) was difficult to be observed from neither outside nor inside of the nickel foam. Most of the nickel foam surface, was covered with large AuNP (diameter larger than 100 nm) and short AuNW (length shorter than 200 nm). Without the growth of longer AuNW, most of the Au source was deposited on the AuNS, leading to the growth of AuNS, and the diameter of these AuNP was much larger than 5 nm, even over 100 nm (blue circles in Figure 2-3-1). The reason for the increasing diameter of the AuNP should be the

insufficiency of ligand confinement, meaning that the concentration of 4-MBA is not high enough to cover the exposed Au surface. For the successful growth of ultrathin AuNW, most of the AuNS and the AuNW surface should be firmly covered with 4-MBA, and the only exposed space comes from the gap between the AuNS and the nickel foam substrate. With less concentrated or lower efficiency of the strong ligand in the growth solution, the reduced Au precursor could be easily deposited on the surface of AuNP, forming larger AuNPs. In addition, the observation of short AuNW indicates that insufficient Au precursor could reach the active growth point. This might result from either the low concentration of the Au precursors or the low efficiency of transportation in the solution. When the incubation time was doubled to 60 min, the amount of Au reduced onto the AuNW did not increase much. On the basis of these results, both the amount of 4-MBA and the Au precursor is not enough to reach the growth point on nickel foam.

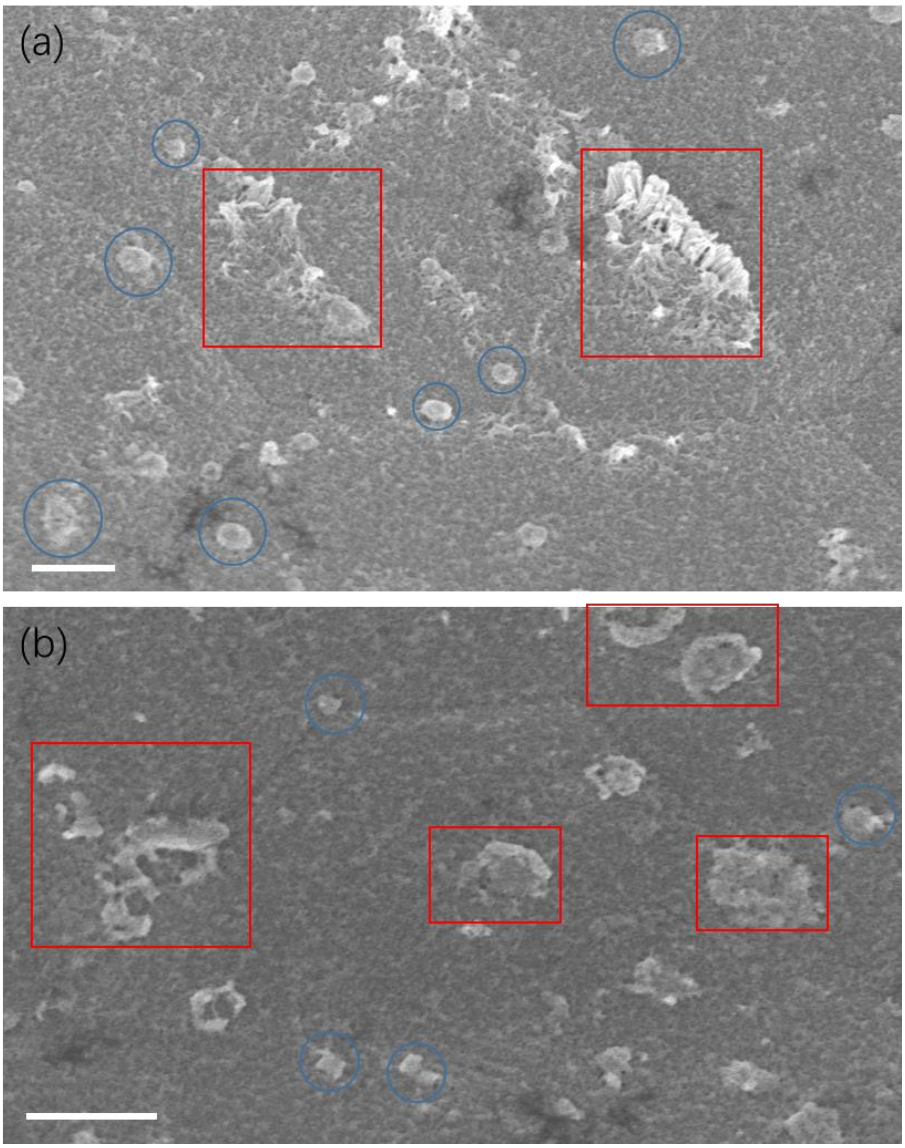

Figure 2-3-1. SEM images of the short AuNW and AuNP on the surface of (a) outside and (b) inside nickel foam by using the standard AuNW growing method. The blue circles and red rectangles indicate the area of growth large AuNP and short AuNW, respectively (scale bar: 1 μm).

To overcome the insufficiency of the ligand or the Au source, the concentration of the chemicals added into the Au growth solution, including $HAuCl_4$, 4-MBA and ascorbic acid was increased by two times. However, similar results were observed from

the SEM images, and there was no long AuNW forest outside or inside the nickel foam. The average length of AuNWs on nickel foam was less than 200 nm. It seems that most of the Au ions was consumed by the increased surface area of nickel foam. Even doubled concentration and time cannot relieve the short supplies of Au precursors. In order to qualitatively determine the residue amount of $HAuCl_4$ after the AuNW growth step, equivalent amount of strong reducing agent (sodium borohydride) was added into the solution. The color of the solution immediately turned to purple-blue, as soon as the reducing agent was added. The changed solution color proved that there would still be large amount of $HAuCl_4$ left in the solution, without being reacted. It should be figured out whether the amount of Au is enough for the growth of long AuNW forest.

In order to quantitatively test the concentration of Au source during the process of AuNW growing on nickel foam surface, a piece of silicon wafer (0.5*0.5 cm^2) was put near the nickel foam as the control experiment, during all the three AuNW growth steps. Other conditions still remained the same as the growth of AuNW on nickel foam. After all three steps, the silicon wafer was taken out and washed with water. Then the nanostructure on the silicon wafer was characterized by SEM. As shown in Figure 2-3-2, the ultrathin AuNW with length over 1 μm can be vertically aligned on the silicon wafer surface. However, it cannot be grown on the nickel foam, just near this silicon wafer. This phenomenon verified that there was enough amount of Au precursor in the solution to support the successful growth of AuNW forest, but they were somehow difficult to reach the nickel foam surface. The chemical transportation is enough for

AuNW growing on flat substrate, but limits the growth on high surface area substrates, such as nickel foam. Therefore, it is the low mass transport efficiency that seriously obstruct the growth of longer AuNW on the nickel foam surface.

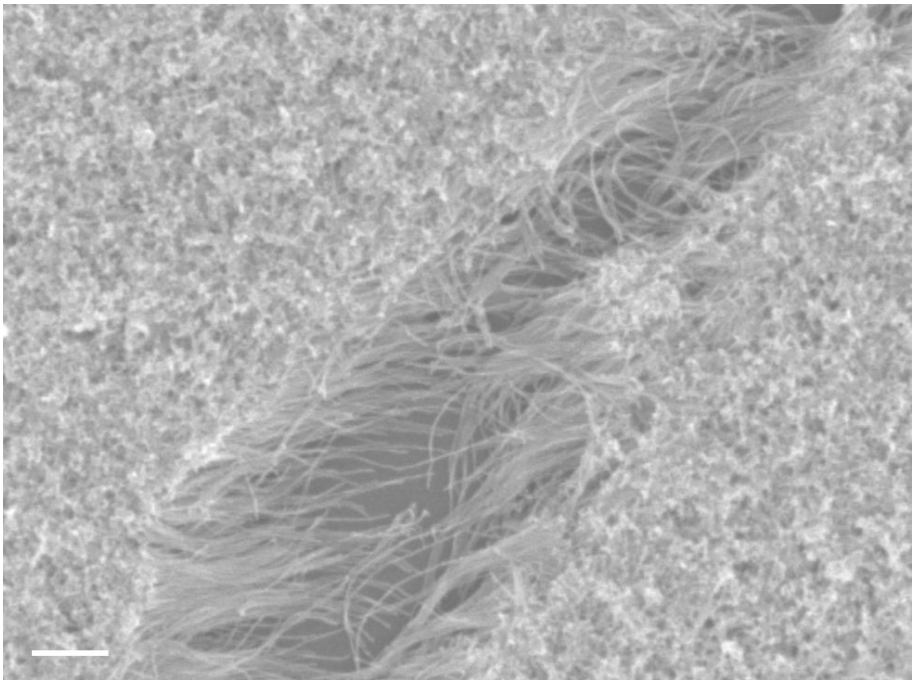

Figure 2-3-2. SEM image of AuNW forest grown on silicon wafer during the process of growing AuNW on nickel foam (scale bar: 200 nm).

Applying the stirring condition. In order to enhance the transportation efficiency of Au source from the solution onto the nickel foam surface, the stirring should be one of the most convenient method. It is quite effective to promote the mixing and supplying efficiency of various solutes near and inside the nickel foam, simply by stirring. One main drawback of the stirring in AuNW growth system is the high possibilities of AuNW peeling off during vigorous stirring. The mechanical stability of the AuNW on silicon wafer was not strong enough to bear the vigorous stirring over one hour. To

avoid the peeling off of AuNW, lower stirring speed around 100 rpm and small stir bar was applied in all three growth steps.

In the APTES modification step, 0.1 % APTES ethanol/water 1:1 solution was freshly prepared. After incubated in the solution with stirring for 30 min, the nickel foam was taken out on the filter paper to remove large amount of the APTES solution inside. Then the nickel foam was washed with ethanol twice and water twice to remove the excess APTES residual on the nickel foam surface. In the AuNS adsorption step, the APTES modified nickel foam was incubated in the AuNS solution with stirring for 60 min. The AuNS solution for adsorption was usually diluted by water five times from the original synthesized AuNS solution, since the amount of AuNS in solution was much larger than the adsorption amount on nickel foam. Then the nickel foam was washed with water twice to remove unabsorbed AuNS inside the nickel foam. For the AuNW growth step, Au growth solution containing $HAuCl_4$ and 4-MBA was prepared. Then the ascorbic acid was quickly added into the solution with stirring for 30 min, just after the nickel foam was dropped into the solution. The interval between the adding of ascorbic acid and the dropping of nickel foam should be as little as possible, otherwise the $HAuCl_4$ would soon be reduced by active nickel metal, undergoing galvanic replacement reactions. Finally, the nickel foam with AuNW was washed by ethanol to remove the excess solution inside nickel foam.

After the stirring condition was introduced into the AuNW growth system, there was obvious long AuNW (mostly over 500 nm) decorated on the nickel foam substrate,

(Figure 2-3-3). The AuNW forest could remain vertically on the nickel foam, but there was serious caking problem at the top, different from normally prepared AuNW forest (Figure 2-3-2). The main purpose of designing this AuNW substrate was to catalyze electrochemical reactions. However, with this kind of serious caking on top, the electrochemical active surface of Au, as well as the transportation efficiency of reactants and products would be significantly reduced. The surface area of caked AuNW was almost equal to that of the packing AuNP, since most of the AuNW was covered by the caking part. This substrate cannot be used as effective catalyst for electrochemical reaction, judging from the morphology. The reasons for serious caking should be found out and the growing methods must be readjusted.

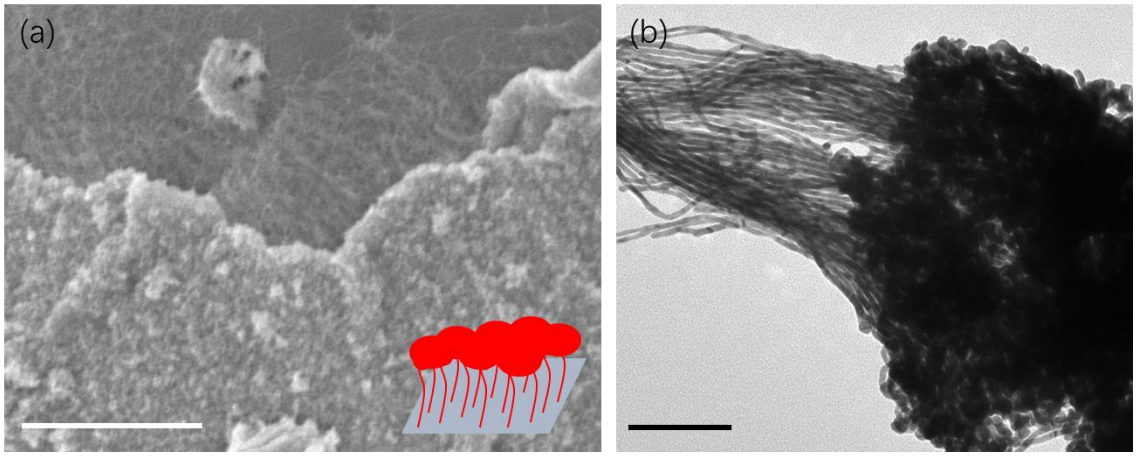

Figure 2-3-3. (a) SEM (scale bar: 1 μm) and (b) TEM (scale bar: 100 nm) images of AuNW grown on nickel foam by standard APTES method with stirring. Inset is the illustration for caking (red standing for gold)

From our previous experience, the amino group on APTES could help the nucleation of Au.[9] Some other positively charged functional groups could also increase the degree

and the speed of nucleation. The positively charged amino group would attract more negatively charged ions in the solution, which was the Au precursor $AuCl_4^-$.[12] When there was no stirring in solution, the nucleation phenomenon was not clearly enough for observation. However, when it comes to the stirring condition, the Au precursors obtained more chances to be nucleated at the sites of amino group on APTES. In the experiment, when there was no stirring condition, only the solution near nickel foam was colorless, meaning that the amount of $HAuCl_4$ reaching the nickel foam surface was gradually increasing and not all Au ions have the chances to be deposited on the nickel foam in 30 min. While within the stirring condition, the color of the Au growth solution was almost colorless with no obvious color difference between the bottom and the top solution, by naked eye. From the observations in experiments and our previous knowledge, we proposed that the serious caking on top of AuNW mainly comes from the combination of stirring condition and the amino group on APTES.

In order to prove the hypothesis and solve the caking problem, the APTES has to be replaced by some other silanes without positive charged functional group, since the stirring was the necessary condition for AuNW growth on nickel foam. So the (3-aminopropyl) triethoxysilane (APTES) was replaced with two different silanes, (3-mercaptopropyl) triethoxysilane (MPTES) and (3-cyanopropyl) triethoxysilane (CPTES). The mercapto group and cyano group was negatively charged functional groups, which are different from positively charged amino group. This might reduce the possibilities of the nucleation of Au near the nickel foam surface. All the other

reaction conditions kept unchanged, with the only difference of replacing APTES with MPTES and CPTES.

Judging from Figure 2-3-4a, the aggregation of AuNW heads almost disappeared with MPTES functionalized nickel foam. There was no obvious caking on the top of AuNW anymore and most of the AuNW can be clearly figured out on SEM images. However, the density of AuNW was relatively low on the MPTES functionalized nickel foam substrate. Most of the nickel foam was covered with short AuNW (less than 500 nm) and AuNS. Although stirring condition has already applied, the AuNW was still not long and dense enough for electrochemical application. The silane MPTES seemed to hinder the Au nucleation degree too much. Both the caking of AuNW and the growth of AuNW were restricted by MPTES.

After the silane was replaced with CPTES, the degree of caking on the top of AuNW obviously decreased. As shown in Figure 2-3-4b, the density of AuNW was quite high, almost covering all the nickel foam surface. From the TEM image, the diameter of heads on AuNW forest (6.0 nm) was almost the same as that of AuNW body (5.8 nm). The diameter of original AuNS head only increased less than 1 nm and no obvious caking on top from SEM or TEM could be observed. The cyano functionalized silane CPTES can reduce the degree of nucleation at the top of AuNW compared with APTES (no caking) and does not hinder the growth of AuNW too much compared with MPTES (higher density and increased length). In short, comparing with different silanes, the CPTES was a relatively suitable and effective silane for the growth of AuNW on the

surface of nickel foam.

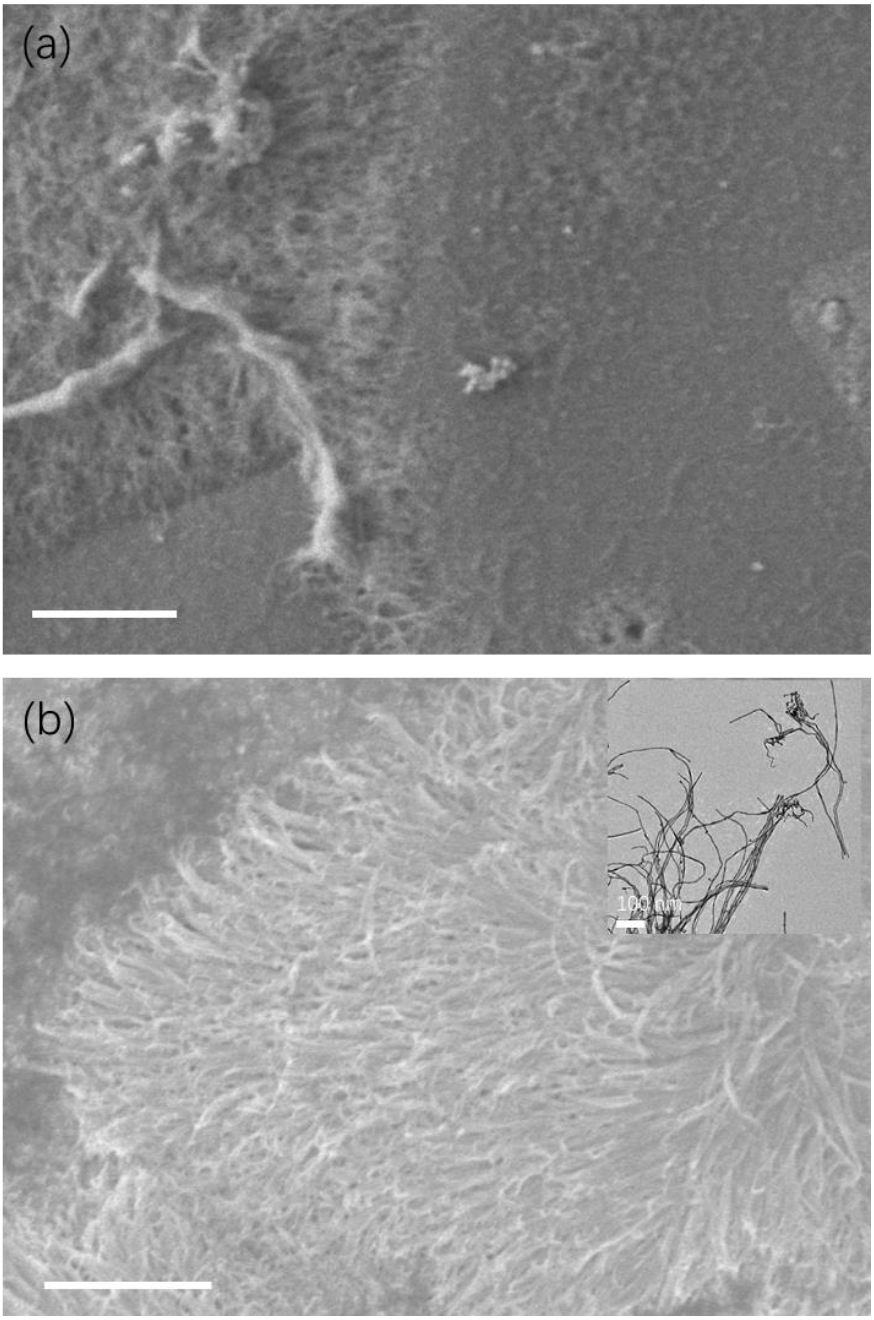

Figure 2-3-4. SEM images of AuNW grown on the surface of nickel foam by stirring condition method with (a) MPTES and (b) CPTES (scale bar: 1 μm). Inset is the TEM image of sonicated AuNW from nickel foam by CPTES method (scale bar: 100 nm).

In order to find out whether the growth density of AuNW inside the nickel foam was

worse or equal to the surface of nickel foam, the growth condition inside the nickel foam was also characterized. After the surface nickel foam was carefully cut off, the inside part of nickel foam was characterized by SEM. As shown in Figure 2-3-5, the length, the density and the alignment of AuNW was almost the same as the AuNW on the surface of nickel foam. Meanwhile, this kind of AuNW on nickel foam was similar to the AuNW grown on silicon wafer by the standard method, judging from TEM images. To conclude, by applying the stirring condition and changing the surface silane from APTES to CPTES, AuNW can be successfully grown on both the surface and inner part of nickel foam.

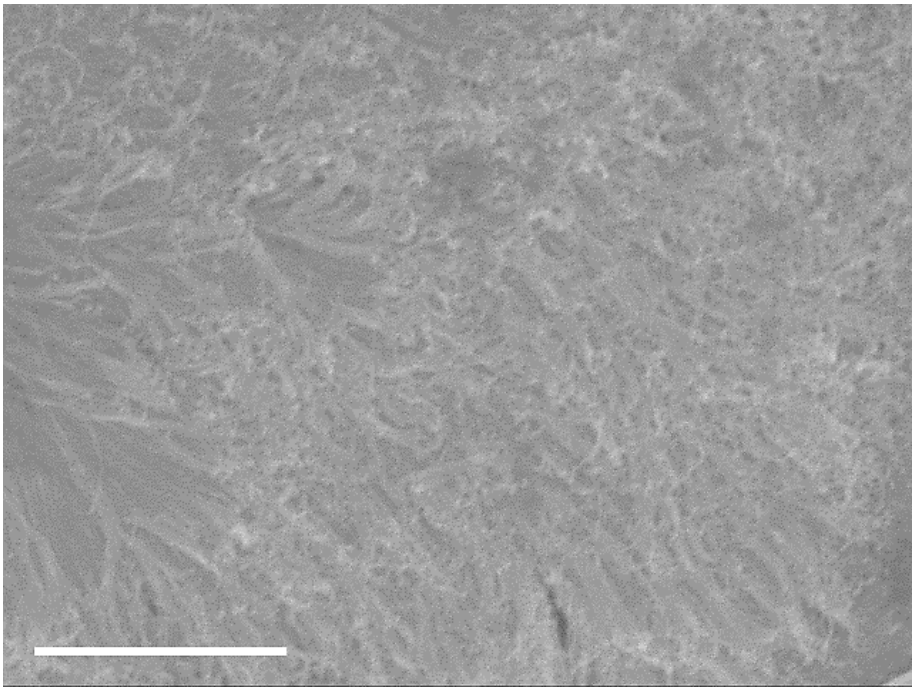

Figure 2-3-5. SEM image of AuNW grown inside the nickel foam by stirring method with CPTES as silane (scale bar: 1 μm).

Growth of AuNW on nickel foam without AuNS. The standard method for the

growth of AuNW on nickel foam or silicon wafer usually includes three steps, functionalizing silane (CPTES or APTES), AuNS adsorption and AuNW growing. The AuNS on the substrate was served as the initiation point for the growth of AuNW. If there was no AuNS on the surface, the reduced Au had little chance to be deposited unless the random nucleation of Au on the surface with very low possibility. As shown in Figure 2-3-6, most part of the silicon wafer was vacant, with very few AuNW bundles. Without the decoration of AuNS, the AuNW forest cannot be formed on silicon wafer, due to the lack of deposition site for Au nucleation. Without nucleation point, AuNW could not be grown on the silicon wafer, and most of the Au precursors would undergo homogeneous nucleation in the solution.

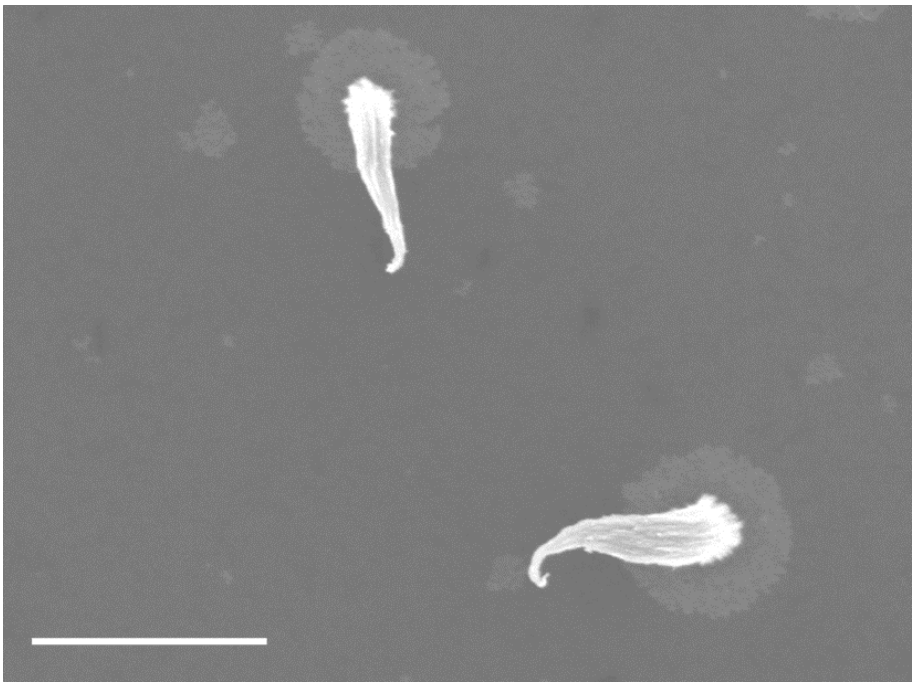

Figure 2-3-6. SEM image of AuNW growing on silicon wafer by standard method without the adsorption of AuNS (scale bar: 1 μm).

However, when it comes to the nickel foam substrate, the nickel was a relatively active metal compared with silicon or some other oxide substrate and the Au precursor $HAuCl_4$ can be easily reduced to Au (0) through galvanic replacement reaction. The intrinsic properties of metal state Au (0) was similar with the AuNS adsorbed on the substrate. It is possible that the two kinds of Au, reduced Au (0) and adsorbed AuNS on substrate, would have similar functions and effects. If this worked, the AuNS adsorption step could be removed for the successful growth of AuNW forest on nickel foam, which would be much easier than growth on the silicon wafer.

Nickel foam was firstly functionalized by CPTES, and washed with ethanol and water twice and finally was directly dropped into the Au growth solution. After 30 min of AuNW growing, the substrate turned to black, indicating the successful deposition of Au nanomaterials (Figure 2-3-7 inset). From the SEM image in Figure 2-3-7, the AuNW could be clearly observed on most of the nickel foam surface and the structure was quite similar with the growth of AuNW on nickel foam by normal CPTES-AuNS method. The length of most AuNW on nickel foam is over 1 μm. There was no caking on the top of the AuNW and almost every single AuNW separated well, verifying that without the addition of AuNS, nickel foam itself can help reduce the $HAuCl_4$ to AuNS on the surface of nickel foam as the initiated Au seeds.

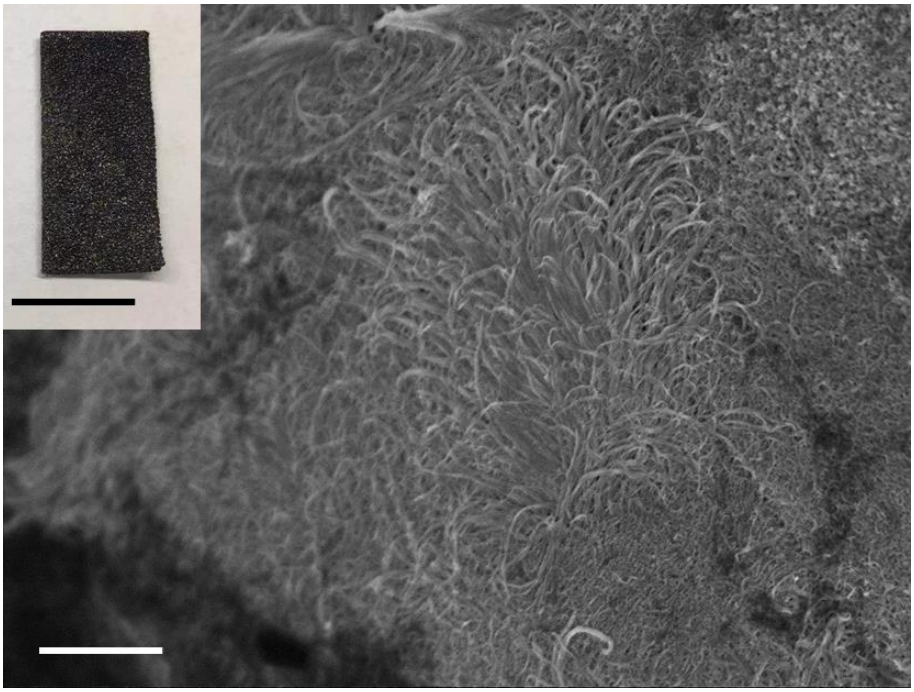

Figure 2-3-7. SEM image of AuNW growing on nickel foam modified with CPTES without the adsorption of AuNS step (scale bar: 1 μm). Inset is the photo of the nickel foam after the growth of AuNW without AuNS decoration (scale bar: 1 cm).

Understanding the growth mechanism and the difference between silicon wafer and nickel foam are the key points to explain the reasons why without AuNS, the AuNW could still grow on the nickel foam, but not on silicon wafer. To grow AuNW on the substrate, there are two necessary conditions. One is the exposed Au surface and the other is enough distance between the Au surface and the substrate. When it comes to the growth of AuNW on CPTES functionalized silicon wafer functionalized, there is no exposed Au surface on silicon wafer. The small heads at the top of each bundle of AuNW all result from the random nucleation of Au on the silicon surface or in the solution near the substrate. When there is one exposed Au surface, more fresh Au

precursors would be gathered and nucleated between the original Au surface and the substrate. But the random nucleation was too less on the silicon surface, leading to very few AuNWs grown on the silicon wafer. What differentiates nickel foam from silicon wafer is reducibility and the active nickel can help reduce the Au (III) ions to Au (0) metal. With the reduction of Au, the AuNP can be easily deposited on the nickel foam surface, which meets the necessary condition of exposed Au surface. The surface silanes, such as APTES or CPTES on nickel foam create enough distance between the Au and the substrate. The combination of nickel foam surface and Au ions in the solution mimic the condition of AuNS functionalized substrate. This is why after the nickel foam was functionalized with silanes, the modification step of AuNS could be skipped, while the silicon wafer could not.

To further prove the function of nickel foam as the reducing agent, APTES is used as the silane on nickel foam surface instead of CPTES, with all other conditions unchanged. A shown in Figure 2-3-8, similar morphology with the growth of AuNW on CPTES functionalized nickel foam could be observed on most of the nickel foam and the average length was over 1 μm. The main difference between the two methods, APTES and CPTES, was the caking degree of the heads of AuNW. The APTES could help the nucleation and aggregation of Au precursor at the top of AuNW, which is the beginning state of AuNW growth. At the very first moment after the Au growth solution reached APTES sites, the amino group promoted the nucleation and growth of AuNP, leading to the caking heads at top.

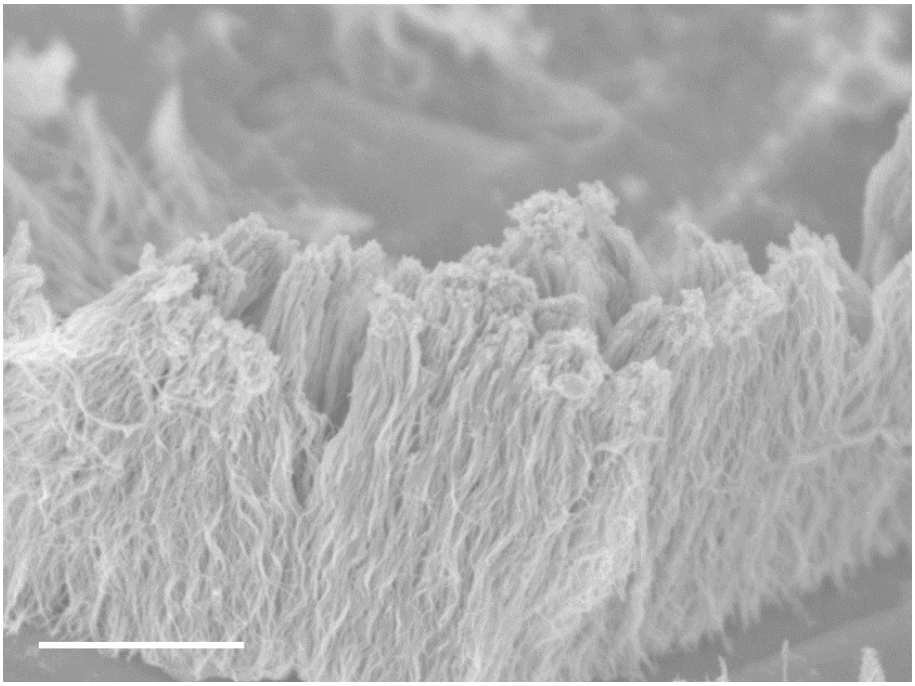

Figure 2-3-8. SEM image of AuNW growing on nickel foam modified with APTES without the adsorption of AuNS (scale bar: 1 μm).

Among these methods of growing AuNW on nickel foam, the most suitable and effective one should be picked up for the electrochemical reactions. Some important factors should be carefully examined and considered to enhance the electrochemical catalysis ability, such as the mechanical stability, the active surface area, and the mass transport efficiency. In order to choose the most suitable substrate for electrochemical reaction, the three factors should be compared among the three substrates, CPTES-AuNS (Figure 2-3-4b), CPTES-noNS (Figure 2-3-7) and APTES-noNS (Figure 2-3-8).

To compare the mechanical stability, the AuNW grown on nickel foam was much better than the growth on FTO, due to the existence of metal-metal bonds between nickel foam and AuNW. So the three nickel foam growth methods all obtain better

stability than the growth of AuNW on FTO. The AuNW was easily peeled off from FTO surface, due to the capillary effect between every nanowire. If the AuNW was lined up in good order on a flat substrate, the bundles of AuNW could be more easily peeled off by vibration or gas bubbles between nanowires. So from SEM images, the growth of AuNW by CPTES-AuNS and CPTES-noNS method was not that dense and lined compared with APTES-noNS method. So from the mechanical stability aspect, the CPTES-AuNS and CPTES-noNS was better.

For the comparison of surface area, the coverage of AuNW on each substrate has to be carefully examined. From SEM images, it roughly shows that both the APTES-noNS and CPTES-AuNS obtained quite high coverage. So over ten SEM images were randomly extracted for each method to find out the average coverage for the AuNW on nickel foam. For CPTES-AuNS, the average coverage was around 85 %, CPTES-noNS around 67 % and APTES-noNS around 68 %. Without the adsorption of AuNS, AuNW could be deposited on the nickel foam on the fresh reduction sites of AuNP. The amount of AuNW mainly depends on the numbers of Au sites on the nickel foam surface. For the growth methods with AuNS, the amount of AuNW was confirmed and determined by the adsorbed AuNS and the coverage of AuNS was higher than other two methods. For the two growth methods without AuNS, the number of Au sites was uncertain and the reduced Au source was mainly divided into two competitive parts, forming AuNS sites and growth of AuNW. Right now, the controllability of the Au reaching more nickel foam surface forming fresh Au sites is low. So from the surface area aspect, the

CPTES-AuNS growth method was better than the methods without the adsorption of AuNS.

When it comes to the mass transport in AuNW system, the distance between each AuNW and the flexibility of AuNW on nickel foam should be under consideration. The top distance between two AuNW was carefully measured in three growing methods. The average distance of CPTES-AuNS, CPTES-noNS and APTES-noNS is 54.7, 58.6 and 15.3 nm respectively. From both the characterized data and the observation from SEM images, APTES-noNS obtains less distance between every AuNW. With higher flexibility, the mass transport could be much easier. Among all the three methods, apparently, the APTES-noNS was worse than the other two, since the heads of AuNW was all caked together and could not move freely in the solution (Figure 2-3-8). But for CPTES-AuNS and CPTES-noNS, the heads of AuNW all spread out and could move freely to help the mass transport more efficient while catalyzing electrochemical reactions. So from the mass transport aspect, the CPTES-AuNS and CPTES-noNS was better.

In short, Table 2-3-1 summarizes three main aspects for electrochemical reactions, the mechanical stability, the surface area and the mass transportation efficiency, of the three methods on the growth of AuNW on nickel foam. From the previous discussions, the CPTES-AuNS decorated nickel foam was the best among the three. So here, the nickel foam substrate, undergoing CPTES and AuNS modification steps, will be used for the electrochemical reactions in the next few steps.

Table 2-3-1. Three aspects of AuNW growing on nickel foam with three different growth methods (underlying the relatively better ones among the three)

Methods	Mechanical stability (lining up)	Coverage (surface area)	Distance between AuNW (mass transport)
CPTES-AuNS	good	85 %	54.7 nm
CPTES-noNS	good	67 %	58.6 nm
APTES-noNS	bad	68 %	15.3 nm

Electrochemical deposition of Pd on Au surface. For different kinds of electrochemical reactions, various composition of catalyst was required, not only the Au surface. However, after the growth of AuNW forest on nickel foam, the exposed active surface area was Au and other noble metal nanowires was difficult to be vertically grown on the nickel foam surface via similar method. So the coating methods should be applied to replace the Au surface with various catalytic metal surfaces instead, to improve the generality of AuNW nickel foam system.

Reproducibility and scalability were the two main reasons to choose the electrochemical deposition method. For electrochemical deposition methods, the coating substrate, the electrolyte, the electrochemical settings, and the deposition procedures could be precisely controlled, which makes the results easier to be reproduced. The conditions in chemical bath deposition methods, such as, the time, the

temperature or the stirring speed, are difficult to be precisely controlled, which would have large impacts on the final structure and composition. Another advantage was the outstanding scalability for electrochemical deposition method. For substrate with larger project or surface area, connection with the electric circuit and immersing into the electrolyte would be the same as the small surface area one. While for the typical chemical solution deposition, large container and large amount of solution are needed, and the deposition solution is difficult to be recycled. The concentration, the temperature and the stirring condition would be quite different at different positions of the large container. In addition, the distribution uniformity of the coating layer was uncontrollable when the substrate surface is increased. While for the electrochemical deposition method, it is easy to enlarge the coating substrate, owing to the uniform electron distribution all over the substrate surface.

So the electrochemical deposition method is used to coat Pd on AuNW nickel foam. Here, the graphite rod was served as the counter electrode, the saturated calomel electrode (SCE) as the reference electrode, and the nickel foam with AuNW as the working electrode. The electrolyte for the Pd coating was 1.0 mM $PdCl_2$ and 0.5 M pH = 6 phosphate aqueous buffer solution. The stirring speed during the coating step was 250 rpm all the time. During the coating step, the -2.5 mA current was applied on the working electrode for 20 s, and then 0 mA was applied for another 20 s with stirring to ensure the efficient flowing of the Pd deposition solution inside the nickel foam. The pulsed current is applied for 12 min to ensure the full coverage of Pd overlayer.

As shown in Figure 2-3-9a, the Pd deposited AuNW became thicker and most of the AuNW remained vertical alignment on the nickel foam surface, after the electrochemical coating of Pd on AuNW nickel foam. In addition, little caking could be clearly observed at the top of AuNW forest. After dissolved in the aqua regia and test in the inductively coupled plasma optical emission spectrometry (ICP-OES), the Pd coated AuNW nickel foam contains 0.18 mg/cm^2 Pd and 0.19 mg/cm^2 Au, verifying the successful growth of Pd onto the substrate. In addition, the energy-dispersive X-ray spectroscopy (EDS) line scan shows the element information of Pd on AuNW, indicating the uniform Pd shell deposited on AuNW (Figure 2-3-9b). Measured from the TEM images, the diameter of AuNW increased from 5.71 ± 0.67 nm to 7.75 ± 1.02 nm after the electrochemical deposition of Pd shell (Figure 2-3-9c and 9d). The increased 2.04 nm results from the Pd shell on AuNW and the estimated average thickness of the Pd overlayer is around 1.02 nm. As shown in Figure 2-3-9c, most of the Pd shell on AuNW is smooth and uniform, with few branch, island or exposed Au surface. As shown in the high-resolution TEM (HRTEM) image (Figure 2-3-9e), both the AuNW core and the Pd shell was quasi-single-crystalline. All these characterizations demonstrate that the Pd shell was successfully deposited on the AuNW nickel foam substrate.

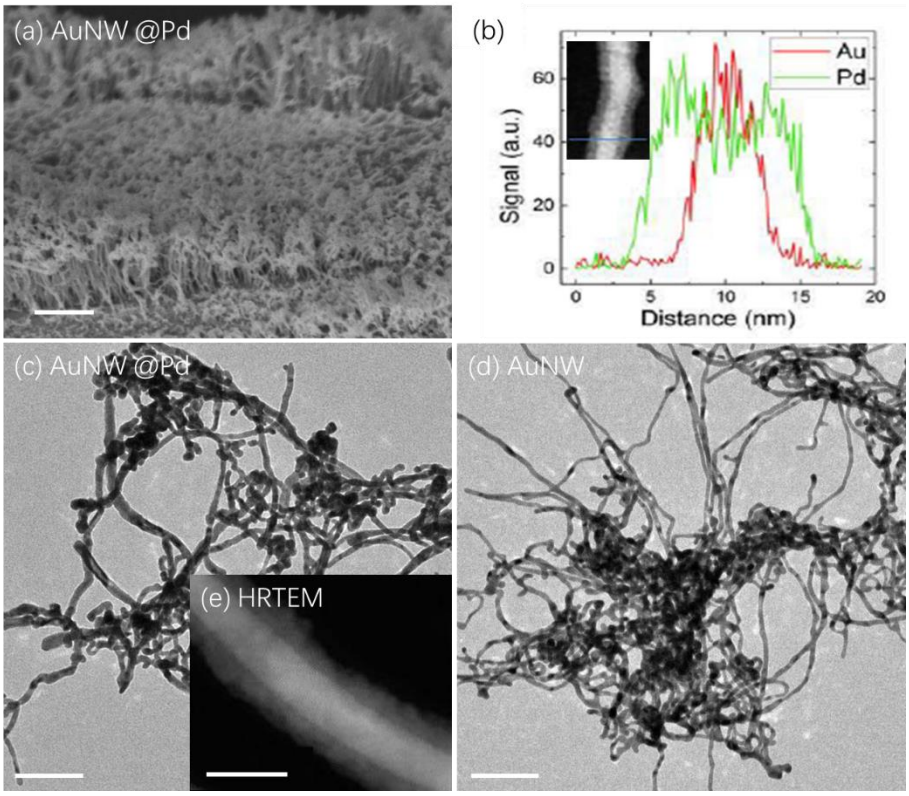

Figure 2-3-9. (a) SEM image and (b) EDS line scan of Pd coated AuNW grown on the nickel foam by CPTES-AuNS method (scale bar: 1 μm). TEM images of AuNW sonicated from nickel foam (c) with and (d) without Pd coating (scale bar: 100 nm). (e) HRTEM of sonicated Pd coated AuNW grown on nickel foam (scale bar: 10 nm).

Electrochemical characterizations of ethanol oxidation reaction. After the successful deposition of Pd on AuNW nickel foam substrate, the ethanol electro-oxidation reaction was turned out to be one of the best choices for two reasons. The Pd-based electrocatalyst is an appropriate catalyst for the ethanol oxidation reaction in alkaline solution. Compared with Au surface, the Pd metal obtains the intrinsic advantage of higher catalysis activity. Usually, the Pd obtains higher current density and more negative onset potential than the Au.[13] Moreover, the bottle neck for ethanol

oxidation reaction right now is the low efficiency. Theoretically, simply increasing the active surface area could enhance the catalysis efficiency incredibly.[14] As a two-pronged strategy, the combination of porous three-dimensional platform nickel foam and the one-dimensional catalyst ultrathin AuNW forest could dramatically increase the surface area, compared with simply packing zero-dimensional catalysts on flat two-dimensional substrate.[1c, 15]

So the Pd coated AuNW nickel foam electrode was served as the working electrode to electrochemically catalyze the ethanol oxidation reactions. The graphite rod and the saturated calomel electrode (SCE) was served as the counter and the reference electrode, respectively. The catalysis activity test for the ethanol oxidation reaction was carried out with three-electrode system in the electrolyte containing 1.0 M sodium hydroxide and 1.0 M ethanol. As shown in Figure 2-3-10, the cyclic voltammetry (CV) curves clearly demonstrate that the peak current density of Pd coated AuNW nickel foam (543.4 mA/cm^2) was 3.3 times, 11.2 times and 48.1 times higher than that of Pd coated bare nickel foam, Pd coated AuNW on FTO and the state-of-the-art Pd-based catalyst, Pd on activated carbon (Pd/C), respectively. The enhanced current density of the AuNW nickel foam substrate mainly results from the greatly increased active surface area. Owing to the large surface area of the three-dimensional substrate nickel foam, the peak current density of Pd coated AuNW nickel foam enhanced over 10 times than that of Pd coated AuNW on the flat substrate FTO, and this is similar to the difference of surface area between the bare nickel foam and the bare FTO. To conclude, the satisfying

peak current density data verifies that the combination of ultrathin AuNW and porous nickel foam substrate, can be served as the promising platform for the enhancement of the current density to a large degree, which might effectively solve the problem of insufficient catalytic activity for the ethanol oxidation reactions.

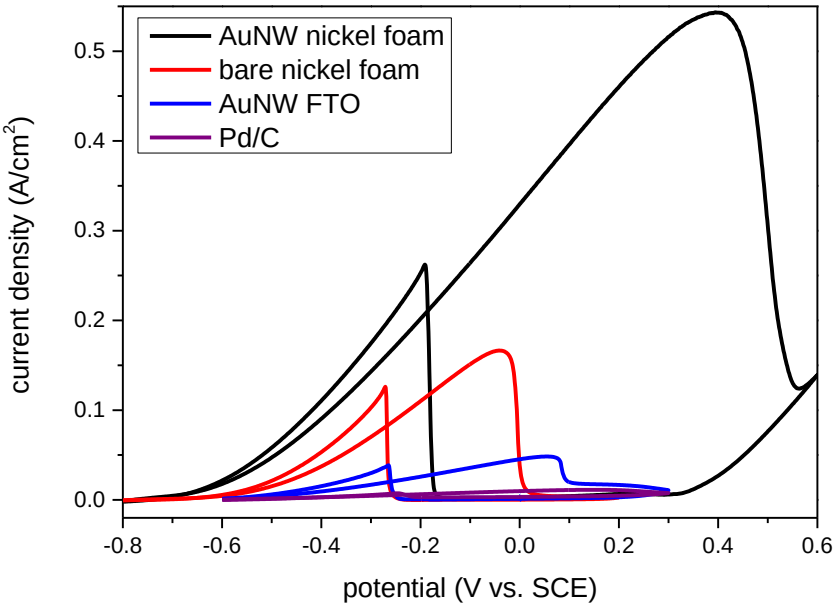

Figure 2-3-10. Cyclic voltammograms of palladium coated AuNW on nickel foam (black line), bare nickel foam (red line), AuNW on FTO (blue line) and Pd/C (purple line) in 1.0 M sodium hydroxide and 1.0 M ethanol aqueous solution.

Besides the high peak current density, the stability is also critical for the practical electrochemical applications. The long term stability tests for Pd coated AuNW nickel foam, bare nickel foam, AuNW on FTO, and Pd/C were carried out by the chronoamperometry technique at the potential of -0.2 V vs. SCE in 1.0 M sodium hydroxide and 1.0 M ethanol aqueous solution for 30 min. As shown in Figure 2-3-11,

all these four curves dropped with the increasing of testing time, indicating that there was severe poison accumulating at the Pd surface during the ethanol oxidation reactions. The quickly dropped current density of the stability test was a common phenomenon for various types of Pd-based catalysts in alkaline electrolyte.[16] The stable current density measured after 30 min at -0.2 V were 86.0, 3.18, 5.10 and 0.605 mA/cm^2 for these four electrodes. The stable current density after 30 minutes of Pd coated AuNW nickel foam was around 27, 17 and over 140 times higher than that of Pd coated bare nickel foam, AuNW on FTO, and Pd/C. The nickel foam system obtains higher starting current density than the flat substrate, so only comparing the absolute value is unfair to the lower surface area ones. To acquire the remaining percentage of current density, the stable current density is divided by the starting current density. As shown in Figure 2-3-12, the remaining percentage of the Pd coated AuNW nickel foam electrode (41 %) was still higher than that of bare nickel foam (5 %), AuNW on FTO (26 %) and Pd/C (10 %). It verifies that this high surface area electrode, Pd coated AuNW nickel foam, is much more efficient and better poison resistant elctrocatalyst than the others on ethanol oxidation reactions in alkaline electrolyte.

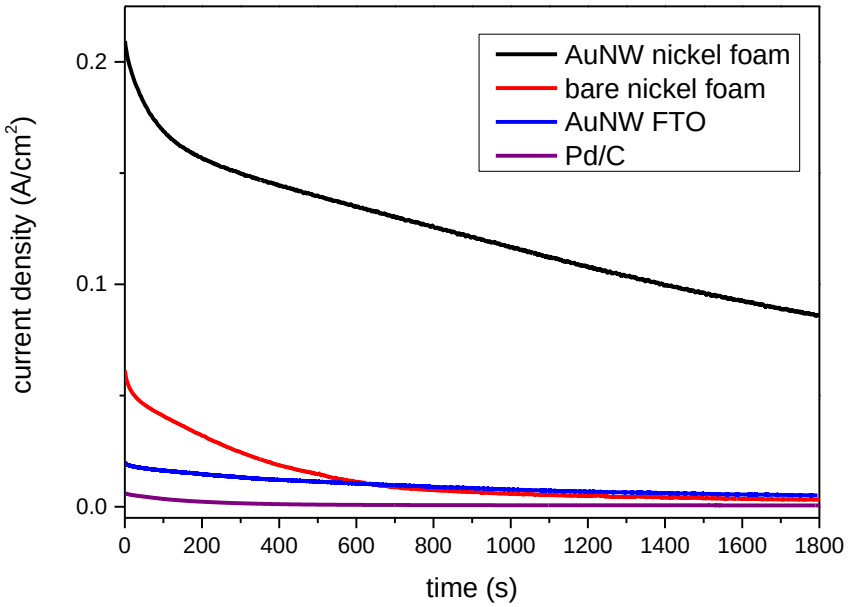

Figure 2-3-11. Chronoamperometry of palladium coated AuNW on nickel foam (black line), bare nickel foam (red line), AuNW on FTO (blue line) and Pd/C (purple line) in 1.0 M sodium hydroxide and 1.0 M ethanol aqueous solution at potential -0.2 V vs. SCE for 30 min.

To figure out the reasons for better stability of the prepared Pd-based high surface area electrode, the examination of surface structure differences of each substrate was carried out carefully. Essentially, the stability test is used to measure the poison tolerance ability of the surface Pd atoms. The poisons in ethanol oxidation reactions, such as, hydroxide group, ethanol intermediate (ethoxy group) and carbon monoxide, would be bound on the surface Pd atoms to deactivate its catalysis ability.[17] For the flat substrate or surface, like the Pd coated bare nickel foam in this case, the surface would soon be occupied with various poisons and little surface could be used as active catalyst

any further, once firmly bound by the poisons. So over 95 % of the starting current density would drop in 30 min. While for the Pd coated AuNW nickel foam substrate, the intermediate was not that easy to cover all the active surface, due to the roughness of the electrode surface or the depth from the top to the bottom of AuNW forest. With over 1 μm length of AuNW, the concentration gradient was formed in between each AuNW. When the top AuNW was poisoned, the bottom part could remain catalyzing ethanol oxidation reactions and this gave enough time for other parts of the AuNW to recover when the concentration of electrolyte is lowered. This is why the two AuNW substrates are far more stable than the other two. The packed Pd/C catalyst worked as the “weak version” of AuNW, since the inside Pd/C could still be served as the new catalytic surface when the outside was poisoned, with much lower efficiency than AuNW. This clearly explained why the Pd coated AuNW nickel foam owns the best poisoning tolerance ability and the reason for higher stable current density of Pd coated AuNW FTO than that of Pd coated bare nickel foam.

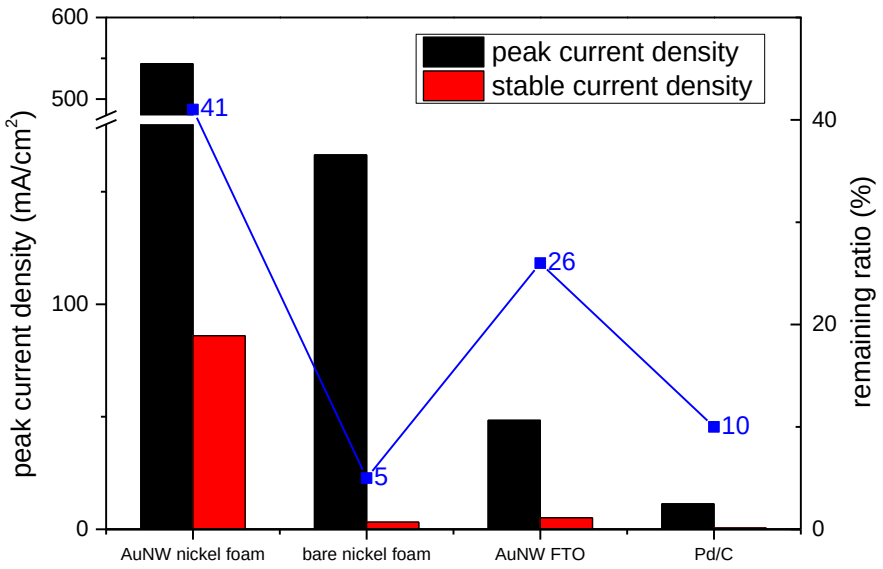

Figure 2-3-12. Peak current density (black bar), stable current density (red bar) and remaining percentage (blue curve) comparison of palladium coated AuNW on nickel foam, bare nickel foam, AuNW on FTO and Pd/C.

As control experiments to prove the influence of concentration gradient, the correlation between the concentration of sodium hydroxide and the binding strength of the –OH group on Pd surface was established, by added different concentration of sodium hydroxide into the electrolyte. Here, the Pd coated AuNW nickel foam were served as the working electrode with other conditions remaining the same, to avoid unnecessary ambiguities. As shown in Figure 2-3-13, the negative shift of backward peak onset potentials can be clearly observed with the increasing concentration of sodium hydroxide. The onset of this backward peak indicates the binding strength of the -OH group on Pd surface. At the starting point of reverse scan, the Pd surface is all

covered with -OH group and no ethanol can be oxidized. The onset potential indicated the initiation of ethanol oxidation, where the surface is refreshed again without strongly bound –OH group and the current density increases dramatically. The onset potential of backward peak moved from -0.03 V to -0.19 V, when the concentration of hydroxide group increases from 0.2 M to 2.0 M. The more negative onset potential demonstrates the stronger binding affinity of –OH group, since it needs more energy to refresh the Pd surface. So higher concentration of sodium hydroxide in the solution would lead to the stronger binding affinity on the Pd surface and it is more difficult to be removed. This explains why the concentration gradient could result in different poisoning degree and the good stability of AuNW nickel foam electrocatalyst.

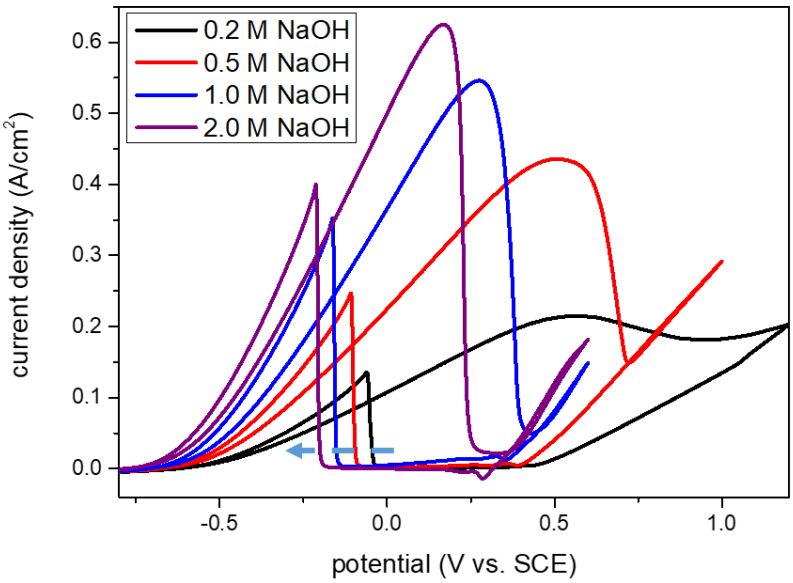

Figure 2-3-13. Cyclic voltammograms of Pd coated AuNW on nickel foam catalyzing 1.0 M ethanol with 0.2 M (black), 0.5 M (red), 1.0 M (blue) and 2.0 M (purple) sodium hydroxide aqueous solution.

Table 2-3-2 listed the current density (mA/cm^2), the mass-specific current (A/g) and the remaining percentage (%) after 30 min stability test of Pd coated AuNW nickel foam electrode and other 49 representative Pd-based electrodes for the catalysis of ethanol oxidation reactions. The current density of the nickel foam electrode in this work is unparalleled than that of listed electrodes, over five times higher than that of most Pd-based electrodes. Similar with previous FTO CV curve in Figure 2-3-10, the current density of nickel foam is over 10 times larger than that of the flat electrode. The advantage of the nickel foam surface is obvious. Only the utilize of some high surface area substrates could lead to the comparable current density with as-synthesized Pd deposited AuNW nickel foam, such as, titania nanotube arrays (the No. 38[18] electrode) and carbon nanotube arrays (the No. 47[19] electrode). Furthermore, the specific current per project surface area of the higher surface area electrode usually would gain more advantages than the flat electrodes. The specific current of AuNW nickel foam electrode in this work is over five times higher than that of most listed electrodes. The high efficiency of Pd atoms mainly results from the vertically aligned AuNW, where most of the atoms on surface could take part in the catalysis step. On the contrary, for the simple packing of zero-dimensional nanomaterials, most of the active surface is useless and inhibited by the outside part of the nanomaterials. The electrolyte was very difficult to go through or reach the inside section of these materials. This table clearly reveals that some relatively high specific current is all related with one-dimensional

nanostructure (nanowire, nanotube or carbon fiber cloth) or by well separated method (aerogel), such as, the No. 29,[9] 33,[20] 36,[21] 37[22] and 48[23] electrode. So the combination of large surface area substrate (nickel foam) and high utilization efficiency of surface atom (Pd coated AuNW) could bring about higher current density and specific current than other listed electrodes. As for the stability test, the remaining percentage after 30 min is used as the evaluation criteria to compare the poison resistant ability of these electrodes. Table 2-3-2 clearly demonstrates that the remaining percentage of most listed materials is lower than that of this work (41 %) and some electrocatalysts even dropped over 90 % after 30 min, which is difficult to be used in any practical applications. When continuous potential was applied on the Pd-based working electrode, the Pd surface would soon be poisoned by hydroxide group and ethanol intermediates. In stability test, the current dropped fast in the first 3 min, and usually over 50 % of the current would be decreased in most cases. With Pd coated AuNW nickel foam electrode, the current only dropped 25 % after the first 3 min.

In short, the existence of AuNW greatly enhanced the catalysis efficiency of Pd atoms and the utilization of porous nickel foam substrate significantly increased the current density per project surface area. Compared with these listed representative Pd-based electrocatalysts, both the catalysis efficiency and the stability of the Pd coated AuNW nickel foam is better than any other electrodes.

Table 2-3-2. Some representative Pd-based electrocatalysts for ethanol oxidation reactions. (Here, MWCNT stands for multi-wall carbon nanotube, ITO stands for indium tin oxide, NWA stands for nanowire array, CNT stands for carbon nanotube, PANI stands for polyaniline and TNTA stands for titania nanotube array)

Entry	Name	Current density (mA/cm^2)	Specific current (A/g)	Remaining percent after 30 min (%)	Electrolyte
this work	Pd coated AuNW nickel foam	543.4	2951	41	1 M NaOH + 1 M EtOH
1	PdNP/WMCNT [6]	25	125	-	1 M KOH + 1 M EtOH
2	Pd-NiO/C [24]	90	300	-	1 M KOH + 1 M EtOH
3	HF treated Pd/MWCNT [25]	40	400	-	1 M KOH + 1 M EtOH
4	1 %wt Pd/1 %wt Ni/MWCNT [26]	96.9	421	28	1 M KOH + 1 M EtOH
5	Pd on carbon microsphere [27]	65	650	10 % after 15 min	1 M KOH + 1 M EtOH
6	AuPd-WC/C [28]	160	1600	-	1 M KOH + 1 M EtOH
7	50 %wt Pd-WC/C [29]	121	404	-	1 M KOH + 1 M EtOH
8	PdNP on WC/MWCNT [30]	137	458	-	1 M KOH + 1 M EtOH
9	Pd/NiO (4:1)/C [31]	74	246	-	1 M KOH + 1 M EtOH
10	Pd/NiO (6:1)/C [32]	95	317	-	1 M KOH + 1 M EtOH
11	Pd-NiO/C [33]	15	492	-	1 M KOH + 1 M EtOH
12	Pt-Pt/ITO [34]	7	-	-	1 M KOH + 1 M EtOH
13	Pd NWA [35]	70	292	14	1 M KOH + 1 M EtOH
14	Pd/In_2O_3 (10:3)/CNT [36]	61	305	26	1 M NaOH + 1 M EtOH
15	Pd carbonized porous anodic alumina [37]	68	227	-	1 M KOH + 1 M EtOH
16	Pd on carbonized TiO_2 NW [38]	75	250	-	1 M KOH + 1 M EtOH

17	Pt_1Pd_1/C [39]	24	36	-	0.5 M H_2SO_4 + 1 M EtOH
18	$Pd_{86}Sn_{14}/C$ [40]	8.4	199	17	0.5 M KOH + 0.5 M EtOH
19	PtPdRh nanocube [41]	0.6	-	39	0.1 M $HClO_4$ + 1 M EtOH
20	PdAu nanowire [42]	84	-	11	1 M KOH + 1 M EtOH
21	$Pd_{0.5}Ag/C$ [43]	4	1873	45	0.5 M KOH + 2 M EtOH
22	$Pd_{40}Ni_{50}Sn_{10}/C$ [44]	169	2111	29	1 M NaOH + 1 M EtOH
23	Pd_4Ag_1/C-500 [45]	8	800	28	1 M NaOH + 1 M EtOH
24	Pd NWA [46]	74	308	-	1 M KOH + 1 M EtOH
25	$Pd_{41}Au_{29}Ni_{30}/C$ [47]	160	208	57	0.5 M NaOH + 1 M EtOH
26	PdNiP/C [48]	70	2450	21	0.5 M NaOH + 1 M EtOH
27	PdSn-SnO_2/C [49]	68	1908	19	1 M KOH + 1 M EtOH
28	Pd-SeO_2/C [50]	85	85	-	2 M KOH + 2 M EtOH
29	PdCo NWA on carbon fiber cloth [9]	-	1500	21 % after 10 min	1 M KOH + 1 M EtOH
30	PdSn alloy nanosheet dendrite [51]	-	576	-	1 M KOH + 1 M EtOH
31	Pd/PANI/Pd nanotube array [52]	-	350	15	1 M NaOH + 1 M EtOH
32	Pd nanomembranes [53]	50	500	-	0.5 M NaOH + 1 M EtOH
33	Pd/TiO_2 NWA web [20]	-	1176	-	2 M NaOH + 2 M EtOH
34	Pd shell on Au nanocube [54]	0.5	40	-	0.2 M KOH + 1.62 M EtOH
35	PdNP-graphene oxide [55]	12	-	-	1 M NaOH + 0.5 M EtOH

36	$Pd_{45}Pt_{55}$ nanowire [21]	-	900	50 % after 3 min	0.5 M NaOH + 1 M EtOH
37	$Pd_{83}Ni_{17}$ aerogel [22]	-	3600	8	1 M NaOH + 1 M EtOH
38	Pd/TNTA [18]	201	11167	-	2 M KOH + 10 %wt EtOH
39	Pd nanochestnut bur [56]	0.56	566	9 % after 16 min	0.1 M KOH + 0.1 M EtOH
40	Pd-polyethyleneimine [57]	197	-	-	1 M NaOH + 1 M EtOH
41	Pd nanodentrite [58]	5.5	-	12	0.1 M KOH + 1 M EtOH
42	Pd-CeO_2 [59]	6.2	565	15 % after 15 min	1 M NaOH + 0.5 M EtOH
43	Pd nanoflower [60]	-	3761	14	1 M KOH + 1 M EtOH
44	Pd nanocrystal [61]	222	1000	20 % after 16 min	1 M KOH + 1 M EtOH
45	Pd nanowire [62]	-	114	33	1 M KOH + 1 M EtOH
46	Pd spherical spongelike particle [63]	77	-	8	1 M KOH + 1 M EtOH
47	Pd/CNT array [19]	208	1304	-	1 M KOH + 1 M EtOH
48	Pd on carbon nanofiber [23]	74.5	1262	3	1 M KOH + 1 M EtOH
49	Pd/nickel foam [5]	107.7	979	-	1 M KOH + 1 M EtOH

Flexibility test for Pd coated AuNW nickel foam. The flexibility is also one of the critical factors of the electrodes in fuel cells, besides the previously mentioned high current density, specific current and good stability. The flexibility characterizations were carried out in the exactly same ethanol oxidation reactions and the effect of the electrode flexibility is mainly based on the catalytic activity performance, which is the

height of peak current density.

When the substrate was bended to different degree, the ethanol oxidation peak current density of the bended electrode was characterized. Here, the nickel foam was bended at 30, 60, and 90 degree, respectively (Figure 2-3-14 inset) and soaked into the 1.0 M sodium hydroxide and 1.0 M ethanol aqueous solution for CV scans to check its catalysis activity. As shown in Figure 2-3-14, the peak current density of the bended electrode still remained 99.6 %, 97.5 % and 99.4 %, after the nickel foam was bended 30, 60 and 90 degree, respectively, compared with the electrode without bended. The four CV curves almost overlapped with each other, indicating that no apparent property changes occurred on the electrode. In short, after the nickel foam substrate was bended even to the vertical state, the catalytic performance (peak current density) could still remain almost unchanged, which shows the bright future for the applications of foldable screens or portable fuel cells.

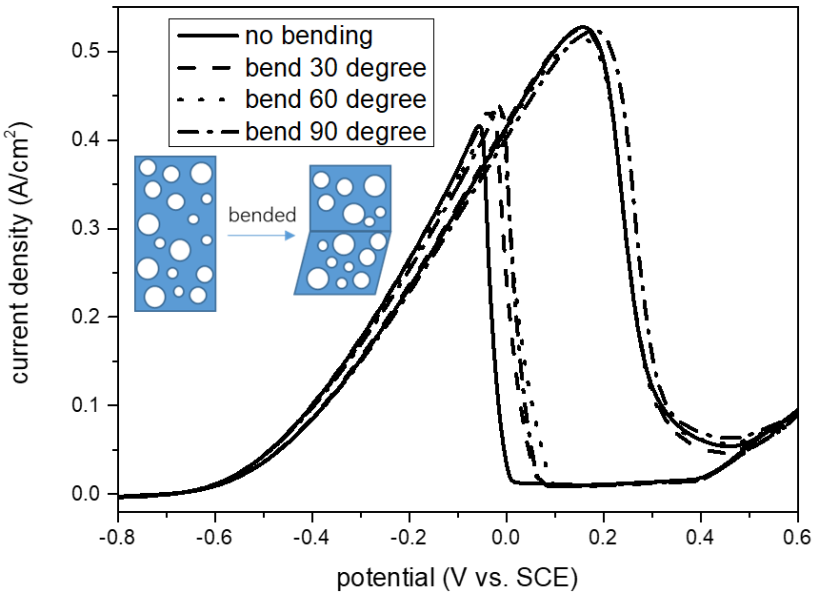

Figure 2-3-14. Cyclic voltammograms of Pd coated AuNW nickel foam without bending (solid line), 30 degree bending (dash line), 60 degree bending (dot line) and 90 degree bending (dash dot line) in 1.0 M sodium hydroxide and 1.0 M ethanol aqueous solution.

After the test of the flexibility with different bended degrees, the effect of bending times on catalytic activities of nickel foam substrate was also carried out in the same condition. Here, the nickel foam was bended 30 degree for 3, 15 and 50 times. The CV curves in Figure 2-3-15 clearly shows that after bended 30 degree for 50 times, the peak current density only slightly dropped and the curve kept almost the same as the one without bended. No obvious decrease of the peak current could be easily observed. After bended 3, 15 and 50 times, the peak current still remained 100.3 %, 98.4 % and 93.7 %, compared with that of the electrode without bended. These results implied that

the catalytic activities would be slightly affected by the bending of nickel foam substrate with the continuously increasing bending times, but the influence was not that significant. It still performed quite well after 50 times continuous bending. In practical applications, there would be low possibility for continuous bending over 50 times. Therefore, the Pd coated AuNW nickel foam was a quite excellent flexible electrocatalyst for ethanol oxidation, without any significant influence on catalytic activities by different bending angles and bending times.

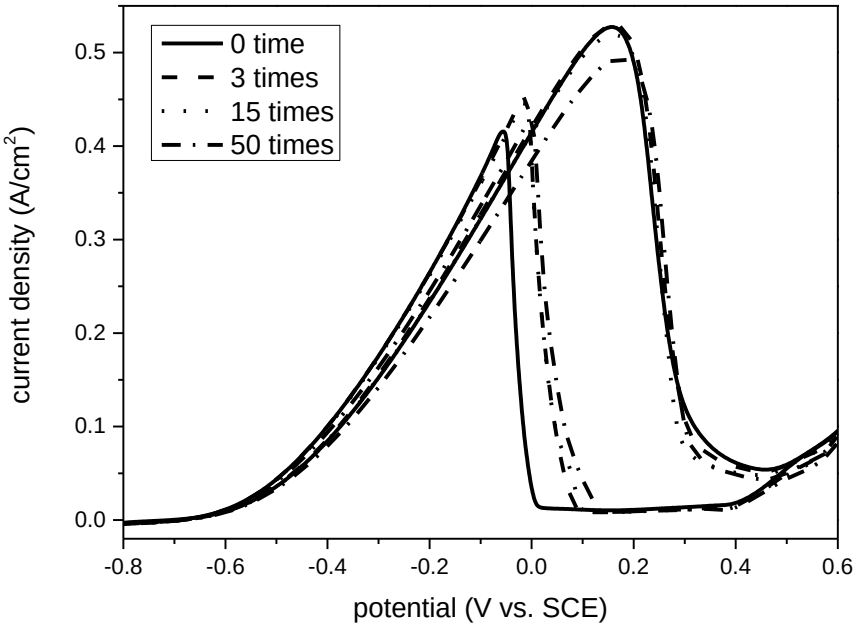

Figure 2-3-15. Cyclic voltammograms of palladium coated AuNW on nickel foam without bended (solid line) and after bended 30 degree for 3 times (dash line), 15 times (dot line) and 50 times (dash dot line) in 1.0 M sodium hydroxide and 1.0 M ethanol aqueous solution.

2.4. Conclusion

We have successfully transplanted the AuNW silicon wafer system to the AuNW nickel foam system by changing the silanes from APTES to CPTES and applying stirred condition. After coated with 1 nm Pd overlayer on AuNW surface by electrochemical method, the catalytic activity can be enhanced 3.3, 11.2 and 48.1 times compared with Pd coated bare nickel foam, AuNW on FTO and the state-of-the-art catalyst Pd/C, respectively. The final stable current density in stability tests of Pd coated AuNW nickel foam substrate could be improved to 27, 17 and over 140 times than that of Pd coated bare nickel foam, AuNW on FTO and Pd/C. In addition, the current density, the specific current and the remaining percentage of stable current density of Pd coated AuNW nickel foam electrode are all higher than that of recent representative Pd-based electrodes, due to the extraordinary large surface area and high active atom utilization efficiency. For the flexibility test, the nickel foam electrode could be bended at different angles with less than 3 % loss of the peak current density and after 15 times of bending, the peak current still remained over 98 %. In the future, the Pd coated AuNW nickel foam electrode would be used as one of the potential anodes for practical applications of portable or foldable direct ethanol fuel cells, due to its large surface area, high catalysis performance, good stability and flexibility.

2.5. Reference

1. (a) Lamy, C.; Lima, A.; Lerhun, V.; Delime, F.; Coutanceau, C.; Léger, J. M., Recent advances in the development of direct alcohol fuel cells (DAFC). *Journal of*

Power Sources **2002,** *105* (2), 283-296; (b) Antolini, E., Catalysts for direct ethanol fuel cells. *Journal of Power Sources* **2007,** *170* (1), 1-12; (c) Bianchini, C.; Shen, P. K., Palladium-based electrocatalysts for alcohol oxidation in half cells and in direct alcohol fuel cells. *Chemical Reviews* **2009,** *109* (9), 4183-4206.
2. Goldemberg, J., Ethanol for a Sustainable Energy Future. *Science* **2007,** *315* (5813), 808-810.
3. Cheng, X.; Shi, Z.; Glass, N.; Zhang, L.; Zhang, J.; Song, D.; Liu, Z. S.; Wang, H.; Shen, J., A review of PEM hydrogen fuel cell contamination: Impacts, mechanisms, and mitigation. *Journal of Power Sources* **2007,** *165* (2), 739-756.
4. Bambagioni, V.; Bianchini, C.; Marchionni, A.; Filippi, J.; Vizza, F.; Teddy, J.; Serp, P.; Zhiani, M., Pd and Pt–Ru anode electrocatalysts supported on multi-walled carbon nanotubes and their use in passive and active direct alcohol fuel cells with an anion-exchange membrane (alcohol = methanol, ethanol, glycerol). *Journal of Power Sources* **2009,** *190* (2), 241-251.
5. Hu, F. P.; Wang, Z.; Li, Y.; Li, C.; Zhang, X.; Shen, P. K., Improved performance of Pd electrocatalyst supported on ultrahigh surface area hollow carbon spheres for direct alcohol fuel cells. *Journal of Power Sources* **2008,** *177* (1), 61-66.
6. Zheng, H. T.; Li, Y.; Chen, S.; Shen, P. K., Effect of support on the activity of Pd electrocatalyst for ethanol oxidation. J Power Sources. *Journal of Power Sources* **2006,** *163* (1), 371-375.
7. Wang, H.; Xu, C.; Cheng, F.; Zhang, M.; Wang, S.; Jiang, S. P., Pd/Pt core–shell nanowire arrays as highly effective electrocatalysts for methanol electrooxidation in direct methanol fuel cells. *Electrochemistry Communications* **2008,** *10* (10), 1575-1578.
8. Marco, C.; Hiroyuki, M.; Shū, K.; Victor, C., Spin trapping of Au-H intermediate in the alcohol oxidation by supported and unsupported gold catalysts. *Journal of the American Chemical Society* **2009,** *131* (20), 7189.
9. Wang, A. L.; He, X. J.; Lu, X. F.; Xu, H.; Tong, Y. X.; Li, G. R., Palladium-cobalt nanotube arrays supported on carbon fiber cloth as high-performance flexible electrocatalysts for ethanol oxidation. *Angewandte Chemie* **2015,** *127* (12), 3740-3744.
10. He, J.; Wang, Y.; Feng, Y.; Qi, X.; Zeng, Z.; Liu, Q.; Teo, W. S.; Gan, C. L.; Zhang, H.; Chen, H., Forest of Gold Nanowires: A New Type of Nanocrystal Growth. *Acs Nano* **2013,** *7* (3), 2733-40.
11. Liu, F.; Song, S.; Xue, D.; Zhang, H., Folded structured graphene paper for high performance electrode materials. *Advanced Materials* **2012,** *24* (8), 1089-1094.
12. Wang, Y.; He, J.; Yu, S.; Chen, H., Exploiting Rayleigh Instability in Creating Parallel Au Nanowires with Exotic Arrangements. *Small* **2016,** *12* (7), 930-938.
13. Kua, J.; Goddard, W. A., Oxidation of methanol on 2nd and 3rd row group VIII transition metals (Pt, Ir, Os, Pd, Rh, and Ru): application to direct methanol fuel cells. *Journal of the American Chemical Society* **1999,** *121* (47), 10928-10941.
14. Liu, J.; Ye, J.; Xu, C.; Jiang, S. P.; Tong, Y., Electro-oxidation of methanol, 1-propanol and 2-propanol on Pt and Pd in alkaline medium. *Journal of Power Sources* **2008,** *177* (1), 67-70.

15. Bambagioni, V.; Bianchini, C.; Filippi, J.; Oberhauser, W.; Marchionni, A.; Vizza, F.; Psaro, R.; Sordelli, L.; Foresti, M. L.; Innocenti, M., Ethanol oxidation on electrocatalysts obtained by spontaneous deposition of palladium onto nickel-zinc materials. *Chemsuschem* **2010,** *2* (1), 99-112.
16. Liang, Z. X.; Zhao, T. S.; Xu, J. B.; Zhu, L. D., Mechanism study of the ethanol oxidation reaction on palladium in alkaline media. *Electrochimica Acta* **2009,** *54* (8), 2203-2208.
17. Huang, W.; Wang, H.; Zhou, J.; Wang, J.; Duchesne, P. N.; David, M.; Zhang, P.; Han, N.; Zhao, F.; Zeng, M., Highly active and durable methanol oxidation electrocatalyst based on the synergy of platinum–nickel hydroxide–graphene. *Nature Communications* **2015,** *6*, 10035.
18. Chen, Y. X.; Lavacchi, A.; Chen, S. P.; Di, B. F.; Bevilacqua, M.; Bianchini, C.; Fornasiero, P.; Innocenti, M.; Marelli, M.; Oberhauser, W., Electrochemical milling and faceting: size reduction and catalytic activation of palladium nanoparticles. *Angewandte Chemie International Edition* **2012,** *51* (34), 8500-8504.
19. Hu, F.; Cui, X.; Chen, W., Ultralong-CNTA-Supported Pd-Based Anodes for Ethanol Oxidation. *Journal of Physical Chemistry C* **2010,** *114* (47), 20284–20289.
20. Chen, Y. X.; Lavacchi, A.; Miller, H. A.; Bevilacqua, M.; Filippi, J.; Innocenti, M.; Marchionni, A.; Oberhauser, W.; Wang, L.; Vizza, F., Nanotechnology makes biomass electrolysis more energy efficient than water electrolysis. *Nature Communications* **2014,** *5* (5), 4036.
21. Zhu, C.; Guo, S.; Dong, S., PdM (M = Pt, Au) Bimetallic Alloy Nanowires with Enhanced Electrocatalytic Activity for Electro‐oxidation of Small Molecules. *Advanced Materials* **2012,** *24* (17), 2326-2331.
22. Cai, B.; Wen, D.; Liu, W.; Herrmann, A. K.; Benad, A.; Eychmüller, A., Function-Led Design of Aerogels: Self-Assembly of Alloyed PdNi Hollow Nanospheres for Efficient Electrocatalysis. *Angewandte Chemie* **2015,** *54* (44), 13101.
23. Qin, Y. H.; Yang, H. H.; Zhang, X. S.; Li, P.; Ma, C. A., Effect of carbon nanofibers microstructure on electrocatalytic activities of Pd electrocatalysts for ethanol oxidation in alkaline medium. *International Journal of Hydrogen Energy* **2010,** *35* (15), 7667-7674.
24. Shen, P. K.; Xu, C., Alcohol oxidation on nanocrystalline oxide Pd/C promoted electrocatalysts. *Electrochemistry Communications* **2006,** *8* (1), 184-188.
25. Hu, F. P.; Shen, P. K.; Li, Y. L.; Liang, J. Y.; Wu, J.; Bao, Q. L.; Li, C. M.; Wei, Z. D., Highly Stable Pd‐Based Catalytic Nanoarchitectures for Low Temperature Fuel Cells. *Fuel Cells* **2010,** *8* (6), 429-435.
26. Singh, R. N.; Singh, A.; Anindita, Electrocatalytic activity of binary and ternary composite films of Pd, MWCNT, and Ni for ethanol electro-oxidation in alkaline solutions. *Carbon* **2009,** *47* (1), 271-278.
27. Xu, C.; Cheng, L.; Shen, P.; Liu, Y., Methanol and ethanol electrooxidation on Pt and Pd supported on carbon microspheres in alkaline media. *Electrochemistry Communications* **2007,** *9* (5), 997-1001.

28. Nie, M.; Tang, H.; Wei, Z.; Jiang, S. P.; Shen, P. K., Highly efficient AuPd–WC/C electrocatalyst for ethanol oxidation. *Electrochemistry Communications* **2007,** *9* (9), 2375-2379.
29. Feng, P. H.; Pei, K. S., Ethanol oxidation on hexagonal tungsten carbide single nanocrystal-supported Pd electrocatalyst. *Journal of Power Sources* **2007,** *173* (2), 877-881.
30. Hu, F.; Cui, G.; Wei, Z.; Shen, P. K., Improved kinetics of ethanol oxidation on Pd catalysts supported on tungsten carbides/carbon nanotubes. *Electrochemistry Communications* **2008,** *10* (9), 1303-1306.
31. Xu, C.; Tian, Z.; Shen, P.; Jiang, S. P., Oxide (CeO, NiO, CoO and MnO)-promoted Pd/C electrocatalysts for alcohol electrooxidation in alkaline media. *Electrochimica Acta* **2008,** *53* (5), 2610-2618.
32. Xu, C.; kang Shen, P.; Liu, Y., Ethanol electrooxidation on Pt/C and Pd/C catalysts promoted with oxide. *Journal of Power Sources* **2007,** *164* (2), 527-531.
33. Hu, F.; Chen, C.; Wang, Z.; Wei, G.; Shen, P. K., Mechanistic study of ethanol oxidation on Pd–NiO/C electrocatalyst. *Electrochimica Acta* **2007,** *52* (3), 1087-1091.
34. Stojanovic, I.; Cuzzocrea, S.; Mangano, K.; Mazzon, E.; Miljkovic, D.; Wang, M.; Donia, M.; Al, A. Y.; Kim, J.; Nicoletti, F., Spontaneous formation of platinum particles on electrodeposited palladium. *Electrochemistry Communications* **2007,** *9* (7), 1563-1566.
35. Xu, C. W.; Wang, H.; Shen, P. K.; Jiang, S. P., Highly Ordered Pd Nanowire Arrays as Effective Electrocatalysts for Ethanol Oxidation in Direct Alcohol Fuel Cells. *Advanced Materials* **2010,** *19* (23), 4256-4259.
36. Chu, D.; Wang, J.; Wang, S.; Zha, L.; He, J.; Hou, Y.; Yan, Y.; Lin, H.; Tian, Z., High activity of Pd–InO/CNTs electrocatalyst for electro-oxidation of ethanol. *Catalysis Communications* **2009,** *10* (6), 955-958.
37. Wang, Z.; Hu, F.; Shen, P. K., Carbonized porous anodic alumina as electrocatalyst support for alcohol oxidation. *Electrochemistry Communications* **2006,** *8* (11), 1764-1768.
38. Hu, F.; Ding, F.; Song, S.; Shen, P. K., Pd electrocatalyst supported on carbonized TiO 2 nanotube for ethanol oxidation. *Journal of Power Sources* **2006,** *163* (1), 415-419.
39. Zhou, W.; Zhou, Z.; Song, S.; Li, W.; Sun, G.; Tsiakaras, P.; Xin, Q., Pt based anode catalysts for direct ethanol fuel cells. *Applied Catalysis B: Environmental* **2003,** *46* (2), 273-285.
40. Du, W.; Mackenzie, K. E.; Milano, D. F.; Deskins, N. A.; Dong, S.; Teng, X., Palladium–Tin Alloyed Catalysts for the Ethanol Oxidation Reaction in an Alkaline Medium. *Acs Catalysis* **2012,** *2* (2), 287-297.
41. Zhu, W.; Ke, J.; Wang, S.-B.; Ren, J.; Wang, H.-H.; Zhou, Z.-Y.; Si, R.; Zhang, Y.-W.; Yan, C.-H., Shaping single-crystalline trimetallic Pt–Pd–Rh nanocrystals toward high-efficiency C–C splitting of ethanol in conversion to CO2. *ACS Catalysis* **2015,** *5* (3), 1995-2008.

42. Cheng, F.; Dai, X.; Wang, H.; Jiang, S. P.; Zhang, M.; Xu, C., Synergistic effect of Pd–Au bimetallic surfaces in Au-covered Pd nanowires studied for ethanol oxidation. *Electrochimica Acta* **2010,** *55* (7), 2295-2298.
43. Feng, Y. Y.; Liu, Z. H.; Kong, W. Q.; Yin, Q. Y.; Du, L. X., Promotion of palladium catalysis by silver for ethanol electro-oxidation in alkaline electrolyte. *International Journal of Hydrogen Energy* **2014,** *39* (6), 2497-2504.
44. Sheikh, A.; Silva, E.; Moares, L.; Antonini, L.; Abellah, M. Y.; Malfatti, C., Pd-based catalysts for ethanol oxidation in alkaline electrolyte. *Am. J. Min. Metal* **2014,** *2*, 64-69.
45. Li, G.; Jiang, L.; Jiang, Q.; Wang, S.; Sun, G., Preparation and characterization of PdxAgy/C electrocatalysts for ethanol electrooxidation reaction in alkaline media. *Electrochimica Acta* **2011,** *56* (22), 7703-7711.
46. Wang, H.; Xu, C.; Cheng, F.; Jiang, S., Pd nanowire arrays as electrocatalysts for ethanol electrooxidation. *Electrochemistry Communications* **2007,** *9* (5), 1212-1216.
47. Dutta, A.; Datta, J., Outstanding Catalyst Performance of PdAuNi Nanoparticles for the Anodic Reaction in an Alkaline Direct Ethanol (with Anion-Exchange Membrane) Fuel Cell. *Journal of Physical Chemistry C* **2012,** *116* (49), 25677–25688.
48. Guo, W.; Niu, S.; Shi, W.; Zhang, B.; Yu, W.; Xie, Y.; Ji, X.; Wu, Y.; Su, D. S.; Shao, L., Pd-P Nanoalloys Supported on Porous Carbon Frame as Efficient Catalyst for Benzyl Alcohol Oxidation. *Catalysis Science & Technology* **2018,** *8* (9).
49. Mao, H.; Wang, L.; Zhu, P.; Xu, Q.; Li, Q., Carbon-supported PdSn–SnO 2 catalyst for ethanol electro-oxidation in alkaline media. *International Journal of Hydrogen Energy* **2014,** *39* (31), 17583-17588.
50. Wang, L.; Lavacchi, A.; Bevilacqua, M.; Bellini, M.; Fornasiero, P.; Filippi, J.; Innocenti, M.; Marchionni, A.; Miller, H. A.; Vizza, F., Energy Efficiency of Alkaline Direct Ethanol Fuel Cells Employing Nanostructured Palladium Electrocatalysts. *Chemcatchem* **2015,** *7* (14), 2214-2221.
51. Ding, L. X.; Wang, A. L.; Ou, Y. N.; Qi, L.; Rui, G.; Zhao, W. X.; Tong, Y. X.; Li, G. R., Hierarchical Pd-Sn Alloy Nanosheet Dendrites: An Economical and Highly Active Catalyst for Ethanol Electrooxidation. *Scientific Reports* **2013,** *3* (2), 1181.
52. Wang, A. L.; Xu, H.; Feng, J. X.; Ding, L. X.; Tong, Y. X.; Li, G. R., Design of Pd/PANI/Pd sandwich-structured nanotube array catalysts with special shape effects and synergistic effects for ethanol electrooxidation. *Journal of the American Chemical Society* **2013,** *135* (29), 10703-10709.
53. Wu, H.; Li, H.; Zhai, Y.; Xu, X.; Jin, Y., Facile synthesis of free-standing Pd-based nanomembranes with enhanced catalytic performance for methanol/ethanol oxidation. *Advanced Materials* **2012,** *24* (12), 1594-1597.
54. Lu, C. L.; Prasad, K. S.; Wu, H. L.; Ho, J. A.; Huang, M. H., Au Nanocube-Directed Fabrication of Au−Pd Core−Shell Nanocrystals with Tetrahexahedral, Concave Octahedral, and Octahedral Structures and Their Electrocatalytic Activity. *Journal of the American Chemical Society* **2010,** *132* (41), 14546-14553.
55. Chen, X.; Wu, G.; Chen, J.; Chen, X.; Xie, Z.; Wang, X., Synthesis of “clean” and

well-dispersive Pd nanoparticles with excellent electrocatalytic property on graphene oxide. *Journal of the American Chemical Society* **2011,** *133* (11), 3693-3695.
56. Ye, S. J.; Kim, d. Y.; Kang, S. W.; Choi, K. W.; Han, S. W.; Park, O. O., Synthesis of chestnut-bur-like palladium nanostructures and their enhanced electrocatalytic activities for ethanol oxidation. *Nanoscale* **2014,** *6* (8), 4182-4187.
57. Mourdikoudis, S.; Chirea, M.; Altantzis, T.; Pastoriza-Santos, I.; Pérez-Juste, J.; Silva, F.; Bals, S.; Liz-Marzán, L. M., Dimethylformamide-mediated synthesis of water-soluble platinum nanodendrites for ethanol oxidation electrocatalysis. *Nanoscale* **2013,** *5* (11), 4776-4784.
58. Gao, Q.; Gao, M. R.; Liu, J. W.; Chen, M. Y.; Cui, C. H.; Li, H. H.; Yu, S. H., One-pot synthesis of branched palladium nanodendrites with superior electrocatalytic performance. *Nanoscale* **2013,** *5* (8), 3202-3207.
59. Q, T.; C, D.; Y, S.; L, D.; G, Y.; Y, G., A palladium-doped ceria@carbon core-sheath nanowire network: a promising catalyst support for alcohol electrooxidation reactions. *Nanoscale* **2015,** *7* (32), 13656-13662.
60. Qi, K.; Wang, Q.; Zheng, W.; Zhang, W.; Cui, X., Porous single-crystalline palladium nanoflowers with enriched {100} facets for highly enhanced ethanol oxidation. *Nanoscale* **2014,** *6* (24), 15090-15097.
61. Wang, Q.; Wang, Y.; Guo, P.; Li, Q.; Ding, R.; Wang, B.; Li, H.; Liu, J.; Zhao, X., Formic acid-assisted synthesis of palladium nanocrystals and their electrocatalytic properties. *Langmuir* **2014,** *30* (1), 440-446.
62. Ksar, F.; Surendran, G.; Ramos, L.; Keita, B.; Nadjo, L.; Prouzet, E.; Beaunier, P.; Hagège, A.; Audonnet, F.; Remita, H., Palladium Nanowires Synthesized in Hexagonal Mesophases: Application in Ethanol Electrooxidation. *Chemistry of Materials* **2009,** *21* (8), 1612-1617.
63. Shen, Q.; Min, Q.; Shi, J.; Jiang, L.; Zhang, J. R.; Hou, W.; Zhu, J. J., Morphology-Controlled Synthesis of Palladium Nanostructures by Sonoelectrochemical Method and Their Application in Direct Alcohol Oxidation. *Journal of Physical Chemistry C* **2009,** *113* (4), 1267-1273.

3. Enhancement in Catalytic Activities of Ethanol Oxidation Reactions by Primary Cell Deposition of Pd Shell and the Mechanism Study on the Movement of Pd

3.1. Introduction

Nowadays, more and more attentions are focusing on the property modifications of a solid surface by foreign atom or molecular.[1] Generally, the inner part is the major component with functional properties, while the functions of the outer shell are to protect the inner core, to strengthen the core performance or to introduce new properties.[2] The coating shell could be assembled onto zero-, one-, two- or three-dimensional morphology structures with nano or micro scale and exhibits better physical and/or chemical properties than normal core composition. This kind of core-shell structure is widely used in optics, sensors, drug delivery and energy conversion.[3] The layer deposition method is very crucial not only in fundamental research studies, but also in various industrial applications, such as, catalysis, electronics, and corrosion protection. To master the mechanism and procedure to coat different shell materials on various core structure became more and more important.

For different electrochemical catalysis applications, to find out the suitable and effective methods for the deposition of thin layer onto substrate is essential to enhance the catalysis performance.[4] The direct growth of perfect alloys usually needs complex and time-consuming steps. While for various coating method, two or more chemical

combinations are relatively easier to be realized. The ratio of the combination is difficult to be precisely controlled for the direct growth, due to the different deposition rate of targeted materials. Usually the coating method is applied instead of directly growth method to specifically manipulate and tune the chemical composition by the new deposition overlayer.

Right now, different thin layer deposition methods are mainly classified into two categories by different reaction phase, the gas phase and the solution phase. For gas phase, atomic layer deposition (ALD)[5] and chemical vapor deposition (CVD)[6] are two widely used and well established methods. While for solution phase, chemical solution growth method[7] and electrochemical deposition method[8] are two widely reported methods for the deposition of metal or oxide shells.

For two widely used coating methods in gas phase, usually the shell material would be heated to gaseous state and then be deposited on the target substrate or be reacted with the substrate materials. Generally, the thickness of the growth overlayer could be precisely controlled to atomic level. But the drawbacks are very notable, such as, time-consuming steps, high cost for each trial, harsh requirements for substrate and limited choice of shell materials.[5c] When any condition during the deposition process was changed, such as, the lattice structure of the substrate or the starting material, serval rounds of trials must be carried out before the successful coating. Plenty of time and money would be easily consumed to expand one new serial of reaction conditions. In addition, since the experiment condition is not that mild, the starting materials as well

as the substrates are required not to be easily decomposed or spoiled in the relatively high temperature or under extreme pressure (vacuum). Sometimes, the targeted substrate is even demanded to be uniformly high quality lattice crystal, such as, Si (111), Ge (100), GaAs (111) and Pt (111).[9]

While for the solution phase coating methods, at first, the substrate is usually immersed into the solution containing the ions of target shell material. Then the ions are reduced back onto the targeted substrate by reducing agents (the chemical reagent or the reducing current). There are serval advantages of the solution coating method compared with the gas phase, like the convenience for performance tests, simple handling steps, and various choices for different substrates and metal ions. In most cases, the demands of temperature and pressure for deposition are much lower than the gas phase one. However, in return, the controllability and the reproducibility of this method is not that high. Usually, the thickness of the coating layer is up to tens or hundreds of nanometers and it is challenging to fine-tune the layer thickness.[10] Normally, the thickness directly corresponds to the reaction time and the reaction rate, which is related with many other factors and difficult to be precisely controlled.

When it comes to the practical applications, how to cut down the production cost is one of the most concerned problems, not only from the production steps, but also from the starting materials. Therefore, to efficiently use the catalysts (in other words, use less catalysts) becomes one meaningful and essential project. This is highly relevant with the synthesis or deposition method. Typically, only the serval surface layers of atoms

are crucial to the catalysis activity and the rest inner atoms could not help much to enhance the performance. Usually, the ultrathin layer catalyst obtains the same or even better catalytic activities than thick layer with the same amount of surface material. So the effective surface material should fulfill the following two key characters, ultralow loading amount and good catalytic activity.[11] The deposition of the ultrathin layer could be one of the satisfactory solutions for both low loading amount and high catalytic activity.

In the electrochemical catalysis reactions, the mass-specific current density is one of the most critical standard measuring indexes. It values the catalysis efficiency of total catalyst atoms and usually higher mass-specific catalytic activity is caused by higher catalyst utilization.[11a, 12] However, most of the representative electrochemical noble metal catalysts are composed of nanoparticles, nanocubes, or nanowires with tens of diameters.[13] In these cases, the inner parts of the materials are almost useless and could not provide much help to increase the catalytic activity. The shell is too thick for these inner atoms to influence the outside atoms. These nanostructures clearly revealed the weakness of the chemical solution deposition method, obstacle to control the thickness for the deposition of desired thin overlayer.

Atomic monolayer deposition could be realized by some gas phase deposition methods, like ALD and CVD, but these methods would cost much time and money for the deposition of ultrathin overlayers, especially for multi-layer depositions. While for normal chemical solution deposition methods, the low controllability of the thin layer

is its main drawback. There is one blank method, which combines the advantages of both gas and solution phase deposition methods, obtaining the simplicity as well as the efficiency.

Here, we reported one convenient and effective deposition method to coat Pd shell on AuNW nickel foam substrate via the primary cell principles. By this method, the amount of Pd coated on Au can be easily tuned by the amount of Pd ions added in the solution. In addition, after serval rounds of cyclic voltammetry (CV) scans, the uneven Pd domains on Au surface would gradually spread out to cover the exposed Au surface. By decreasing the deposited Pd amount, the peak current density of ethanol oxidation reaction almost kept the same as that of the electrochemical deposited one. While the mass-specific current density (A/g) enhanced over two times, due to the reduced deposition amount. Interestingly, on the basis of the control experiments, the physical movement of Pd was found out to be irrelevant with the ethanol in the electrolyte, the existence of nickel foam or the relative position of Pd/Au, verifying that the Pd domains on the substrate would be oxidized to Pd ions into the electrolyte and then be reduced back onto the Au surface.

3.2. Materials and Methods

3.2.1. Materials

All the aqueous solutions used in the experiments were prepared with deionized water (resistivity > 18 $M\Omega \cdot cm^{-1}$). Hydrogen tetrachloroaurate(III) ($HAuCl_4$, 99.9%, Au 49%

on metals basis, Alfa Aesar), palladium chloride (98%, Sigma Aldrich), 4-mercaptobenzoic acid (4-MBA, 90%, Sigma Aldrich), (3-aminopropyl)triethoxysilane (APTES, Sigma Aldrich), 3-cyanopropyltriethoxysilane (CPTES, Sigma Aldrich), sodium citrate tribasic dihydrate (99.0%, Sigma Aldrich), L-ascorbic acid (Sigma Aldrich), sodium borohydride (98%, Sigma Aldrich), sodium hydroxide (98%, Sigma Aldrich), palladium on activated charcoal (Pd/C, Sigma Aldrich), ethanol for electrochemistry test (analytical grade, Merck) and ethanol for AuNW growing (99.86% technical grade) were used as received. Nickel foams (0.5 mm thickness) were purchased from Suzhou JSD Co. Fluorine doped tin oxide (FTO) glasses and silicon wafers were purchased from Sigma Aldrich.

3.2.2. Methods

Characterization methods. All transmission electron microscopy (TEM) images were collected on a JEM-1400 (JEOL) operated at 100 kV. All scanning electron microscopy (SEM) images were collected on a JSM-6700F (JEOL). All electrochemistry data were collected on a CHI-760e electrochemical workstation.

Preparation of TEM samples. TEM copper grids were treated with oxygen plasma in a Harrick plasma cleaner/sterilizer for 30 s to improve the surface hydrophilicity. Then the sample solution was dropped onto the hydrophilic face of TEM copper grids placed on the filter paper in less than 30 min. The filter paper below TEM copper grids was used to wick off the excess sample solution around the TEM grid, which was then

dried in air for 1 h.

Synthesis of 3-5 nm gold nanoseed (AuNS). A 50 mL round bottom flask was filled with 20 mL deionized water. Then 160 μL sodium citrate (1 wt%) aqueous solution and 100 μL $HAuCl_4$ (50 mM) aqueous solution was added into the flask and kept stirring for 1 min. Then 620 μL ice-cold $NaBH_4$ (0.1 M) aqueous solution was added in one shot with vigorous stirring. The solution turned from light yellow to reddish orange, indicating the formation of AuNS. The solution was kept stirring for 10 min and waited for use after overnight for the consumption of unreacted $NaBH_4$.

Synthesis of AuNW nickel foam substrate. Before the growth of AuNW forest on nickel foam, the purchased nickel foam was first sonicated in ethanol/acetone 1:1 solution for 15 min for three times to remove the surface organic residual. After that, the nickel foam was continuously sonicated in deionized water for 15 min for three times to remove excess organic solution inside nickel foam. Then the nickel foam was dried on the filter paper and waited for use. The nickel foam was firstly functionalized with cyano group and was immersed in CPTES water/ethanol 1:1 solution (1 μL/mL) for 30 min. Then the cyano functionalized nickel foam was washed with ethanol twice and then water twice to remove the excess silanes on and inside the surface of nickel foam. Between each washing step, the excess ethanol or water inside nickel foam was removed by filter paper. After functionalized with CPTES, the nickel foam was soaked in excess citrate-stabilized AuNS (diameter 3-5 nm) solution for 1 h to ensure the adsorption of AuNS on nickel foam surface. Then the nickel foam was washed with

water twice to remove the excess and unabsorbed AuNS. The AuNS-adsorbed nickel foam was then immersed in the AuNW growing solution containing the solvent ethanol 2 mL, the ligand 4-MBA in ethanol 400 μL (10 mM), the gold source $HAuCl_4$ in water 100 μL (50 mM) and the reducing agent L-ascorbic acid in water 600 μL (20 mM) for 30 min. Finally, the nickel foam was rinsed with ethanol and dried on filter paper. Within all these three steps, a stir bar was added in the solution and kept stirring to force the solution exchanging more frequently inside the nickel foam.

Coating Pd on AuNW nickel foam substrate via the primary cell principle. The nickel foam decorated with AuNW was immersed into the 10 mM $PdCl_2$ aqueous solution for 30 minutes and then washed with water twice to remove excess unreacted Pd ions. The Pd was successfully coated on the AuNW surface. During the deposition process, the nickel foam worked as the anode and the AuNW worked as the cathode, assembling as one primary cell and the electrolyte was the coating material, $PdCl_2$.

Galvanic replacement deposition of Pd shell on nickel foam. The purchased nickel foam was first sonicated in ethanol/acetone 1:1 solution for 15 min for three times to remove the surface organic residual. After that, the nickel foam was continuously sonicated in deionized water for 15 min for three times. Then it was dried on filter paper and waited for use. Before the coating of Pd shell, firstly the nickel foam was sonicated in 0.1 M HCl solution for 5 min to remove its surface oxides and quickly washed with water. After that, the nickel foam with fresh nickel surface was immediately immersed into the 10 mM $PdCl_2$ aqueous solution. After one minute, the nickel foam was

successfully coated with Pd shell. At last, the Pd coated nickel foam was washed with water twice and waited for use.

Electrochemical deposition of Pd on AuNW nickel foam. To coat Pd layer on AuNW on nickel foam or FTO, the electrochemical coating method was carried out by the CHI-760e electrochemical workstation. The counter electrode used during the process was a graphite rod. A saturated calomel electrode (SCE) was served as the reference electrode and all potential in this section was reported with respect to the SCE without any other instructions. The working electrode was served as the nickel foam with AuNW or FTO with AuNW. The electrolyte used for the Pd coating was 1.0 mM $PdCl_2$, 0.5 M pH = 6 phosphate aqueous buffer solution. The stirring speed during the coating step was 250 rpm all the time. During the coating step, the -2.5 mA current was applied on the working electrode for 20 s, then kept stirring with 0 mA for another 20 s in order to transfer the Pd solution inside the nickel foam thoroughly. Usually, these two steps kept undergoing for 12 min. With other coating times or method, it will be mentioned in the specific section.

Electrochemical property characterizations for ethanol oxidation reaction. The electrochemical property measurements of our different catalysts were carried out in the standard three-electrode cell. The CHI-760e electrochemical workstation was used for cyclic voltammetry tests, stability tests and some other electrochemical tests mentioned in this section. The platinum foil (1*2 cm^2) and the saturated calomel electrode (SCE) served as the counter electrode and the reference electrode,

respectively. The working electrode was the Pd coated AuNW on nickel foam or on FTO. Cyclic voltammetric and chronoamperometric experiments for ethanol oxidation reactions were performed in 1.0 M sodium hydroxide and 1.0 M ethanol aqueous solution saturated with nitrogen gas. The stirring speed during the purging N_2 gas and electrochemical tests was 250 rpm all the time. The scan rate of cyclic voltammetry test was 50 mV/s. The stability test was carried out at -0.2 V vs. SCE. The entire electrochemical test was carried out at ambient temperature (25 ± 1 ℃).

3.3. Results and Discussion

When catalyzing the ethanol oxidation reactions, it is well established that only serval atomic layers of surface catalysts are involved in the catalysis process.[12] The catalytic activity would be tremendously improved, when the dimension of the active catalyst was reduced to less than one nanometer.[14] In the Pd coated AuNW system here, when the thickness of Pd overlayer was less than one nanometer, the catalytic efficiency would be greatly enhanced. Therefore, fine-tuning the deposition amount of Pd, an expensive noble metal catalyst, is critical to control the cost of production during the manufactural process.

As previously shown in Figure 2-3-9, the thickness of the electrochemically deposited Pd shell on AuNW was over 1 nm, which could be further reduced, while remaining the catalytic properties the same or even better. However, by using this deposition method, the thickness of 1 nm seemed to be the thinnest, forming as the complete Pd shell. When

the concentration of $PdCl_2$ or the deposition time was reduced, the exposure of Au surface could easily be observed on CV curves. In addition, the deposition amount of Pd was very difficult to be precisely controlled. As a result, if complete thinner Pd shell could be synthesized with tunable amount, the deposition method must be altered to a more controllable one.

Deposition of Pd on AuNW nickel foam with primary cell coating method. It has been thoroughly studied that for the typical primary cell (copper-zinc primary cell), when the copper (II) sulfate was served as the electrolyte of the cathode half-cell, pure copper metal could be easily deposited on the cathode electrode (Figure 3-3-1). The copper ions in the electrolyte would be reduced to copper metal onto the electrode surface by the electrons transferring from zinc electrode to the copper electrode. The deposition of pure copper metal could be easily obtained on the desired cathode, which is a convenient and effective approach for the deposition of relatively inactive metal onto the substrate. The only requirement for the substrate is conductive without any limitation of the shape or the intrinsic property. This is a commonly used and well developed method for pure metal deposition via the primary cell structure. The coating condition requires two different conductive metal electrodes with different electrode potential in the targeted metal ion solution and the two electrodes cannot be too active to react with water directly.

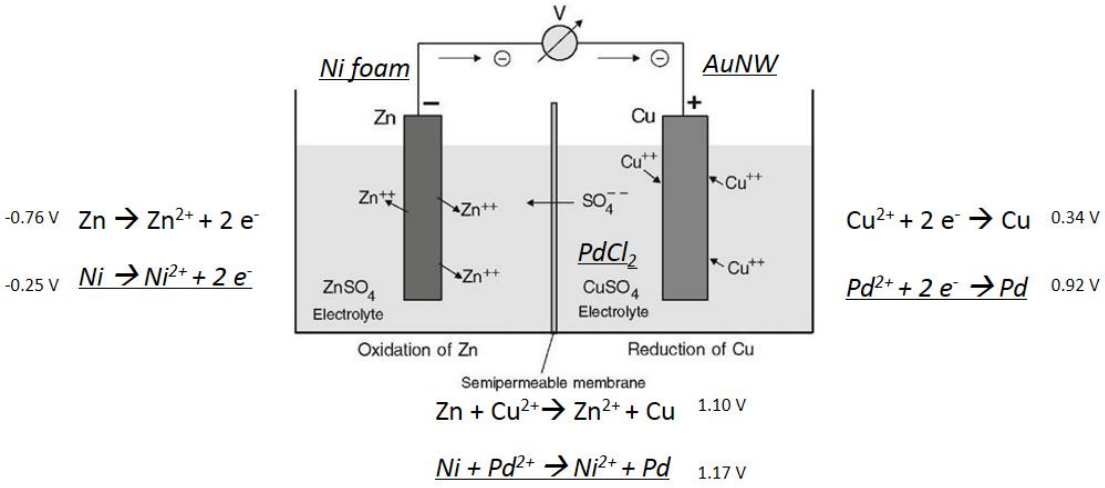

Figure 3-3-1. Illustration of the structure and the standard electrode potential (no underline) of copper-zinc primary cell for the deposition copper on cathode side and the virtual model and standard electrode potential (underline) for the deposition palladium on AuNW on nickel foam with primary cell coating system.

Compared with copper-zinc primary cell system, the structure of the AuNW decorated nickel foam substrate corresponds to the requirements of primary cell. The nickel foam could be treated as the active metal, instead of the zinc electrode in the copper-zinc system and the AuNW forest can be served as the less active metal, instead of the copper electrode. Furthermore, the electrolyte could be replaced with the palladium chloride instead of the copper sulfate for the deposition of Pd onto the cathode. For these two alternative reactions, their standard electrode potentials were listed in Figure 3-3-1 (underline).[15] The potential difference between these two Ni/Pd reactions was almost the same as that of the Cu/Zn ones. The electric potential difference between Ni and Pd was 1.17 V, which was very close to the previous Cu-Zn

potential difference (1.10 V).[15b, 16] According to the theoretical basis of primary cell as well as the calculation of electric potential differences, pure metal Pd could theoretically be reduced onto the Au surface in the AuNW nickel foam primary cell system.

This primary cell deposition method was applied for the coating Pd overlayer on AuNW nickel foam substrate. After the fabrication of the nickel foam with AuNW by the CPTES-AuNS method (previously discussed in Section 2.3), the as-synthesized nickel foam was merely immersed into the 10 mM $PdCl_2$ aqueous solution and incubated for 30 minutes. During the incubation process, the color of the nickel foam turned from grey (AuNW nickel foam) to dark grey (Pd coated AuNW nickel foam) and the color of the deposition solution turned from yellow (containing 10 Mm $PdCl_2$) to light yellow (containing less $PdCl_2$), meaning that the Pd ions in the solution have been successfully reduced onto the nickel foam. As shown in Figure 3-3-2, most of the AuNW remains vertically aligned and the surface was successfully coated with Pd shell. The diameter of AuNW increased from 4.8 nm to 6.1 nm after the deposition of Pd, measured from TEM images of the sonicated AuNWs. During the fabrication steps, the only chemical reagents in the solution was $PdCl_2$, so the increase of diameter should result from the deposition of Pd shell. Figure 3-3-2a clearly shows that most of the AuNW surface was uniformly coated by the Pd shell and there was almost no exposed Au surface. The electron microscopy images could only give part information of the

whole electrode, and further proof of the successful deposition of Pd shell was carried out in the electrochemical tests to obtain its total information.

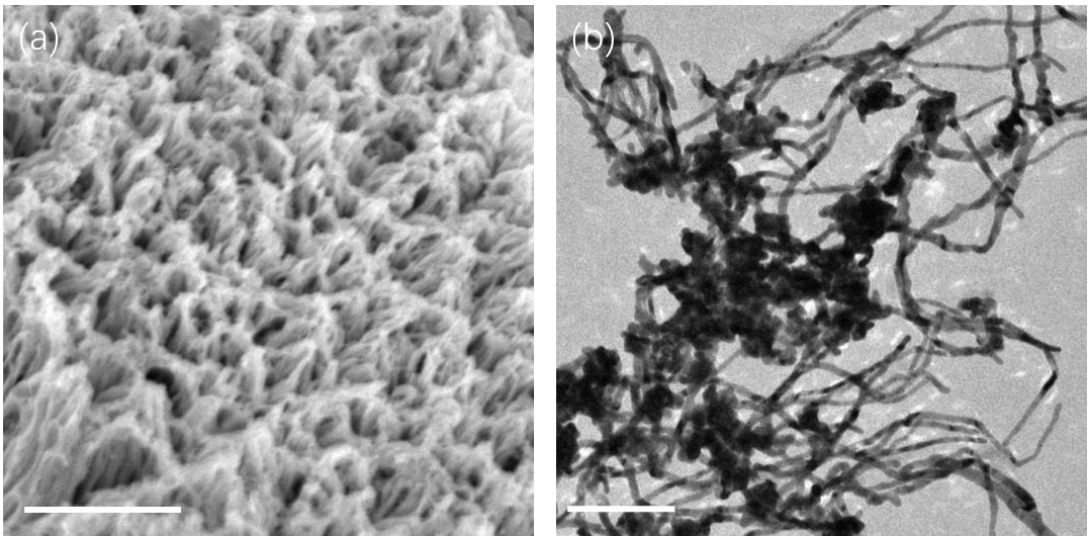

Figure 3-3-2. (a) SEM images (scale bar: 1 μm) and (b) TEM images (scale bar: 100 nm) of Pd coated AuNW on nickel foam by the primary cell coating method.

Electrochemical tests for the Pd coated AuNW nickel foam substrate. The ethanol oxidation electrochemical activities of Pd coated AuNW nickel foam by the primary cell method were investigated in 1.0 M sodium hydroxide and 1.0 M ethanol aqueous solution at room temperature. As shown in Figure 3-3-3, the peak current density of the Pd coated AuNW on nickel foam (0.480 A/cm^2) was 3 and 42.5 times higher than that of Pd coated bare nickel foam (0.160 A/cm^2) and the state-of-the-art catalyst, Pd/C (0.011 A/cm^2), respectively. The enhancement of the current density from bare nickel foam to the growth of AuNW on nickel foam mainly results from the dramatically increased surface area of AuNW. In addition, there is no recognizable branch or any shoulder peak in both the forward and backward peaks of Pd coated AuNW nickel foam,

meaning that there was almost no impurity, like Au, remaining on the surface of active Pd shell. Otherwise, there would be one clear Au forward appears at the potential of ca. -0.3 V. Both the electron microscopy images and the CV curves could lead to the conclusion that through the primary cell coating method, the Pd shell can be successfully and exclusively deposited on the AuNW nickel foam substrate.

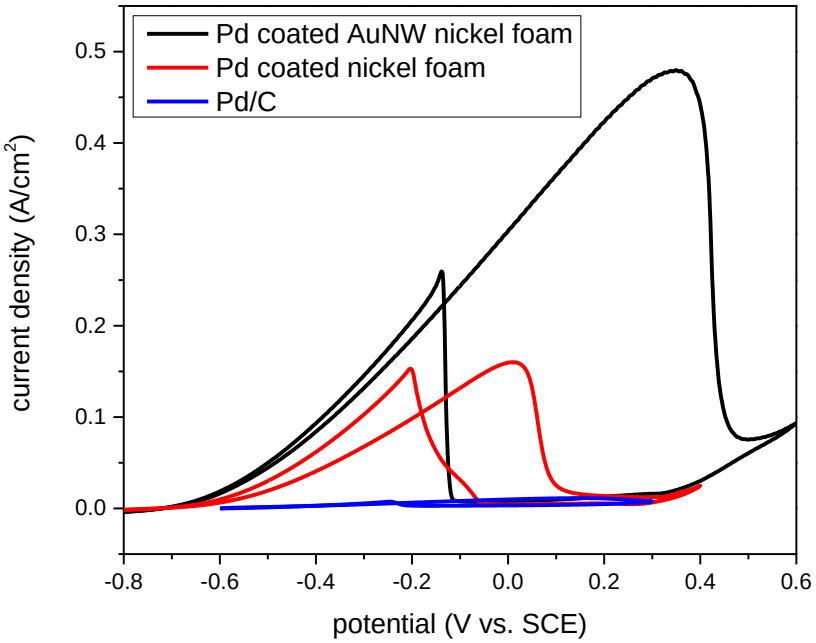

Figure 3-3-3. Cyclic voltammograms of Pd coated AuNW on nickel foam by primary cell coating method (black line), Pd coated nickel foam by galvanic replacement method (red line) and Pd/C (blue line) in 1.0 M sodium hydroxide and 1.0 M ethanol aqueous solution at room temperature.

The primary cell coated Pd on AuNW nickel foam was also compared with the electrochemical deposited one (previously discussed in Section 2.3). The shape of two

curves was almost the same (Figure 2-3-10 black line and Figure 3-3-3 black line), revealing that the composition and morphology of two as-synthesized Pd structure was similar. Moreover, the two peak current densities were close to each other and equally in the same magnitude (0.480 and 0.543 A/cm^2), still over ten times and 40 times higher than that of Pd coated AuNW on FTO and Pd/C, respectively.

In order to test the stability of the synthesized substrate, -0.2 V vs. SCE potential was continuously applied on Pd coated nickel foam with or without AuNW for 30 minutes. As shown in Figure 3-3-4, the chronoamperometric results indicate that the stable current density of Pd coated AuNW nickel foam (60.3 mA/cm^2) is over 18 and 100 times higher than that of Pd coated bare nickel foam (3.2 mA/cm^2) and Pd/C (0.6 mA/cm^2), respectively. Similar with the previous results of stability tests in Section 2.3, the poison resistant ability could be largely improved after the active surface area was increased. The entire active Pd surface could not be fully covered in a short period of time by various poisons, such as, hydroxide group and ethanol intermediates, when the large surface area AuNW forest was grown on the three-dimensional substrate, nickel foam. Compared with the electrochemical deposited substrate (Figure 2-3-11, black line), the shape and the decreasing speed was still almost the same.

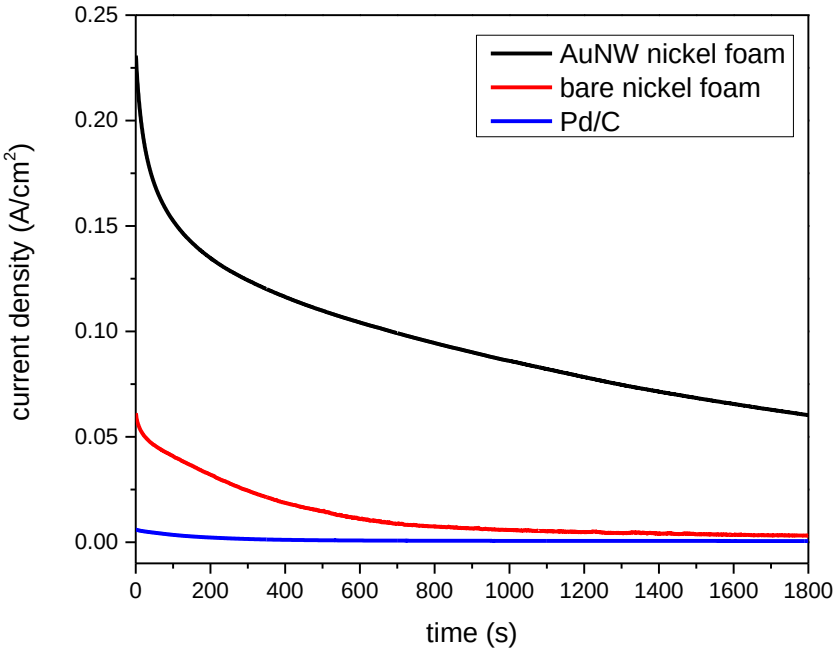

Figure 3-3-4. Chronoamperograms of palladium coated AuNW on nickel foam by primary cell coating method (black line), palladium coated bare nickel foam (red line), and Pd/C (blue line) in 1.0 M sodium hydroxide and 1.0 M ethanol aqueous solution at the potential of -0.2 V vs. SCE at room temperature.

In short, the primary cell deposition method was convenient and efficient for the deposition of Pd overlayer onto Au surface. The entire Au surface could be fully covered with active Pd shell within only one synthesizing step in room temperature and ambient pressure without any complicated instrument or equipment. In addition, the catalytic activity and the stability performance did not change much compared with typical electrochemical deposition method, while the primary cell deposition method owns incredible convenience and simplicity.

Decreased concentration of Pd precursors by primary cell deposition method. The thickness of the deposited Pd shell is around 0.6 nm, measured from the TEM image on Figure 3-3-2b, which could still be further reduced. When the concentration of the palladium (II) chloride in the deposition solution was declined from 10 to 2.5 mM, less amount of Pd would be coated on the AuNW surface, which would ideally result in the deposition of thinner Pd shell onto Au surface. Interestingly, clear Au forward peak (0.3 V vs. SCE) and backward peak (0.1 V vs. SCE) as well as the Pd forward and backward peaks can be simultaneously observed in the second CV cycle catalyzing ethanol oxidation reactions (Figure 3-3-5, dark blue line). The existence of these four peaks clearly verified that the AuNW surface could not be fully covered by the Pd and the active Au and Pd surface coexisted on the electrode. It seems that the deposited amount of Pd is not enough and more Pd should be added.

Surprisingly, when more CV cycles were applied on this Pd partially coated AuNW nickel foam substrate, the Pd forward and backward peaks began to rise, while the Au peaks kept decreasing to stable position (Figure 3-3-5, from dark to light blue). After 15 CV cycles, no Au peak could be clearly observed and the peak current density of the final Pd coated AuNW on nickel foam increased to 0.544 A/cm^2, which is almost the same as that of the electrochemical deposition method one (0.543 A/cm^2). However, the mass-specific current of the primary cell deposition method coated AuNW nickel foam (6464 A/g) is over two times higher than that of electrochemical coated one (2951 A/g), due to the decreased amount of Pd deposited on the electrode. Compared with the

Pd-based electrodes in Table 2-3-2, most of the specific current is lower than that of Pd coated AuNW nickel foam by primary cell. The specific current density of the partially deposited Pd shell on AuNW nickel foam kept gradually increasing after serval rounds of CV circles.

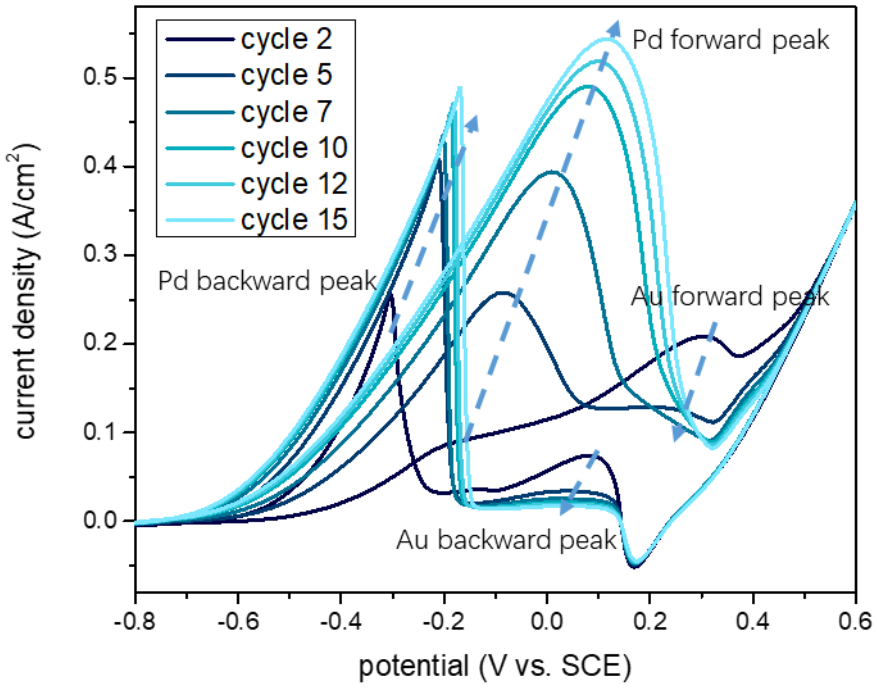

Figure 3-3-5. Cyclic voltammograms of palladium coated AuNW on nickel foam by primary cell coating method with 2.5 mM $PdCl_2$ coating solution from cycle 2 (dark blue) to cycle 15 (light blue) in 1.0 M sodium hydroxide and 1.0 M ethanol aqueous solution. The dash arrows demonstrate the increasing and decreasing trend of the peak current densities of palladium and gold, respectively.

As shown in Figure 3-3-5, the forward and backward peaks of Au decreased, while the two Pd peaks enhanced with the increasing of CV cycle numbers. In the second CV

cycle, there were clearly two forward peaks, one for ethanol oxidation forward peak catalyzed by Pd at ca. -0.2 V and the other Au peak at ca. -0.35 V. While in the 15th CV cycle, only the Pd forward peak could be observed. The improved catalytic peak current can only result from the increased active surface area of Pd, since the total amount of Pd in on the electrode was constant during CV scans. For the Au part, the AuNW itself could not be easily disappeared in 20 cycles of CV and the current density was almost the same or even increased a little after that (Figure 3-3-6). One possible reason to explain the disappearance of the Au peaks could be that the active Au surface was covered with some other materials. From here, took the increasing of Pd peak current density and surface area into account, the most possible explanation would be that the Pd domains on the AuNW surface somehow started to move and cover the Au surface within serval cycles of CV.

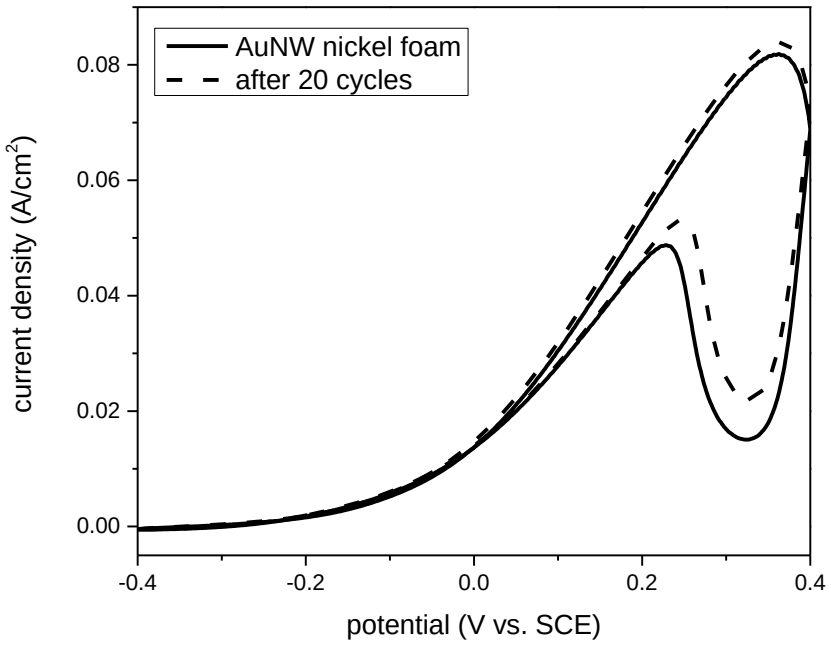

Figure 3-3-6. Cyclic voltammograms of AuNW nickel foam electrode catalyzing ethanol oxidation reactions before (solid line) and after (dash line) 20 CV cycles in 1.0 M sodium hydroxide and 1.0 M ethanol aqueous solution at room temperature with scan rate 50 mV/s.

One possible mechanism was proposed to explain the increasing and decreasing of Pd and Au peaks. Figure 3-3-7 reveals different steps for the deposition of Pd on Au with the help of CV scans. At the very first step, the Pd domains were aggregated on the AuNW at some degree. After that, with more and more CV scans, the Pd nanomaterials started to move and spread along the AuNW surface. In the end, with enough cycles of CV, the entire AuNW would be fully covered with uniform Pd shell and became Pd coated AuNW in the end.

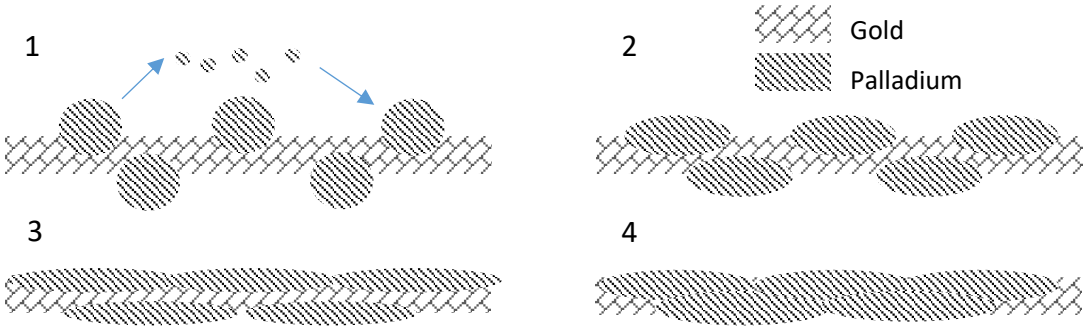

Figure 3-3-7. Illustration of the proposed mechanism to explain how the palladium particles (oblique line) could move to fully cover the active gold surface (brick pattern).

To support this proposed mechanism, the most key question needed to be answered is why the Pd was more likely to be deposited onto the Au surface, but not on Pd domain itself. From the illustration of proposed mechanism in Figure 3-3-7, the trend can be clearly viewed that more Pd atoms moved away from original Pd domains to cover Au surface. Thermodynamically, the atoms would choose a relatively more stable position to be deposited. The bonding energy of Au-Pd (143 kJ/mol) was stronger than that of Pd-Pd (136 kJ/mol), indicating that the formation of more Au-Pd bonds would be thermodynamically more favorable than Pd-Pd bonds.[17] On the basis of bonding energy data, the Pd atoms should be more likely to be deposited on Au, the thermodynamically more favorable position with stronger bonding affinities. This could explain why the Pd atoms would be more deposited on Au rather than on Pd itself. In addition, this could clarify the reason why the forward and backward peak current of Au would decrease and Pd peaks would increase.

Research on necessary conditions for the physical movement of Pd domains. Thermodynamically, Pd atoms would be more favorable to be deposited onto the Au surface, rather than on Pd itself. But the pathway of Pd movement was still unclear. More reasonable and detailed mechanism could be proposed, if the necessary conditions for the Pd movement onto Au surface were thoroughly tested and verified. From the previous experiment results, the electrochemical method could be one unique and simple way to change the wettability of the Au surface. There are only two possible mechanisms for the explanation of this phenomenon, the ripening or the migration of Pd atoms. The Pd atoms may firstly get oxidized at high voltage to free Pd ions in the electrolyte, which are then reduced back to cover the Au surface. Alternatively, the CV scan may promote the surface migration, where the Pd atoms may directly move on the Au surface by breaking and remaking the metal bonds. After the thorough inspection of the necessary conditions, one of the Pd movement mechanism could be more convincing.

To find out the necessary conditions, various experimental conditions were mainly divided into four sections, the electrochemical environment, the composition of the electrolyte, the substrate material, and the relative position of Pd-Au on the electrode. If the removal of some conditions would not lead to the change of Pd and Au peaks, the condition would be confirmed to be one of the necessary conditions. Focusing on these four aspects, different control experiments were carried out to determine the necessary condition for the movement of Pd onto Au.

The first necessary condition experiment is to test in the electrochemical environment without CV scans. Only the fixed reduction or oxidation potential was applied respectively on the AuNW nickel foam with partially covered Pd domains substrate. The potential of -0.4 V was applied for 5 minutes as the continuous reduction potential on the substrate in the aqueous electrolyte containing 1.0 M sodium hydroxide and 1.0 M ethanol. As shown in Figure 3-3-8, before -0.4 V potential was applied, the two forward peaks, Pd (at -0.1 V) and Au (at 0.3 V), indicates the partial coverage of Pd on Au. After applied with the reduction potential, both the Au and the Pd peak currents increased, but the shape of the CV curve did not change much. On the basis of previous experiences, the current density of the first CV scan would always be slightly lower than other CV scans, due to the disequilibrium adsorbed surface reactants.[18] The rough ratio of Pd/Au on the surface could be deduced from the ratio of Pd and Au forward peak current, monitoring whether the amount of surface metal was changed or not. The ratio amount of the reactants catalyzed by exposed electrocatalyst, Pd or Au, could reflect the actual ratio amount of exposed surface catalysts. For this set of experiment, the ratio of peak current of Pd/Au before and after applying -0.4 V reduction potential was 1:1.6 and 1:1.6, respectively. The same two peak ratios implied that the state of surface Pd on AuNW, especially the Pd/Au ratio, did not change much, when only the reduction potential was applied.

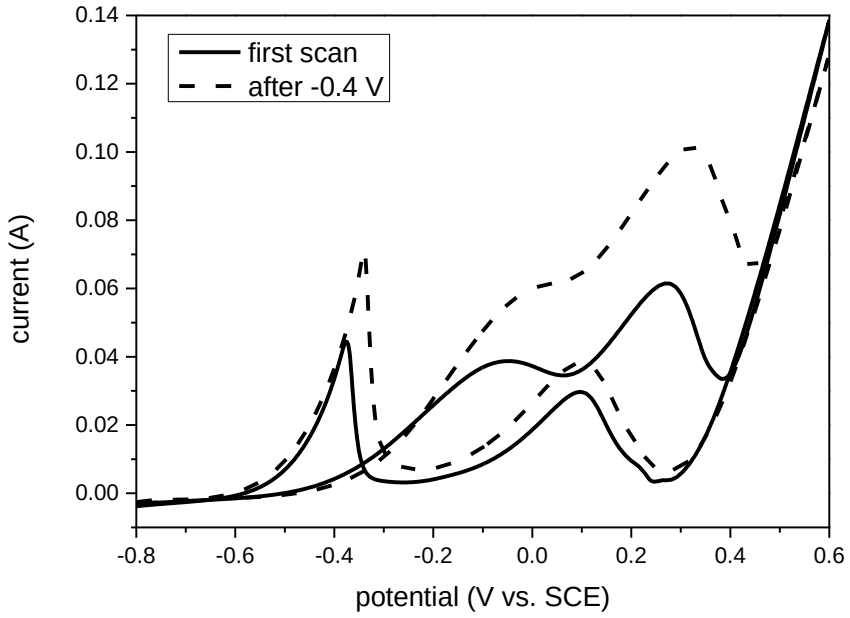

Figure 3-3-8. Cyclic voltammograms of palladium coated AuNW on nickel foam by primary cell coating method with 2.5 mM $PdCl_2$ coating solution before (solid) and after (dash) applying -0.4 V potential on the nickel foam for 5 minutes.

Similarly, the oxidation potential of 0.2 V was applied on the same piece of electrode for 5 minutes. Figure 3-3-9 demonstrates that after the applying of oxidation potential, the shape of CV curve did not alter much, still two clear forward peaks, Pd at around -0.1 V and Au at around 0.3 V. After the comparison of the ratio of Pd/Au peak current before (1:1.6) and after (1:1.4) applying the potential of 0.2 V, the ratio of surface atoms almost remained the same. In short, only the reduction or the oxidation potential can hardly change the surface state or move the surface Pd atoms. The oxidation or reduction potential alone is not the necessary condition for the movement of Pd.

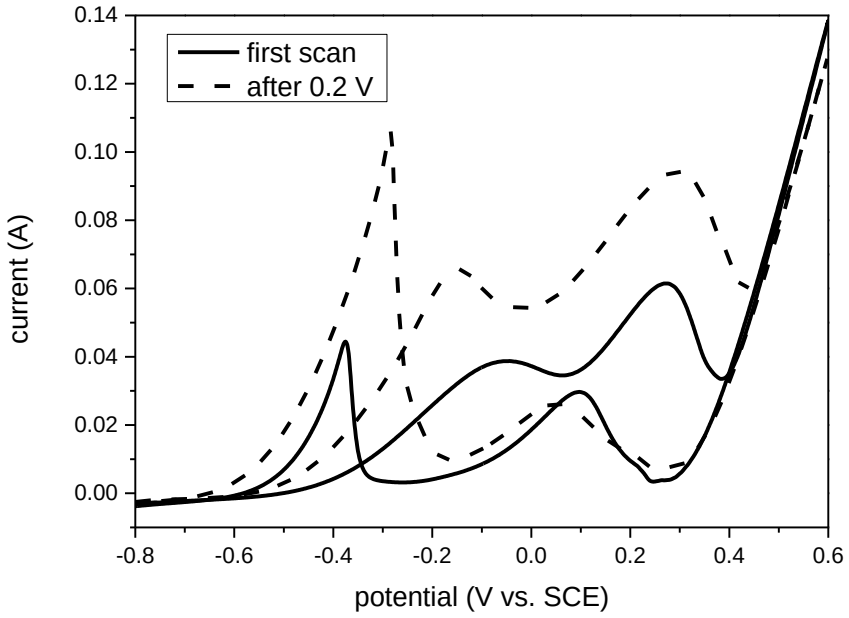

Figure 3-3-9. Cyclic voltammograms of palladium coated AuNW on nickel foam by primary cell coating method with 2.5 mM $PdCl_2$ coating solution before (solid) and after (dash) applying 0.2 V potential on the nickel foam for 5 minutes.

The necessary condition tests for half range of CV was carried out in the similar conditions. The reduction half CV from -0.8 to -0.2 V (Figure 3-3-10a) and the oxidation half CV from 0 to 0.6 V (Figure 3-3-10b) was applied individually. For the reduction half CV scans, after five CV scans, the ratio of Pd/Au peak current was 1:1.1, the same as the ratio of 1:1.1, before applied the reduction CV scans. This result testified that with only reduction half CV scans, the surface Pd islands could not move to cover the Au surface. While for the oxidation half CV scans, Figure 3-3-10b clearly demonstrated that after five CV cycles, the Pd/Au peak current ratio decreased from 1:1.1 to 1:0.6. Only judging from the change of ratio, it seems that the Pd started to

move and cover part of the Au surface during the five oxidation half CV scans. Considering the occurrence of oxidation of Pd in the solution, the increase of the Pd peak current would not completely result from the Pd deposition on Au surface, but also from the reduction of Pd ions by active nickel foam surface. The most possible reducing reagent in this system should be the metal nickel, since there was no strong reduction current during all the CV process.

In short summary, only the fixed potential or half CV scans could not lead to the movement of Pd onto Au surface. When the combination of reducing and oxidizing CV scans was applied on the partially deposited Pd on AuNW, the Pd domains would move and cover the Au surface..

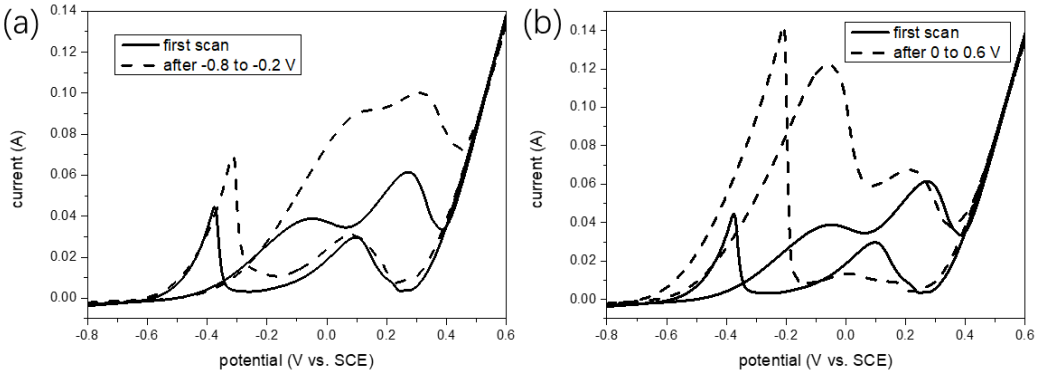

Figure 3-3-10. Cyclic voltammograms of Pd coated AuNW nickel foam by primary cell coating method with 2.5 mM $PdCl_2$ coating solution before (solid) and after (dash) applying (a) -0.8 to -0.2 V and (b) 0 to 0.6 V half CV scans individually on the nickel foam for five cycles.

Next, two compositions in the electrolyte (ethanol and sodium hydroxide) were removed respectively, to confirm whether they were the necessary condition for the movement of Pd. The first experiment was carried out in the electrolyte without any ethanol. Twenty cycles of CV were applied on Pd coated AuNW nickel foam electrode in the 1.0 M sodium hydroxide aqueous solution without ethanol. After that, one more CV cycle was applied to examine whether the ratio of surface atoms was changed or not. As shown in Figure 3-3-11, only pure Pd forward and backward peaks could be observed and there was no Au peaks. This verifies that without ethanol, Pd could still move onto the Au surface, which can be fully covered in 20 CV cycles. On the basis of this result, the ethanol is not the necessary condition for the movement of Pd.

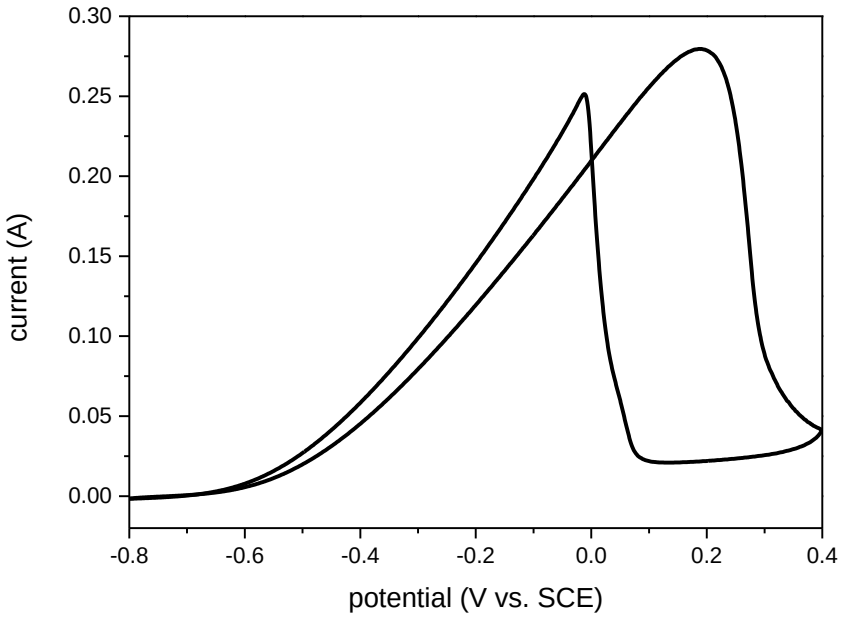

Figure 3-3-11. Cyclic voltammograms of Pd coated AuNW on nickel foam by primary cell coating method with 2.5 mM $PdCl_2$ coating solution after 20 cycles of CV scan in 1.0 M sodium hydroxide aqueous solution without ethanol.

The next control experiment was carried out in the electrolyte without sodium hydroxide. Similarly, 20 rounds of CV scan was applied in 1.0 M sodium sulfate aqueous solution without sodium hydroxide. Figure 3-3-12 indicates that after potential cycling without sodium hydroxide, both the Au (0.3 V) and the Pd (-0.2 V) forward peak can be clearly observed with the peak current ratio of Pd/Au around 1:1.8, similar with the ratio before any electrochemical treatment. Without sodium hydroxide in the electrolyte, the surface Pd/Au atoms did not change much, meaning that the Pd atom was difficult to move and the sodium hydroxide was the necessary condition for Pd movement.

In short summary, the ethanol in the electrolyte is found out not to be the necessary condition for the movement of Pd, only an indicator to amplify the current density (over ten times higher than the current density without ethanol). However, the sodium hydroxide in the electrolyte is the necessary condition leading to the physical movement of Pd domains. Without sodium hydroxide, the surface Pd atom cannot move to cover the Au surface.

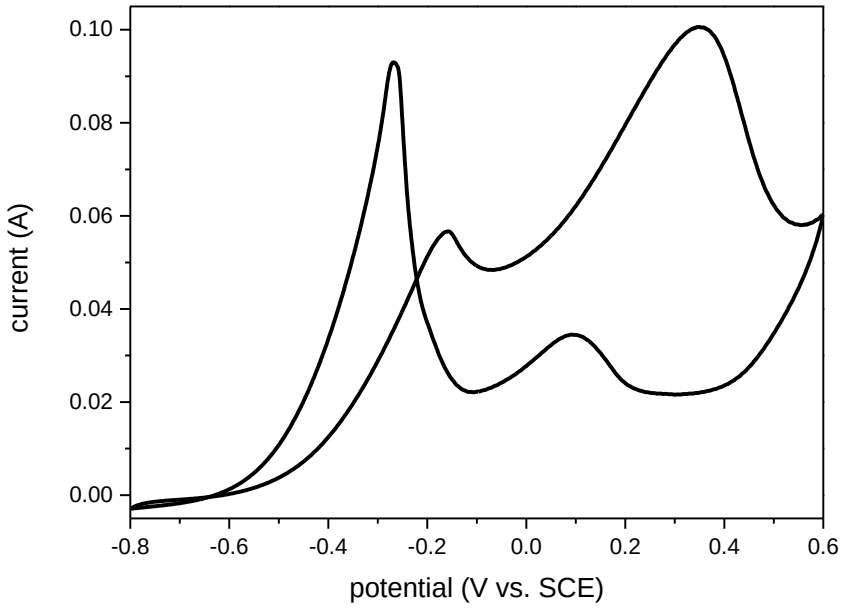

Figure 3-3-12. Cyclic voltammograms of Pd coated AuNW on nickel foam by primary cell coating method with 2.5 mM $PdCl_2$ coating solution after 20 cycles of CV in 1.0 M Na_2SO_4 aqueous solution without NaOH.

The working electrode was mainly composed of two parts, the AuNW and the nickel foam. In order to test whether the AuNW structure was necessary for the movement of Pd, the original one-dimensional Au surface (AuNW) was replaced with the zero-dimensional nanomaterials, the citrate-decorated 15 nm Au nanoparticles (AuNPs). As shown in Figure 3-3-13, the Au peaks kept decreasing, while the Pd peaks kept increasing, very similar with the AuNW nickel foam situation. The AuNP peak was much smaller than AuNW peak, due to the dramatically decreased active surface area of AuNP, but the decreasing trend was the same. The shape of the Au nanomaterials

cannot affect the movement of Pd and the successive Au surface (AuNW) was not the necessary condition for Pd movement.

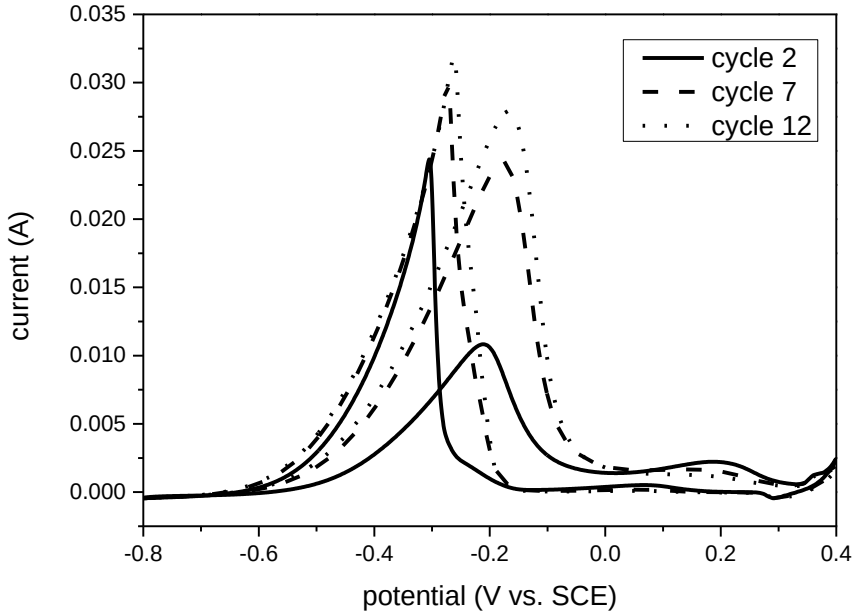

Figure 3-3-13. Cyclic voltammograms of palladium coated AuNP on nickel foam by primary cell coating method with 2.5 mM $PdCl_2$ coating solution with different cycle number (cycle 2 solid, cycle 7 dash and cycle 12 dot) in 1.0 M sodium hydroxide and 1.0 M ethanol aqueous solution at room temperature.

As the anode in the primary cell, the nickel foam was always served as the platform for the electro-oxidation ethanol reactions and it deserves considering whether the nickel foam played an important role in the movement of Pd. The nickel foam substrate was then replaced with the inert conductive substrate, fluorine doped tin oxide (FTO). But the FTO substrate was different from the nickel foam system, since it could not be treated with the primary cell coating method. The activity of FTO was not strong

enough to circulate as one primary cell to reduce palladium chloride onto Au surface. In order to simulate the partially deposited Pd situation, the Pd surface was produced on purpose by dropping the mixture of AuNP and PdNP solution on the FTO. The mixture was dripped on the FTO surface to deliberately create the contact of Pd and Au. Figure 3-3-14 clearly demonstrates the increasing trend of the Pd forward and backward peaks. Without any additional Pd source, the only possible pathway for the increasing of Pd peak should be the spread out of Pd surface to cover the exposed Au surface. As shown in the final CV scan, there was no clear Au peak observed. Without nickel foam, the Pd could still cover on the Au surface and thus the nickel foam should not be the necessary condition for the movement of Pd.

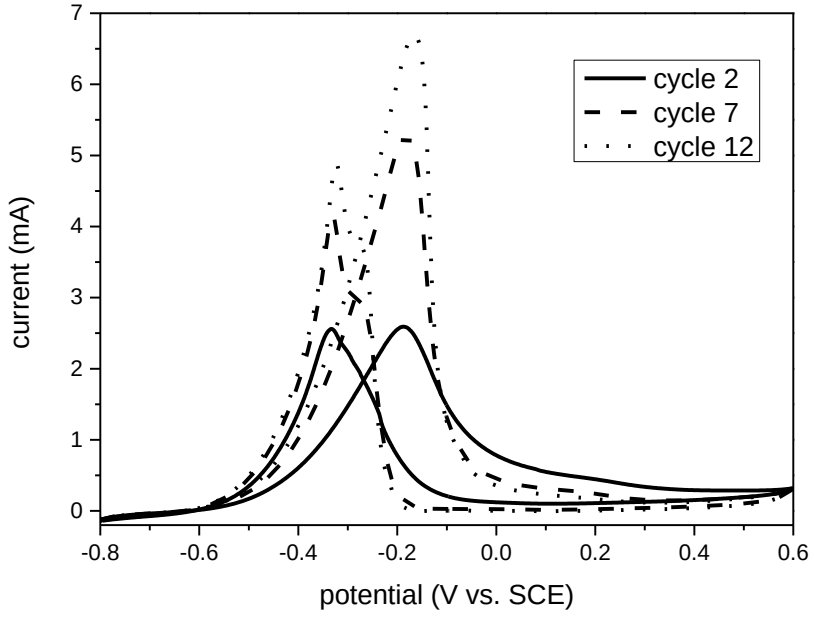

Figure 3-3-14. Cyclic voltammograms of mixed AuNP and PdNP on FTO with different cycle number (cycle 2 solid, cycle 7 dash, cycle 12 dot) in 1.0 M sodium hydroxide and 1.0 M ethanol aqueous solution.

Previously, the active Au surface was always connected to the Pd surface for convenient movement. To figure out whether the relative position of Pd/Au would affect the movement process, the Au and Pd surface should be separated. If the Pd remains moving, the oxidation and reduction of Pd atoms probably occurs during the moving process, likely following the ripening mechanism. Otherwise, the movement of Pd should follows the migration mechanism. For all previous experiments, the primary cell coating method was always used for the deposition of Pd, which would result in the close contact of Pd and Au. So in this experiment, AuNP and PdNP was separated onto different position of the FTO substrate within same conductive surface and this substrate was served as the working electrode (Figure 3-3-15b). With more and more CV cycles, Figure 3-3-15a clearly demonstrates that the Au forward peak current decreased while the Pd increased, similar with previous Pd movement results. The Au surface was gradually covered with Pd and the disconnected two parts of nanoparticles would mix with each other during the CV process. So, the series of CV curves revealed that the connection of Au and Pd surface was not the necessary condition.

Interestingly, during the CV process, there were clearly two types of Pd backward peaks in Figure 3-3-15a inset, one rising at ca. -0.35 V (Peak I) and the other one at ca. -0.25 V (Peak II). The Peak I exists at the very first circle CV scan and lasts during the whole CV cycling steps, meaning that this peak was more like the pure Pd peak from PdNP. While the Peak II did not occur at the very first state and it kept increasing with

more and more CV cycle numbers, indicating that this peak might result from the Pd covering the Au surface. This phenomenon was worth considering why the electrochemical signals of these two kinds of Pd are different from each other.

Usually, the onset potential of the backward peak provides the correlation information about the binding strength of the intermediate. Here, more negative onset potential of the backward peak would corresponds to the stronger binding of –OH group, since more energy is needed for the removal of attached –OH group with more negative potential. So it seems that the binding energy of hydroxide on the pure Pd surface was larger than that on the Pd-Au mixed surface, due to the more negative onset of pure Pd. If previous results were taken into considerations, the onset potential of the backward peak all raised at relatively more positive section (Figure 3-3-5, 3-3-8, 3-3-9, and 3-3-10 at ca. -0.2 V). In these experiments, there was no pure Pd surface and the Pd domains were all deposited on the Au surface. The shouldered negative peaks could be observed in Figure 3-3-14 and 3-3-15 at ca. -0.35 V, with the existence of pure Pd domains on the electrode and this peak position was similar with that of pure Pd. There were two backward peaks when the pure Pd nanomaterials moved and covered the Au surface, implying that there were two types of Pd on the substrate, pure Pd deposited on FTO and strained Pd deposited on Au surface.

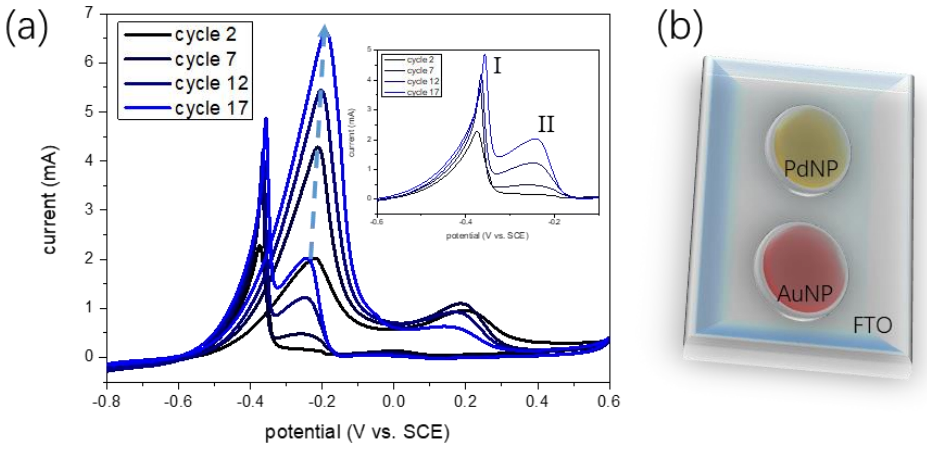

Figure 3-3-15. (a) Cyclic voltammograms of separated AuNP and PdNP on same piece of FTO with different cycle number (from black to blue) in 1.0 M sodium hydroxide and 1.0 M ethanol aqueous solution and inset is the detailed region of two palladium backward peaks. (b) Illustration of the working electrode with separated PdNP and AuNP on FTO conductive side.

Within the same piece of FTO, the Pd could move to cover the Au surface, judging from the increase of Pd and decrease of Au peaks. To further confirm the movement process of Pd domains, the Pd and Au was separated onto two different pieces. The combination of two FTO substrates could easily weaken the flowing efficiency of the electrolyte between two substrates. Hence, Pd coated nickel foam by galvanic replacement reaction was directly used as the Pd source in this experiment to increase the fluidity of the electrolyte. The Au source here was the same as the previous experiment, dripped AuNP on the FTO substrate. The Pd coated nickel foam and the AuNP decorated FTO was connected and served as the working electrode for 20 circles

of CV. Before and after the CV scans, only the FTO with AuNP was served as the working electrode to eliminate the interference from pure Pd domains. As shown in Figure 3-3-16, after 20 circles of CV scan, the forward and backward peaks of Au decreased dramatically, while the Pd peaks started to appear. The Pd and Au nanoparticles were divided at different pieces of substrate and there was no other media except the electrolyte to facilitate the movement of Pd. So this experiment solidified the conclusion that for the Pd movement, the Au and Pd at the same piece was not the necessary condition. The Pd atoms could move freely between two different substrates via the electrolyte media.

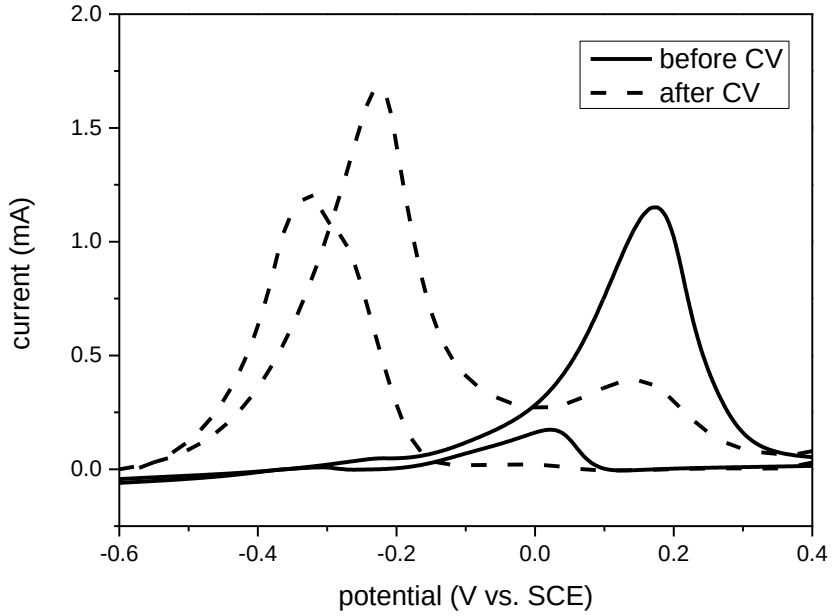

Figure 3-3-16. Cyclic voltammograms of AuNP on FTO before (solid) and after (dash) 20 circles of CV scanning with palladium coated nickel foam in 1.0 M sodium hydroxide and 1.0 M ethanol aqueous solution.

After testing all these possible conditions, no experiment was carried out in the condition without Au surface. So the next necessary condition to be tested was whether the Pd can move without any Au surface. Bare FTO substrate was served as the working electrode without any decoration. Similar with the previous experiment, 20 cycles of CV were applied on the bare FTO in 1.0 M sodium hydroxide and 1.0 M ethanol aqueous solution, and the Pd coated nickel foam was served as Pd source. Figure 3-3-17 clearly shows the differences of peak current between AuNP on FTO and bare FTO after 20 circles of CV. The forward peak current of AuNP on FTO was over 8 times higher than that of bare FTO. Even after another 10 cycles of CV circles, the peak current of bare FTO still did not increase much, only 0.01 mA, meaning that the Pd was much more difficult to cover the bare FTO surface than the Au surface. This phenomenon can be explained by the differences of lattice mismatch between substrates and Pd. The lattice mismatch between two noble metals, Pd and Au (5 %) is much smaller than that between metal and metal oxide, Pd and tin oxide (18 %).[19] Large lattice mismatch would seriously obstruct the deposition of Pd onto substrate and the deposition of Pd on FTO was thermodynamically unfavorable process. Generally, for the successful deposition of metal overlayer, the lattice mismatch should be smaller than 5 %.[20] When choosing the deposition position of Pd ions, the targeted surface should be similar with Pd atom and form strong bonding (bond energy of Au-Pd 142.7 kJ/mol) to stabilize the Pd overlayer.[21] So the deposition of relatively complete Pd overlayer must follow one precondition, the existence of the suitable and stable place

for Pd to be favorably deposited, for example, the Au surface here. To conclude, the Au surface should be the necessary condition for the movement of Pd.

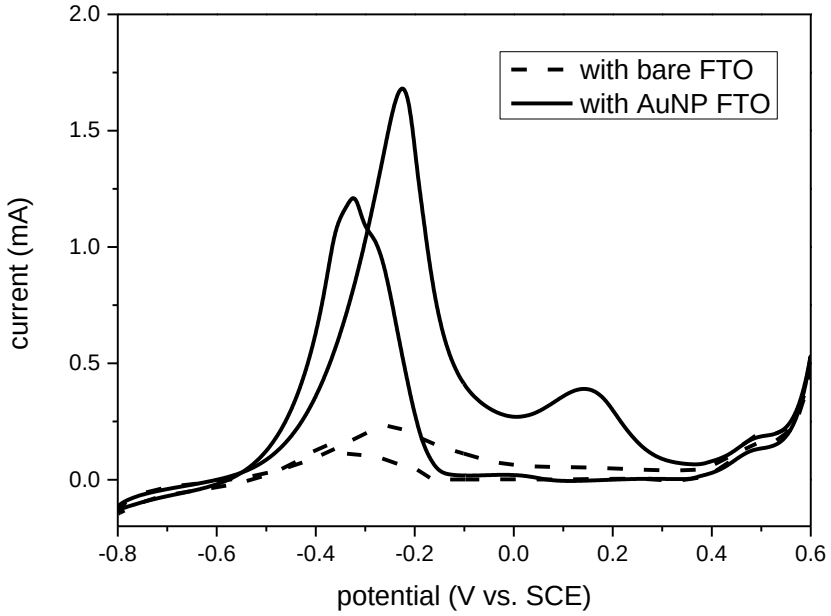

Figure 3-3-17. Cyclic voltammograms of AuNP on FTO (solid) and bare FTO (dash) after 20 cycles of CV scans with palladium coated nickel foam as palladium source in 1.0 M sodium hydroxide and 1.0 M ethanol aqueous solution.

After all these necessary condition experiments, some of the reaction conditions were found out to be of no significance, while some were necessary for the movement of Pd. Therefore, by listing and comparing all these conditions, one possible mechanism could be built up to explain how the Pd would move and cover the Au surface with the help of CV circles.

Firstly, the surface ratio of Pd/Au would not change much, if only fixed or range of oxidation/reduction potential was applied in 5 minutes or 20 circles of CV. This testified

that to move the surface Pd atoms, the combination of oxidation and reduction potential should be one of the necessary conditions. The mechanism of Pd movement could very likely follow the ripening process. The Pd islands on the substrate were firstly oxidized to Pd ions into the solution and then were reduced back onto the Au surface.

Secondly, the ethanol in the electrolyte was test to be the unnecessary condition, while the sodium hydroxide was vital to the ripening of Pd. This phenomenon could not be easily achieved when the electrolyte was neutral. So the electrolyte must be tuned to basic or acid. However, the template for electrochemical tests was nickel foam, which would easily be damaged and spoiled in acid condition. The ethanol did not play an important role in the moving of Pd, but it clearly indicated and amplified the increased amount of Pd and the decreased amount of Au. Without the added ethanol in the electrolyte, the current density would be declined at least ten times and the two backward Pd peaks would be very difficult to be observed or separated.

Thirdly, either the nickel foam substrate or the AuNW nanostructure was not the necessary conditions for the physical movement of Pd. When the nickel foam substrate and the AuNW surface was replaced with the conductive substrate FTO and the citrate-decorated AuNPs with different diameters, respectively, this Pd ripening system could still work effectively. The existence of the metal surface (Au) with different shape or size was vital to the ripening of Pd and there was no other strict requirement for the conductive substrate or the targeted metal to be covered.

At last, the relative position of the Au nanomaterial and Pd domain was found out not to be the key to the Pd ripening process, while the appearance of Au surface played an important role. Even when the Au and Pd surface was separated into two pieces of substrate, the Pd itself can still be dissolved to cover the Au surface. So all these experiment results could verify that the physical movement of Pd follows the ripening process. The Pd domain on the electrode was firstly oxidized to the Pd ion into the electrolyte and then the ion was reduced back onto the Au surface in reduction potentials. This ripening process successfully explained why the position of Au was unrelated with the moving of Pd and why two stages of oxidation and reduction potential was essential.

To prove the Pd movement mechanism, SEM images of Pd deposited on AuNW nickel by primary cell deposition method before and after 20 CV circles were shown in Figure 3-3-18. Before CV scans, the Pd nanoparticles (yellow circles in Figure 3-3-18a) were randomly deposited in between the AuNW forest, with particle size from 50 nm to over 250 nm. The size or the position of these Pd nanoparticles could not be regularly distributed on the nickel foam substrate, indicating the fast reaction rate of galvanic cell reactions. While after 20 circles of CV, no Pd nanoparticles can be clearly observed on the substrate (Figure 3-3-18). These SEM images clearly demonstrated that CV scans could help dissolve these deposited Pd nanoparticles on the substrate and redeposit them back onto AuNW surface. The final deposition destination can be easily proved by CV curves of ethanol oxidation, where no Au peaks can be observed (Figure 3-3-5).

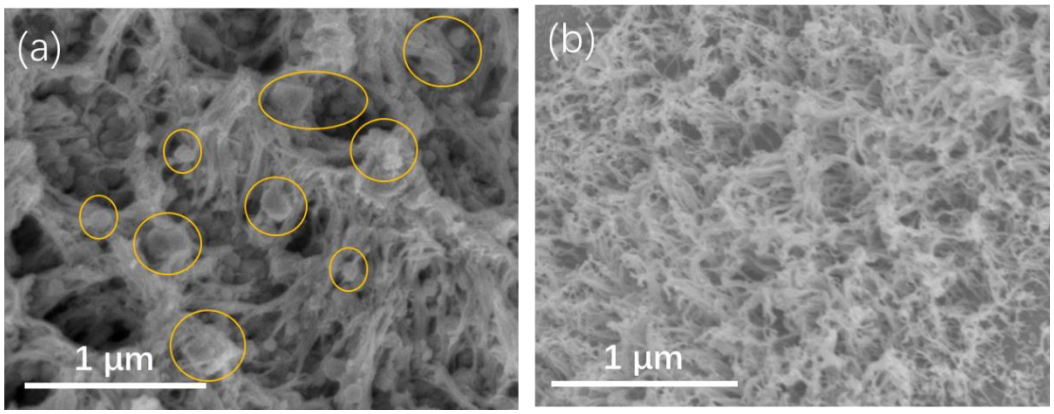

Figure 3-3-18. SEM images of Pd deposited on AuNW nickel foam by primary cell deposition method (a) before and (b) after 20 cycles of CV scanning from -0.8 to 0.6 V vs. SCE (yellow circles standing for Pd nanoparticles deposited on AuNW).

In addition, the appearance of dissolved Pd ions in the electrolyte can be determined by ICP-OES. Before 20 circles of CV, the amount of Pd dissolved in the electrolyte reached 0.8 ng/mL and this number was increased to 342 ng/mL after 20 CV scans, evaluated by ICP-OES. The reason of the existence of Pd ions in the electrolyte can be explained by the oxidation of Pd metal by oxidation of CV scans. Liu group reported the similar phenomenon of the occurrence of Pt ions in the solution when the Pt counter electrode was undergoing potential cycling in hydrogen evolution reactions.[22] They stated that the most obvious dissolution of Pt metal would take place when the CV potential on the Pt counter electrode enables both Pt oxidation and reduction, and the Pt dissolution can be easily enhanced after repetitive oxidation and reduction of Pt. Our proposed Pd movement mechanism essentially matched with their observation and explanation of Pt dissolution.

In short summary, one reasonable mechanism could be proposed to explain how the Pd nanomaterials ripen onto the Au surface (Figure 3-3-19), based on the results of the control experiment. Within the oxidation section of CV, a portion of the surface Pd atoms would be oxidized to Pd ions into the electrolyte. When it comes to the reduction section of CV, the Pd ions would be reduced back with negative potentials and these Pd atoms could choose the relatively favorable position for deposition. It is well known that the FTO surface (tin oxide) was unfavorable for Pd deposition, while the noble metal surface, especially the Au surface on FTO substrate would be the thermodynamically favorable position. In addition, the bond strength of Pd-Au was stronger than that of Pd-Pd, which would easily result in higher possibilities of deposited Pd domains on Au than on Pd itself. With the increasing cycle numbers of CV, the active surface of Au would be decreased, due to the coverage of Pd, while the active surface of Pd would be increased. This is the reason why the decreased current of the Au forward peak and the increased current of Pd forward peak can be clearly observed with more CV circles.

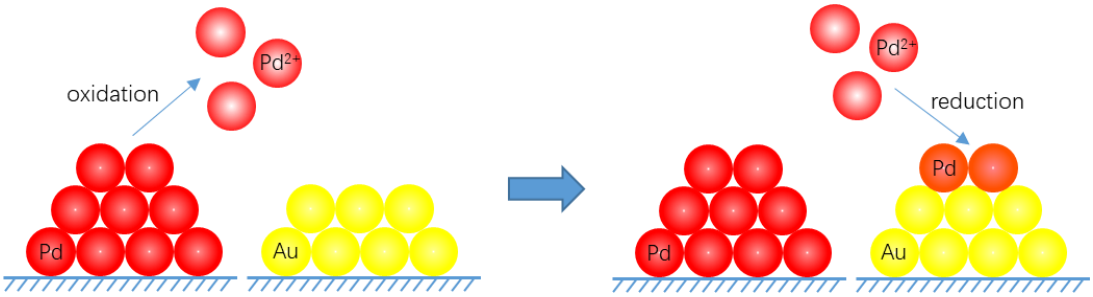

Figure 3-3-19. Illustration of the Pd repining mechanism to explain how the Pd domains (red) would firstly be dissolved and then fully cover the active Au surface (yellow) followed with oxidation and reduction steps.

3.4. Conclusion

One convenient and effective deposition method for the coating of Pd shell on Au surface was readily achieved. The Pd overlayer could be successfully formed on the Au surface, followed with the primary cell principle (constructed with AuNW and nickel foam). The catalytic activity and stability of the primary cell deposited Pd-based electrode could remain almost the same as that of Pd shell fabricated by the electrochemical coating method. When the concentration of Pd precursors was further reduced, the Au surface cannot be fully covered with Pd shell anymore. But with the help of CV circling, the Pd shell could still be successfully spread out on the AuNW. The specific current of primary cell deposited electrode for ethanol oxidation reactions could be dramatically increased to 6464 A/g, higher than most of the recent representative Pd-based electrodes, due to the higher efficiency of active Pd atoms. The function of CV scans was to disperse Pd uniformly onto the high surface area AuNW surface, aiming to achieve higher Pd forward peak current density. Interestingly, during the CV circling process, the Pd domains on the substrate would firstly be dissolved into the electrolyte and then mostly reduced back onto the Au surface, rather than on Pd surface or FTO substrate, on the basis of serval sets of necessary condition experiment results.

3.5. Reference

1. Naohara, H.; Ye, S.; Uosaki, K., Electrochemical Layer-by-Layer Growth of Palladium on an Au(111) Electrode Surface: Evidence for Important Role of Adsorbed Pd Complex. *Journal of Physical Chemistry B* **1998,** *102* (22), 4366-4373.

2. (a) L, S.; Y, J.; Z, Z., Li Ion Battery Materials with Core-Shell Nanostructures. *Nanoscale* **2011,** *3* (10), 3967-3983; (b) Kang, N.; Marieève Perron; ‡, R. E. P. H.; Yubao Zhang; Geneviève Gaucher, A.; Jeanchristophe Leroux, Stereocomplex Block Copolymer Micelles: Core−Shell Nanostructures with Enhanced Stability. *Nano Letters* **2005,** *5* (2), 315-319; (c) Li, Y.; Jin, J.; Wang, D.; Lv, J.; Hou, K.; Liu, Y.; Chen, C.; Tang, Z., Coordination-responsive drug release inside gold nanorod@metal-organic framework core–shell nanostructures for near-infrared-induced synergistic chemo-photothermal therapy. *Nano Research* **2018**, 1-12; (d) Limban, C.; Missir, A.; Caproiu, M.; Grumezescu, A.; Chifiriuc, M.; Bleotu, C.; Marutescu, L.; Papacocea, M.; Nuta, D., Novel Hybrid Formulations Based on Thiourea Derivatives and Core@Shell Fe_3O_4@C18 Nanostructures for the Development of Antifungal Strategies. *Nanomaterials* **2018,** *8* (1), 47; (e) Liz-Marzán, L. M.; Giersig, M.; Mulvaney, P., Synthesis of nanosized gold-silica core-shell particles. *Langmuir* **1996,** *12* (18), 4329-4335.

3. (a) Reiss, P.; Protiere, M.; Li, L., Core/shell semiconductor nanocrystals. *small* **2009,** *5* (2), 154-168; (b) Luo, J.; Wang, L.; Mott, D.; Njoki, P. N.; Lin, Y.; He, T.; Xu, Z.; Wanjana, B. N.; Lim, I. I. S.; Zhong, C. J., Core/shell nanoparticles as electrocatalysts for fuel cell reactions. *Advanced Materials* **2008,** *20* (22), 4342-4347; (c) Zhu, Y.; Shi, J.; Shen, W.; Dong, X.; Feng, J.; Ruan, M.; Li, Y., Stimuli‐responsive controlled drug release from a hollow mesoporous silica sphere/polyelectrolyte multilayer core–shell structure. *Angewandte Chemie* **2005,** *117* (32), 5213-5217.

4. Bang, J. H.; Suslick, K. S., Applications of ultrasound to the synthesis of nanostructured materials. *Advanced Materials* **2010,** *22* (10), 1039-1059.

5. (a) Puurunen, R. L., Surface chemistry of atomic layer deposition: A case study for the trimethylaluminum/water process. *Journal of Applied Physics* **2005,** *97* (12), 121301-121301-52; (b) Miikkulainen, V.; Leskela, M.; Ritala, M.; Puurunen, R. L., ChemInform Abstract: Crystallinity of Inorganic Films Grown by Atomic Layer Deposition: Overview and General Trends. *Journal of Applied Physics* **2013,** *113* (2), 2-159; (c) George, S. M., Atomic Layer Deposition: An Overview. *Chemical Reviews* **2010,** *110* (1), 111-131.

6. (a) Wei, D.; Liu, Y.; Wang, Y.; Zhang, H.; Huang, L.; Yu, G., Synthesis of N-Doped Graphene by Chemical Vapor Deposition and Its Electrical Properties. *Nano Letters* **2009,** *9* (5), 1752; (b) Xomeritakis, G.; Lin, Y. S., Fabrication of a thin palladium membrane supported in a porous ceramic substrate by chemical vapor deposition. *Journal of Membrane Science* **1996,** *120* (2), 261-272; (c) Liang, C.; Xia, W.; Soltani-Ahmadi, H.; Schluter, O.; Fischer, R. A.; Muhler, M., The two-step chemical vapor deposition of Pd(allyl)Cp as an atom-efficient route to synthesize highly dispersed

palladium nanoparticles on carbon nanofibers. *Chemical Communications* **2005,** *2* (2), 282-284; (d) Reina, A.; Jia, X.; Ho, J.; Nezich, D.; Son, H.; Bulovic, V.; Dresselhaus, M. S.; Kong, J., Large area, few-layer graphene films on arbitrary substrates by chemical vapor deposition. *Nano Letters* **2009,** *9* (1), 30-35.

7. (a) Kim, S. W.; Kim, M.; Lee, W. Y.; Hyeon, T., Fabrication of hollow palladium spheres and their successful application to the recyclable heterogeneous catalyst for suzuki coupling reactions. *Cheminform* **2002,** *33* (42), 7642-3; (b) Kim, J. H.; Bryan, W. W.; Chung, H. W.; Chan, Y. P.; Jacobson, A. J.; Lee, T. R., Gold, Palladium, and Gold−Palladium Alloy Nanoshells on Silica Nanoparticle Cores. *Acs Appl Mater Interfaces* **2009,** *1* (5), 1063-1069; (c) Wang, M.; Li, Q.; Yu, H.; Hur, S. H.; Kim, E. J., Phase-controlled preparation of TiO 2 films and micro(nano)spheres by low-temperature chemical bath deposition. *Journal of Alloys & Compounds* **2013,** *578* (11), 419-424.

8. (a) Kolb, D. M.; Przasnyski, M.; Gerischer, H., Underpotential deposition of metals and work function differences. *Journal of Electroanalytical Chemistry & Interfacial Electrochemistry* **1974,** *54* (1), 25-38; (b) Bartlett, P. N.; Birkin, P. R.; Ghanem, M. A., Electrochemical deposition of macroporous platinum, palladium and cobalt films using polystyrene latex sphere templates. *Chemical Communications* **2000,** *17* (17), 1671-1672; (c) Oskam, G.; Long, J. G.; Natarajan, A.; Searson, P. C., Electrochemical deposition of metals onto silicon. *Journal of Physics D Applied Physics* **1999,** *31* (31), 1927.

9. (a) Ku, C. S.; Huang, J. M.; Cheng, C. Y.; Lin, C. M.; Lee, H. Y., Annealing effect on the optical response and interdiffusion of n-ZnO/p-Si (111) heterojunction grown by atomic layer deposition. *Applied Physics Letters* **2010,** *97* (18), 1460; (b) Swaminathan, S.; Oshima, Y.; Kelly, M. A.; Mcintyre, P. C., Oxidant prepulsing of Ge (100) prior to atomic layer deposition of Al2O3: In situ surface characterization. *Applied Physics Letters* **2009,** *95* (3), 4587; (c) Paul, R.; Reifenberger, R. G.; Fisher, T. S.; Zemlyanov, D. Y., Atomic Layer Deposition of FeO on Pt(111) by Ferrocene Adsorption and Oxidation. *Chemistry of Materials* **2015,** *27* (17), 150811102548005; (d) Xu, M.; Wu, Y. Q.; Koybasi, O.; Shen, T.; Ye, P. D., Metal-oxide-semiconductor field-effect transistors on GaAs (111)A surface with atomic-layer-deposited Al2O3 as gate dielectrics. *Applied Physics Letters* **2009,** *94* (21), 294.

10. Hang, S.; Jiating, H.; Jiangyan, W.; Shuang-Yuan, Z.; Cuicui, L.; Thirumany, S.; Subodh, M.; Ming-Yong, H.; Dan, W.; Hongyu, C., Investigating the multiple roles of polyvinylpyrrolidone for a general methodology of oxide encapsulation. *Journal of the American Chemical Society* **2013,** *135* (24), 9099-9110.

11. (a) Wang, R.; Wang, C.; Cai, W. B.; Ding, Y., Ultralow‐platinum‐loading high‐performance nanoporous electrocatalysts with nanoengineered surface structures. *Advanced Materials* **2010,** *22* (16), 1845-1848; (b) Cai, B.; Wen, D.; Liu, W.; Herrmann, A. K.; Benad, A.; Eychmüller, A., Function-Led Design of Aerogels: Self-Assembly of Alloyed PdNi Hollow Nanospheres for Efficient Electrocatalysis. *Angewandte Chemie International Edition* **2015,** *54* (44), 13101.

12. Jones, J.; Xiong, H.; Delariva, A. T.; Peterson, E. J.; Pham, H.; Challa, S. R.; Qi, G.; Oh, S.; Wiebenga, M. H.; Xi, P. H. N., Thermally stable single-atom platinum-on-ceria catalysts via atom trapping. *Science* **2016,** *353* (6295), 150-154.
13. (a) Xu, C. W.; Wang, H.; Shen, P. K.; Jiang, S. P., Highly Ordered Pd Nanowire Arrays as Effective Electrocatalysts for Ethanol Oxidation in Direct Alcohol Fuel Cells. *Advanced Materials* **2010,** *19* (23), 4256-4259; (b) Wang, Q.; Wang, Y.; Guo, P.; Li, Q.; Ding, R.; Wang, B.; Li, H.; Liu, J.; Zhao, X., Formic acid-assisted synthesis of palladium nanocrystals and their electrocatalytic properties. *Langmuir* **2014,** *30* (1), 440-446; (c) Hu, F.; Cui, G.; Wei, Z.; Shen, P. K., Improved kinetics of ethanol oxidation on Pd catalysts supported on tungsten carbides/carbon nanotubes. *Electrochemistry Communications* **2008,** *10* (9), 1303-1306; (d) Wang, A. L.; He, X. J.; Lu, X. F.; Xu, H.; Tong, Y. X.; Li, G. R., Palladium–Cobalt Nanotube Arrays Supported on Carbon Fiber Cloth as High-Performance Flexible Electrocatalysts for Ethanol Oxidation. *Angewandte Chemie* **2015,** *127* (12), 3740-3744.
14. Park, J.; Zhang, L.; Choi, S. I.; Roling, L. T.; Lu, N.; Herron, J. A.; Xie, S.; Wang, J.; Kim, M. J.; Mavrikakis, M., Atomic Layer-by-Layer Deposition of Pt on Pd Octahedra for Enhanced Catalysts toward the Oxygen Reduction Reaction. *Acs Nano* **2015,** *9* (3), 2635-47.
15. (a) Bard, A. J.; Faulkner, L. R.; Leddy, J.; Zoski, C. G., *Electrochemical methods: fundamentals and applications*. wiley New York: 1980; Vol. 2; (b) Haynes, W. M., *CRC handbook of chemistry and physics*. CRC press: 2014.
16. Bard, A., *Standard potentials in aqueous solution*. Routledge: 2017.
17. (a) Fan, F. R.; Liu, D. Y.; Wu, Y. F.; Duan, S.; Xie, Z. X.; Jiang, Z. Y.; Tian, Z. Q., Epitaxial Growth of Heterogeneous Metal Nanocrystals: From Gold Nano-octahedra to Palladium and Silver Nanocubes. *Journal of the American Chemical Society* **2008,** *130* (22), 6949-51; (b) Luo, Y.-R., *Comprehensive handbook of chemical bond energies*. CRC press: 2007.
18. Hu, F.; Chen, C.; Wang, Z.; Wei, G.; Pei, K. S., Mechanistic study of ethanol oxidation on Pd–NiO/C electrocatalyst. *Electrochimica Acta* **2007,** *52* (3), 1087-1091.
19. (a) Meng, M.; Fang, Z.; Zhang, C.; Su, H.; He, R.; Zhang, R.; Li, H.; Li, Z. Y.; Wu, X.; Ma, C., Integration of Kinetic Control and Lattice Mismatch to Synthesize Pd@AuCu Core-Shell Planar Tetrapods with Size-Dependent Optical Properties. *Nano Letters* **2016,** *16* (5), 3036; (b) Kolmakov, A.; Klenov, D. O.; Lilach, Y.; Stemmer, S.; Moskovits, M., Enhanced gas sensing by individual SnO2 nanowires and nanobelts functionalized with Pd catalyst particles. *Nano Letters* **2005,** *5* (4), 667.
20. Feng-Ru, F.; De-Yu, L.; Yuan-Fei, W.; Sai, D.; Zhao-Xiong, X.; Zhi-Yuan, J.; Zhong-Qun, T., Epitaxial growth of heterogeneous metal nanocrystals: from gold nano-octahedra to palladium and silver nanocubes. *Journal of the American Chemical Society* **2008,** *130* (22), 6949-51.
21. Yuan, D. W.; Yang, W.; Zhi, Z., Geometric, electronic, and bonding properties of AuNM (N = 1-7, M = Ni, Pd, Pt) clusters. *Journal of Chemical Physics* **2005,** *122* (11), 611-88.

22. Chen, R.; Yang, C.; Cai, W.; Wang, H.-Y.; Miao, J.; Zhang, L.; Chen, S.; Liu, B., Use of Platinum as the Counter Electrode to Study the Activity of Nonprecious Metal Catalysts for the Hydrogen Evolution Reaction. *Acs Energy Letters* **2017,** *2* (5), 1070-1075.

4. Sub-atomic Layer Deposition of Pd with Real-time Monitoring

4.1. Introduction

Nowadays, the majority of commercial chemical products involve catalysis at some stage of the manufacturing process. The use of nanomaterial-based catalyst can increase the catalytic activity, due to its extremely high surface/volume ratio (S/V) compared with traditional bulk catalyst.[1] Besides size, tuning other factors, such as composition,[2] structure,[3] and shape[4] of nanomaterials, can further increase the catalytic activity. Understanding the underlying mechanisms of these factors would be critical for better synthetic designs.

Fundamentally, the catalytic activity depends on the binding affinity of reactants/products on the exposed surface atoms.[5] If the binding affinity is too weak, the reactants could hardly bind to the catalyst, leaving most of the catalytic surface unutilized; if the binding affinity is too strong, it is difficult for reactants/products to leave the surface once bound. Thus, fine-tuning of the binding affinity is critical to improve the catalytic activity, whereas coarse tuning method could easily miss the optimal condition.

There are mainly three methods to tune the binding affinity: 1) Changing the composition of metal catalyst is a very simple method and widely used.[6] However, the tuning interval is too large given the few suitable metals to choose from. 2) As an improvement, alloys could offer a large number of combinations as the composition

ratio can be continuously varied, that is, if the optimal affinity occurs within the alloy combination. However, the synthesis of ideal alloy at nanoscale is difficult.[7] In the co-reduction method, combinations of metal ions can be simultaneously reduced, but the structure and composition of the product cannot be consistently tuned, often forming alloy, phase-segregated, or core-shell products, depending on the metal combinations and the rate of reduction.[8] 3) Tuning shell thickness is an interesting direction of fine-tuning the binding affinity, as the shell facing the reactants remains constant, whereas the internal core can influence the electronic property of the shell atoms.[9] Typically, the effects are the most pronounced when the overlayer is only a few atoms thick and the influence would be reduced with the increasing thickness of the overlayer.[10] In comparison to the first two methods, fine-tuning the shell thickness would be more accurate and adjustable.

Right now, the methods used for thin layer deposition include atomic layer deposition (ALD),[11] chemical vapor deposition (CVD),[12] underpotential deposition (UPD)[13] and chemical bath deposition (CBD).[14] For ALD, CVD and UPD, precise control for single or sub-monolayer deposition could be realized. Harsh conditions such as high temperature and high vacuum are required for ALD and CVD. For UPD, high purity of the substrate, including uniformity of the surface facets, is necessary to ensure consistent electrode potential for single layer deposition.[13] In comparison, the CBD method is more convenient under ambient condition, but the controllability over the

shell thickness is low. Once the shell is formed, usually the thickness is already tens of nanometers.

Most importantly, for all four methods, it is difficult to real-time monitor the property during the deposition process. Given the complicated procedure, it is tedious and time-consuming to retrieve the sample after each step of the multi-step deposition. Sometimes, the characterization method would spoil the nanostructure and obstruct further steps of modification or characterization. With real-time monitoring, one would easily obtain the structure-property correlation and determine the preparation process that leads to the best performance.

Here, we report a cyclic voltammetry (CV) based deposition method, where sub-monolayer of Pd deposition on Au can be readily achieved. The deposition is carried out during CV scan of ethanol oxidation reaction, where the onset potential of backward peaks would indicate the binding affinity of –OH group, and the peak current would demonstrate the exposed active surface area and the catalytic activity. With such real-time monitoring, the thickness of the Pd layer can be continuously and precisely tuned by the number of CV cycles and directly correlates with the electrochemical properties.

4.2. Materials and Methods

4.2.1. Materials

All the aqueous solutions used in the experiments were prepared with deionized water (resistivity > 18 $M\Omega \cdot cm^{-1}$). Hydrogen tetrachloroaurate(III) ($HAuCl_4$, 99.9%, Au

49% on metals basis, Alfa Aesar), palladium chloride (98%, Sigma Aldrich), 4-mercaptobenzoic acid (4-MBA, 90%, Sigma Aldrich), (3-aminopropyl)triethoxysilane (APTES, Sigma Aldrich), (3-cyanopropyl)triethoxysilane (CPTES, Sigma Aldrich), sodium citrate tribasic dihydrate (99.0%, Sigma Aldrich), sodium borohydride (98%, Sigma Aldrich), sodium hydroxide (98%, Sigma Aldrich), ethanol for electrochemistry test (analytical grade, Merck) and ethanol for AuNW growing (99.86% technical grade) were used as received. Copper specimen grids (200 meshes) with carbon support film were purchased from Beijing XXBR Technology Co. Fluorine doped tin oxide (FTO) glasses were purchased from Sigma Aldrich. Nickel foams with different thickness (0.5 mm, 1.0 mm, 2.0 mm and 5.0 mm) were purchased from Suzhou JSD Co and cut into 1*2 cm^2. Washing steps should be applied on the nickel foam before use.

4.2.2. Methods

Characterization methods. All transmission electron microscopy (TEM) images were collected on a JEM-1400 (JEOL) operated at 100 kV. All field emission scanning electron microscopy (SEM) images were collected on a JSM-6700F (JEOL). All electrochemistry data were collected on a CHI-760e electrochemical workstation.

Synthesis of 3-5 nm gold nanoseed (AuNS). A 50 mL round bottom flask was filled with 20 mL deionized water. Then 160 μL sodium citrate (1 wt%) aqueous solution and 100 μL $HAuCl_4$ (50 mM) aqueous solution was added into the flask and kept stirring for 1 min. Then 620 μL ice-cold $NaBH_4$ (0.1 M) aqueous solution was added in one

shot with vigorous stirring. The solution turned from light yellow to reddish orange, indicating the formation of AuNS. The solution was kept stirring for 10 min and collected to use after overnight for the consumption of unreacted $NaBH_4$.

Growth of ultrathin AuNW on nickel foam substrate. Before the growth of AuNW forest on nickel foam, the purchased nickel foam was first sonicated in ethanol/acetone 1:1 solution for 15 min for three times to remove some organic residual on the surface. Then the nickel foam was sonicated in deionized water for 15 min for three times and dried on the filter paper. The nickel foam was firstly functionalized with cyano silanes by reacting with CPTES water/ethanol 1:1 solution (1 μL/mL) for 30 min with stirring. Then the nickel foam was washed with ethanol twice and then with water twice. The excess ethanol or water residual inside the nickel foam should be removed thoroughly by filter paper. After successfully functionalized with CPTES, the nickel foam was soaked in citrate-stabilized AuNS (3-5 nm) aqueous solution as synthesized for over 1 h with stirring to ensure the adsorption of AuNS onto nickel foam surface. Then the nickel foam was washed with water twice to remove the excess unabsorbed AuNS. The AuNS-functionalized nickel foam was then immersed in the Au growth solution containing the solvent ethanol 2 mL, the ligand 4-MBA (10 mM) in 400 μL ethanol, the Au source $HAuCl_4$ (50 mM) in 100 μL water and the reducing agent L-ascorbic acid (20 mM) in 600 μL water for 30 min with stirring. Finally, the nickel foam was rinsed with ethanol and dried on the filter paper.[15]

Deposition of AuNS on FTO. Before the deposition of AuNS on FTO, the conductive surface of FTO has to be functionalized with APTES first. The conductive side of FTO was firstly functionalized with amino group and was immersed in APTES water/ethanol 1:1 solution (1 μL/mL) for 30 min. Then the FTO was washed with ethanol twice and then water twice to remove the excess silanes on the FTO surface. After the FTO dried enough in the air, we directly dropped 20 μL AuNS stock solution onto the FTO surface and waited the AuNS solution to dry. After the solution was totally dried, the deposition of AuNS on FTO was prepared. By this method, the AuNS was spread quite well compared with methods without APTES decoration.

Layer-by-layer electrochemical coating method for the deposition of Pd on Au. This electrochemical coating method used the standard three-electrode cell. The cyclic voltammetry tests were carried out by using the CHI-760e electrochemical workstation. The counter electrode we used was graphite electrode. The reference electrode we used was saturated calomel electrode (SCE). The working electrode we used was FTO with AuNS or any other surface needed to be coated. The electrolyte we used to do the CV coating was 1.0 M sodium hydroxide, 1.0 M ethanol aqueous solution saturated with N_2 with different concentration of $PdCl_2$ as the Pd source. The stirring speed during the purging N_2 gas and electrochemical test was 250 rpm all the time. The scan rate of cyclic voltammetry test was 50 mV/s. The scan range of CV was from -0.8 V to 0.6 V and back to -0.8 V as one cycle. More CV cycle number would lead to the increasing

thickness of Pd overlayer. The entire electrochemical test was carried out at room temperature, 25 ℃.

Island growth of Pd on Au. All the electrochemical workstation, three electrodes, electrolyte were kept the same as the layer-by-layer method, except the electrochemical method was different. We used fixed potential at -1.0 V vs. SCE for 5 minutes to replace the normal CV scans and then we can get AuNS coated by island Pd.

4.3. Results and Discussion

Previously, we have already proved that the Pd nanomaterial could be dissolved and redeposited back onto the AuNW surface during potential cycling (Figure 3-3-5). The mechanism of Pd movement can be summarized that the Pd atoms firstly get oxidized at oxidation potential to free Pd ions in the solution, which are then reduced back to deposit onto the Au surface. Although, the existence of Pd ions in the electrolyte can be confirmed by inductively coupled plasma optical emission spectrometry (ICP-OES) already, the amount or the valence state of Pd ions cannot be precisely controlled or even predicted during the Pd movement process. The oxidation and reduction of Pd alternatively occurs during the potential cycling process, which caused great uncertainties to the dissolution or deposition of Pd.

In order to solve this problem and testify proposed mechanism, the direct addition of Pd salt (such as, $PdCl_2$) into the electrolyte was used to replace the originally deposited Pd nanomaterials on Au surface. In addition, the potential position of Au and Pd

nanowire should be deeply studied to ensure that the change of peak position and height was analyzed correctly.

Preparation and characterization of Au nanowires and Pd coated Au nanowires. We use porous nickel foam as the substrate for growing a forest of ultrathin Au nanowires (AuNWs), as a two-pronged strategy to enhance the electrochemical active surface. The nickel foam surface was firstly functionalized with (3-cyanopropyl)triethoxysilane to render its surface amenable for the subsequent adsorption of citrated-stabilized 5 nm Au nanoparticles (AuNPs). Then, the nickel foam was immersed into the growth solution, containing the ligand 4-mercaptobenozic acid (4-MBA), the reducing agent L-ascorbic acid, and the gold source $HAuCl_4$.[16] After 30 min, both the surface and the inside part of nickel foam turned black, indicating the thorough growth of Au nanomaterials. As revealed by scanning electron microscopy (SEM), the nickel foam surface was covered with a dense layer of vertically aligned AuNWs, with length over 1 μm (Figure 4-3-1a). The AuNWs were detached from the nickel foam by sonication and characterized by transmission electron microscopy (TEM). As shown in Figure 4-3-1b, the average diameter of these AuNWs was about 5 nm. The successful growth of ultrathin AuNWs on high surface area substrate nickel foam would remarkably enhance the electrochemical active surface area, which would lead to the increase of the catalytic activity.

High surface area Au-based electrodes are highly desirable as the anode of the ethanol fuel cell to enhance its efficiency.[17] Therefore, the AuNW-functionalized nickel foam

(AuNW/NF) substrate is served as the working electrode to catalyze ethanol oxidation reaction. The electrochemical characterizations were carried out in the alkaline electrolyte containing 1.0 M sodium hydroxide and 1.0 M ethanol and all potentials in this chapter refer to saturated calomel electrode (SCE). The resulting CV curves showed two well-defined symmetric peaks (Figure 4-3-2a, black line).[18] The forward peak I at ca. 0.3 V and backward peak II at ca. 0.15 V are the typical features in ethanol oxidation by Au electrodes, matching with the literature data in terms of the peak position and shape.[19]

Pd-based nanomaterials are regarded as a better choice for electro-oxidation of ethanol,[20] and thus the AuNW/NF substrate is coated with Pd shell by pulsed current of -2.5/0 mA for 12 min. As shown in Figure 4-3-1c and 1d, most of the nanowires on the nickel foam remained vertically aligned and the average diameter of this nanowire increased to about 8 nm. The CV curves showed two typical asymmetric peaks of Pd, with forward peak III at ca. 0 V and backward peak IV at ca. -0.2 V (Figure 4-3-2a, red line). The peak position is similar to those of representative Pd nanomaterials.[19a, 20]

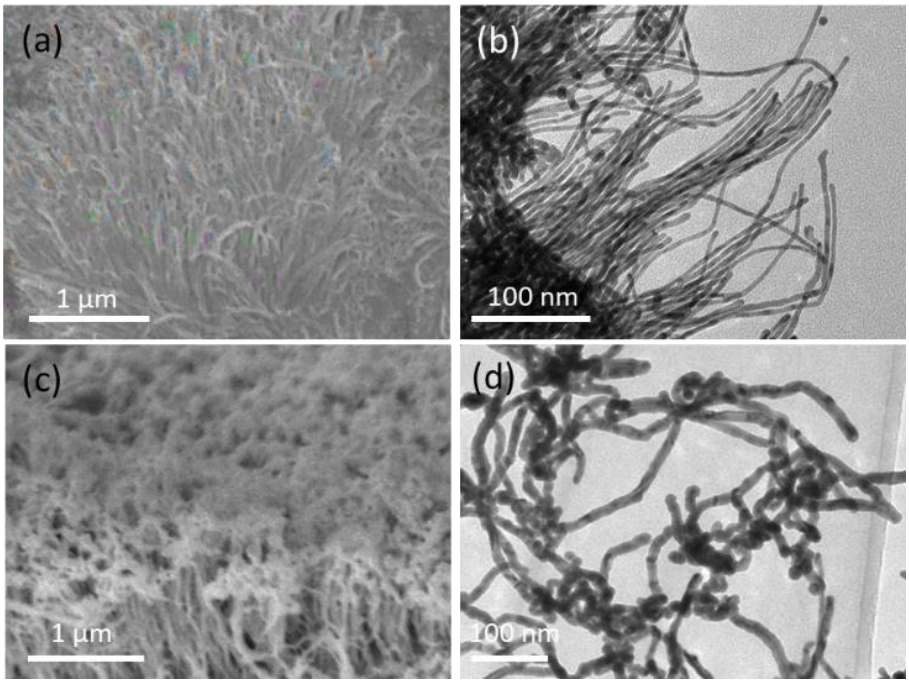

Figure 4-3-1. (a,c) SEM images of AuNW forest grown on nickel foam (a) before and (c) after the deposition of Pd shell. (b,d) TEM images of detached (b) AuNW and (d) Pd coated AuNW from nickel foam.

However, simply reducing the Pd concentration did not lead to a thinner uniform shell on Au surface. Four peaks can be simultaneously observed at the first few CV scans (Figure 4-3-2b, light blue line). The position and shape of these peaks match with that of the typical forward and backward peaks of Au and Pd, respectively (Figure 4-3-2a), indicating the coexistence of active Pd and Au on the surface. This implies that the AuNWs were not fully covered with Pd.

Interestingly, with further CVs, the Au peaks kept decreasing while the Pd peaks kept increasing, indicating progressive Pd coating on the exposed Au surface (Figure 4-3-2b). At the same time, the position of the Pd peaks shift to more positive values (Figure

4-3-2b), indicating the change of electrochemical activity, likely because the gradual spread-out of the Pd domains gives a thinner and more uniform coating. Such physical movement of Pd atoms is intriguing, and provides an unusual means to smooth the rough shell and prepare ultrathin coatings.

This phenomena is likely caused by two possible mechanisms: the Pd atoms may firstly get oxidized at high voltage to free Pd ions in the electrolyte, which are then reduced back to cover the Au surface (Figure 4-3-2c); alternatively, the CV scan may promote the surface migration of Pd domains, where the Pd atoms may directly move on the Au surface by breaking and remaking the metal bonds.

The addition of $PdCl_2$ for the deposition of Pd overlayer on Au. To distinguish the two mechanisms, solution form of Pd precursor (16 μM $PdCl_2$ in the electrolyte) was used to replace the previous form of solid state Pd (the Pd domains on the AuNWs). Considering that the $PdCl_2$ solution would undergo galvanic replacement reaction with the nickel foam, as a model study, fluorine-doped tin oxide (FTO) was used as the inert substrate here. Furthermore, the citrate-stabilized AuNPs were decorated on FTO (AuNP/FTO) as a replacement of the AuNWs, to avoid the unnecessary ambiguities caused by the residual strong ligand 4-MBA on AuNW surface.

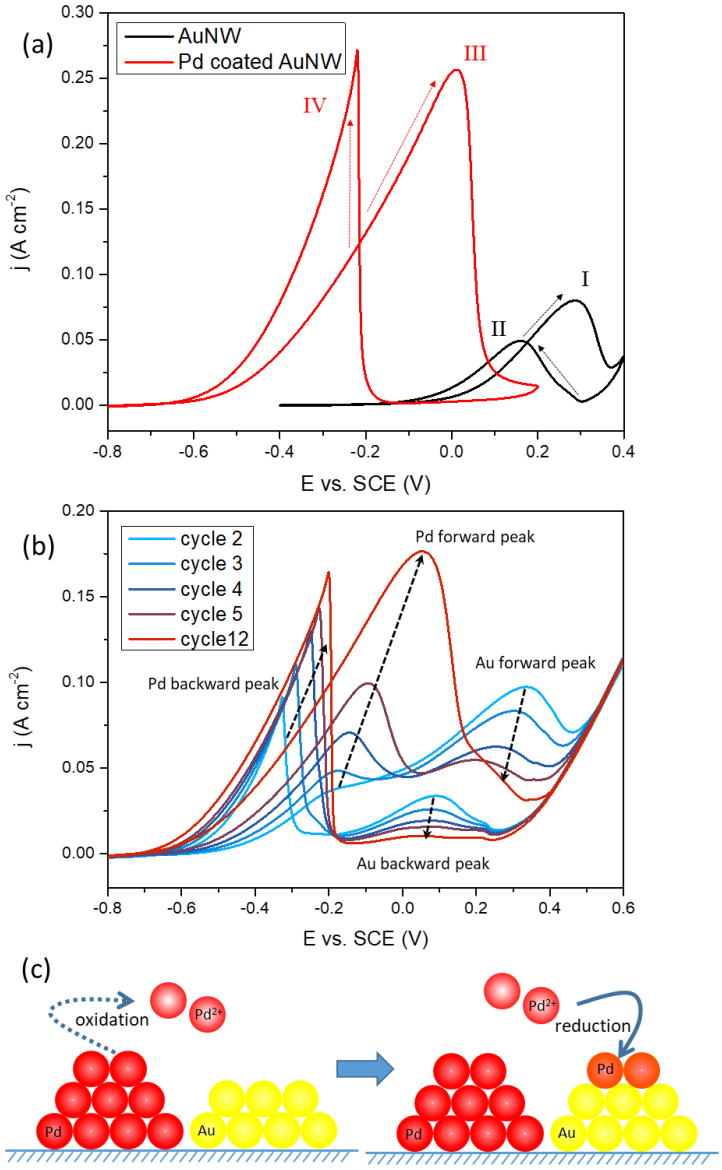

Figure 4-3-2. (a) Cyclic voltammograms of AuNW (black) and Pd coated AuNW (red) catalyzing ethanol oxidation reaction in 1.0 M NaOH and 1.0 M ethanol. Cyclic voltammograms (b) and schematic illustration (c) of the deposition Pd on Au surface in ethanol oxidation system catalyzed by partially coated Pd on AuNW with different cycle numbers in 1.0 M NaOH and 1.0 M ethanol. Scan rate v=50 mV/s.

With the AuNP/FTO as the working electrode for CV scans, increase of Pd forward peak current density and negative shift of Pd backward peak can be observed (Figure 4-4-3a). Due to the significantly decreased active Au surface area from AuNW/NF to AuNP/FTO, the decreasing trend of Au backward peaks can be observed in the magnified CV curves (Figure 4-4-3a, inset). The increase of Pd and decrease of Au peaks indicate that the exposed Au surface was gradually covered with the freshly reduced Pd ions in the electrolyte. Without any solid state Pd, the Au surface can still be fully covered by Pd shell. Therefore, the Pd ion is the key factor for the movement of Pd, following the oxidation-reduction mechanism (Figure 4-3-2c).

On the basis of this result and mechanism, selective coating on the exposed Au surface is more favorable than the deposition back onto the Pd domains. It can be explained by the stronger bond energy of Pd-Au (143 kJ/mol) than that of Pd-Pd (136 kJ/mol).[21] Moreover, the lattice strain between Au and Pd would not be significant (< 5%),due to their matching lattice, so that the bonding between the Au-Pd interface could be effective and stable.[21b] The formation of more Pd-Au bonds would significantly reduce the total surface energy, reaching a more stable state, than the formation of Pd-Pd bonds. The deposition of the first atomic layer of Pd on Au, rather than the growth of Pd islands on Au, is the thermodynamically favored final product, following the thermodynamically controlled deposition process.

Electrochemical characterization of deposited Pd overlayer on Au. Magnified CV curves on the series of Pd deposited AuNP/FTO backward peaks showed negative shift

in the onset potential for ethanol oxidation (Figure 4-3-3b). Before the 6th cycle, the backward peak did not shift much, likely because the electrochemical activity of the first atomic Pd layer was the same, which has not been fully covered yet. After that, the negative shift can be clearly observed with the increasing amount of deposited Pd. This shift starts from the relatively positive potential of -0.22 V, since there is no Pd on the substrate before the first CV and the onset potential of Au is more positive than that of Pd. At this point, the inner Au core greatly influenced the electrochemical property of the deposited Pd domains. With the Pd shell grows thicker and thicker, this effect would be gradually decreased. In the final CV scan, the shift ends at the potential of -0.35 V, very similar to that of pure Pd (-0.37 V, Figure 4-3-4). The Pd shell acts more like the pure Pd without the influence from the inner Au core. These gradually shifted CV curves indicate how the electronic structure of the Pd overlayer is influenced by the Au core.

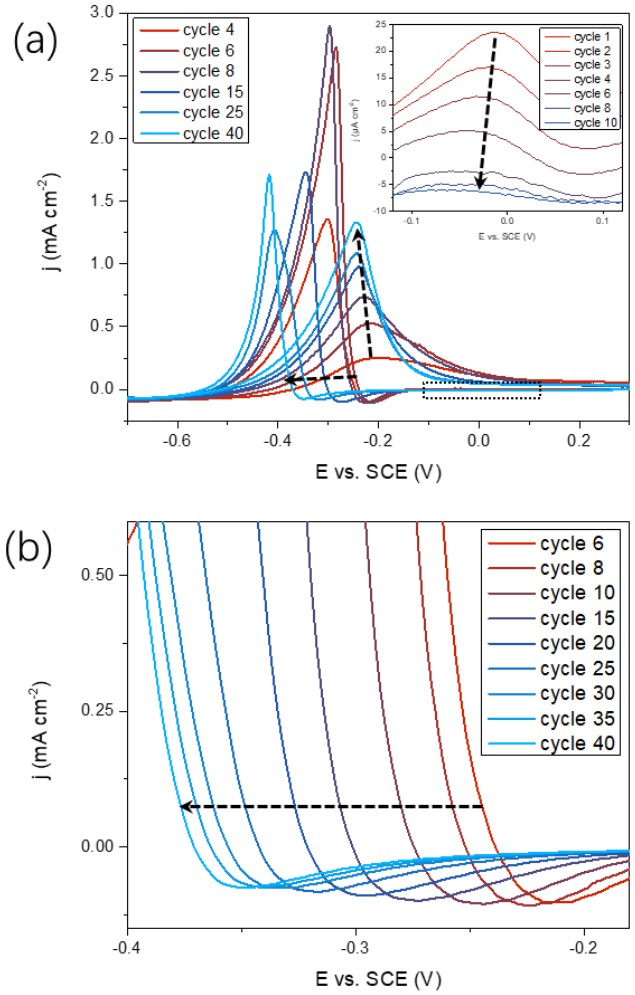

Figure 4-3-3. (a) Cyclic voltammograms of Pd deposited AuNP/FTO substrate with different cycle numbers in 1.0 M NaOH, 1.0 M ethanol and 16 μM $PdCl_2$. Inset is the magnified region for Au backward peak. (b) Magnified CV curves for the negative shift of Pd backward peak.

Similarly, the CV circles of the PdO reduction were obtained on the AuNP/FTO substrate in the electrolyte containing 1.0 M NaOH and 16 μM $PdCl_2$ (Figure 4-3-5a). The onset potential negatively shifted from the potential of -0.22 V to -0.35 V, similar shift range with ethanol oxidation one. After the onset potential of ethanol oxidation

and PdO reduction was extracted and listed in Figure 4-3-5b, the shift rate of the two reactions were almost the same. It is well known that the observed negative shift of PdO reduction peak directly corresponded to the strengthening of -OH binding affinity on thicker Pd shell.[22] It is very likely that the negative shift of ethanol oxidation would result from the stronger binding affinity of –OH group on Pd.

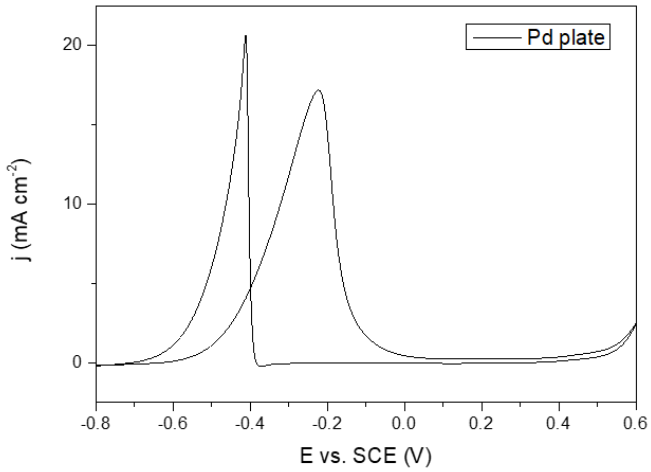

Figure 4-3-4. (a) Cyclic voltammogram of Pd plate substrate in 1.0 M NaOH, and 1.0 M ethanol aqueous electrolyte.

In addition, the $Na_2S_2O_8$ reduction catalytic ability of the series of Pd deposited AuNP/FTO was measured in the electrolyte containing 1.0 M NaOH, 20 mM $Na_2S_2O_8$, and 16 μM $PdCl_2$. As shown in Figure 4-3-6, the backward peak rising at around -0.3 V shows the catalytic performance of $Na_2S_2O_8$ reduction reactions. The series of the backward peaks gradually shifted from -0.22 V to -0.34 V. This shift trend was also

very similar with PdO reduction, indicating that the varied –OH binding affinities have significant impacts on the catalytic activities.

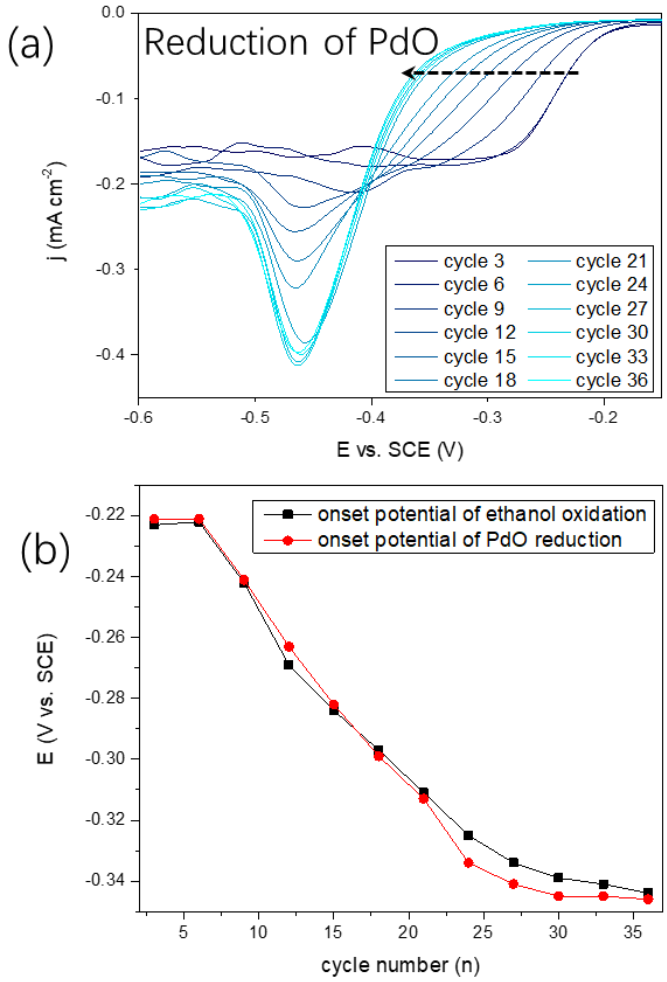

Figure 4-3-5. (a) Onset potential shifting of PdO reduction in 1.0 M NaOH and 16 μM $PdCl_2$ with AuNP/FTO substrate. (b) Cycle number dependence of onset potentials of ethanol oxidation and PdO reduction reactions.

On the basis of these results, we hypothesize that the increasing binding affinity of the –OH group on Pd surface should be responsible for the negative shift of backward

peaks in ethanol oxidation reactions. With stronger binding affinity of -OH group on the gradually thickened Pd surface, the ethanol intermediate (ethoxyl group) is relatively more difficult to reach the catalyst surface or undergo catalysis process, leading to the delayed initiation of ethanol oxidation reaction. And thus, more energy is required to remove the strongly bound –OH group, which leads to the more negative onset potential.

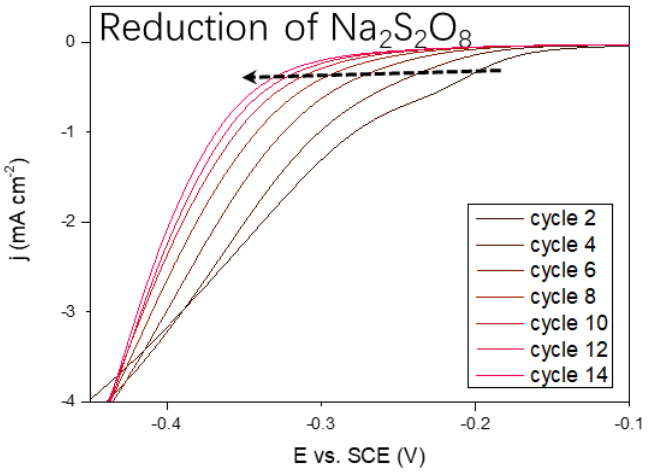

Figure 4-3-6. Onset potential shifting of $Na_2S_2O_8$ reduction in 1.0 M NaOH, 20 mM $Na_2S_2O_8$ and 16 μM $PdCl_2$ with AuNP/FTO substrate.

The catalytic performance mainly depends on the binding affinity of the reaction intermediates. With the gradually strengthened binding affinity of –OH group, the catalytic activity of the fresh Pd surface can be exhibited by the Pd backward peak current density, which was extracted from each CV and listed in Figure 4-3-7a. This

curve describes the trends in catalytic ability of ethanol oxidation, leading to well-known catalytic volcano plot. Before the 7th cycle, the peak current keeps increasing and is almost linear to the cycle number. Likely because the Au surface is not fully covered with sub-monolayer Pd and the amount of deposited Pd is linear to the cycle number. While after the 7th cycle, the peak current density kept decreasing, due to the stronger -OH binding affinity on the thicker Pd shell. This would suppress the binding of ethanol intermediate, leading to the loss of catalytic efficiency. The highest peak current density occurs at the 7th cycle, implying that the state of Pd owns better catalytic activity than others. When the correlation between the backward peak current density and the CV circle number was established, the electrochemical performance of ethanol oxidation can be real-time monitored during the CV deposition process and the best one can be determined by the highest peak current density, at the 7th cycle.

Interestingly, the decrease of Au peak is found out not to synchronize with the shift of Pd peak. To figure out their relationships, the peak current density of Au backward peak as well as the onset potential of Pd backward peak in each CV curve is extracted and organized in Figure 4-3-7b. Before the 6th cycle (Section I), the Au peak keeps decreasing to stable state (dropping only 7 % for the rest 34 cycles), while the onset potential of Pd backward peak remains constant. This non-overlapping phenomenon indicates that the freshly reduced Pd could hardly be deposited on existing Pd layer until the Au surface is fully covered. This verifies that the deposition of the first monolayer of Pd on Au follows the layered growth mode. From the 7th to the 30th cycle

(Section II), the Pd backward peak keeps negatively shifting while the Au peak current remains unchanged. During the growth of strained Pd layer, no multi-peaks or sudden change of onset potential can be observed, meaning that the layered Pd shell was gradually formed with the help of CV. From the 31st to the 40th cycle (Section III), both the Au peak current density and the Pd onset potential remain unchanged (the difference between each cycle less than 1 mV viewed as unchanged). The inner Au core has less significant impact on the Pd shell, which performs more like pure Pd (onset potential of pure Pd plate -0.37 V, Figure 4-3-4). To conclude, the deposition process can be divided into three sections, full covering on Au surface, growth of strained Pd and growth of pure Pd, following the layer-by-layer growth mode, which leads to the thermodynamically stable structure.

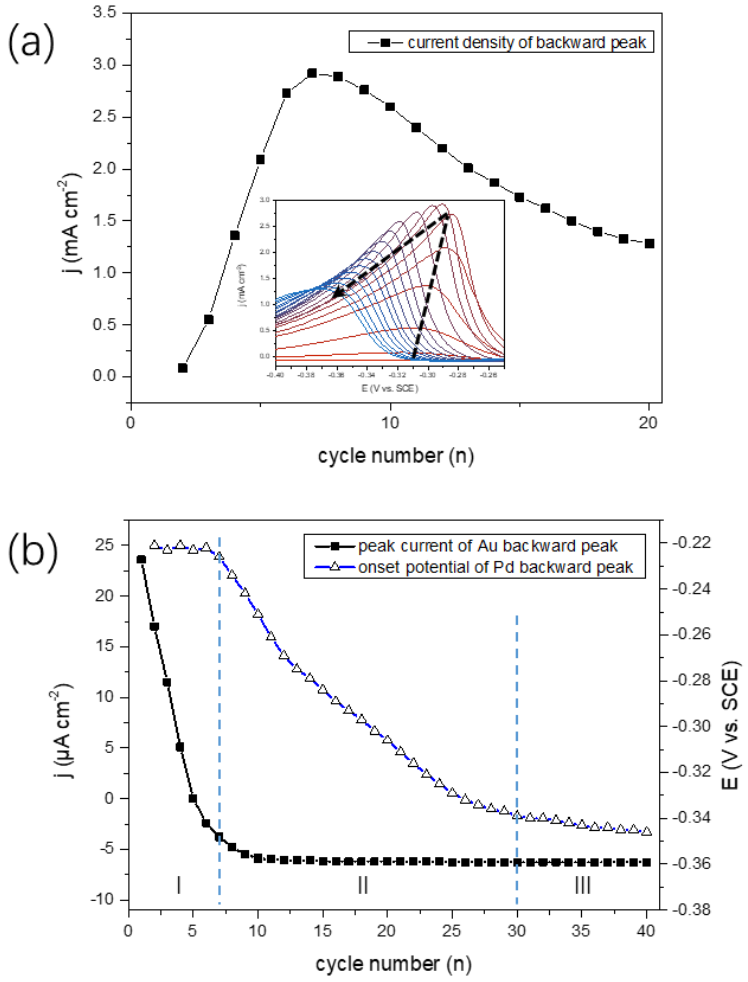

Figure 4-3-7. (a) Cycle number dependence of Pd backward peak current density. The inset is the detailed CV curves at Pd backward peak region with increasing CV cycle numbers. (b) Cycle number dependence of peak current density of Au backward peak (solid square, left axis) and onset potential of Pd backward peak (hollow triangle, right axis).

Detailed morphology and property characterization of Pd overlayer on Au. In order to characterize the monolayer deposition of atomic Pd shell on AuNP, the morphology characterization of the Pd deposited AuNP at the 6th CV cycle was carried

out by the high-angle annular dark-field scanning transmission electron microscopy (HAADF-STEM) and energy-disperse X-ray spectroscopy (EDS), respectively. As shown in Figure 4-3-8a, the STEM images on the atomic monolayer of Pd on AuNP exhibited a distinct contrast difference between the Pd overlayer and the Au core. The monolayer of the Pd shell is uniformly deposited on the 5 nm AuNP after 6 cycles of CV in the electrolyte containing 16 μM $PdCl_2$. No island, branch or multi-layer can be observed on the uniform Pd shell. The EDS mapping and line scan confirms the core and the shell consists of Au and Pd, respectively (Figure 4-3-8d and 8g). In addition, at the 6^{th} CV scan, the peak current density of Au backward peak almost dropped to the stable state, verifying that there is little exposed active Au surface and most of the Au surface was already covered with Pd. Similarly, at 20^{th} CV scan, the thickness of Pd overlayer on Au surface uniformly increased to around three atomic layer (Figure 4-3-8b). Furthermore, after 40 CV scans, the thickness of Pd shell increased to over five atomic layer (Figure 4-3-8c). From these morphology characterization together with previously electrochemical properties (Figure 4-3-7), it could be confirmed that the electrochemical CV deposition method follows the layer-by-layer deposition growth mode and the monolayer deposition of Pd on Au can be realized. Furthermore, sub-monolayer, multi-layer core-shell structure can be prepared as well, by tuning the CV cycle numbers.

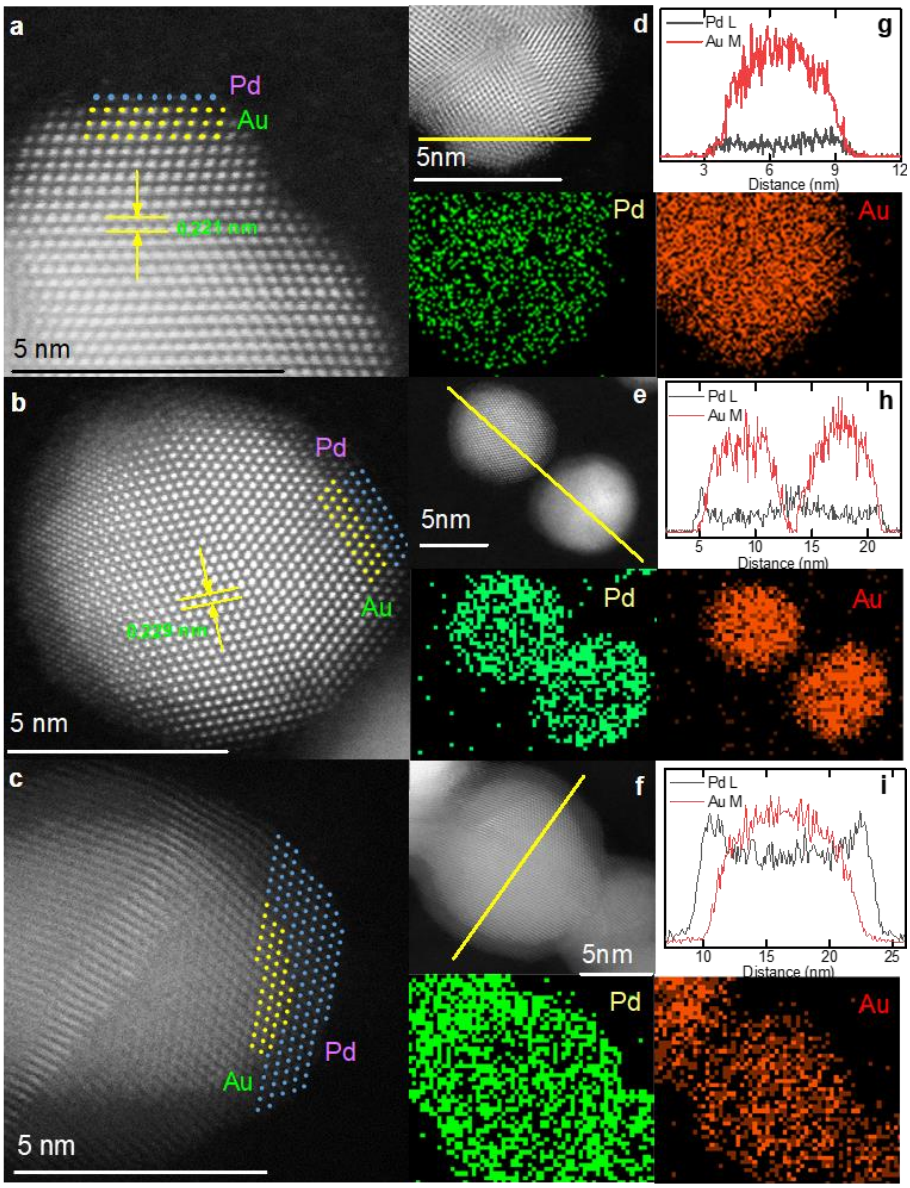

Figure 4-3-8. (a, b, c) HAADF-STEM image, (d, e, f, g, h, i) EDS mapping, and line scan of atomic monolayer deposited Pd on AuNP at the (a, d, g) 6th, (b, e, h) 20th and (c, f, i) 40th CV scan.

X-ray absorption fine structure (XAFS) analysis is one of the most powerful techniques for characterization of fine nanomaterial structure. Here, pure Pd (equal to infinite monolayers of Pd), CV deposited 5 monolayers of Pd on Au, and 1.5

monolayers of Pd on Au were used as three representative samples for XAFS analysis. As shown in Figure 4-3-9a, the main adsorption Pd peaks of the 1.5ML Pd and 5ML Pd have a small energy difference (around 2 eV), indicating that the adsorption energy of Pd atomic layer would be changed when the Pd overlayer on Au was thicker from 1.5ML to 5ML. While, the main adsorption Pd peaks of 5ML Pd on Au and pure Pd was almost the same, which means that after the deposition of over five atomic layer of Pd on Au, the adsorption energies of Pd would not be changed any more. As shown in Figure 4-3-9b, the bond length of Pd-Pd gradually decreased, when the Pd overlayer became thicker, revealing that the Au core would affect the formation of Pd overlayer, and thus have a great impact on the adsorption of intermediates. With thicker Pd shell, the influence from inner core would be gradually decreased.[23] The absolute coordination numbers indicate that with thicker Pd overlayer, the coordination ability of Pd shell became stronger, resulting in stronger binding strength of OH^-, which perfectly fits our electrochemical results (Figure 4-3-5).

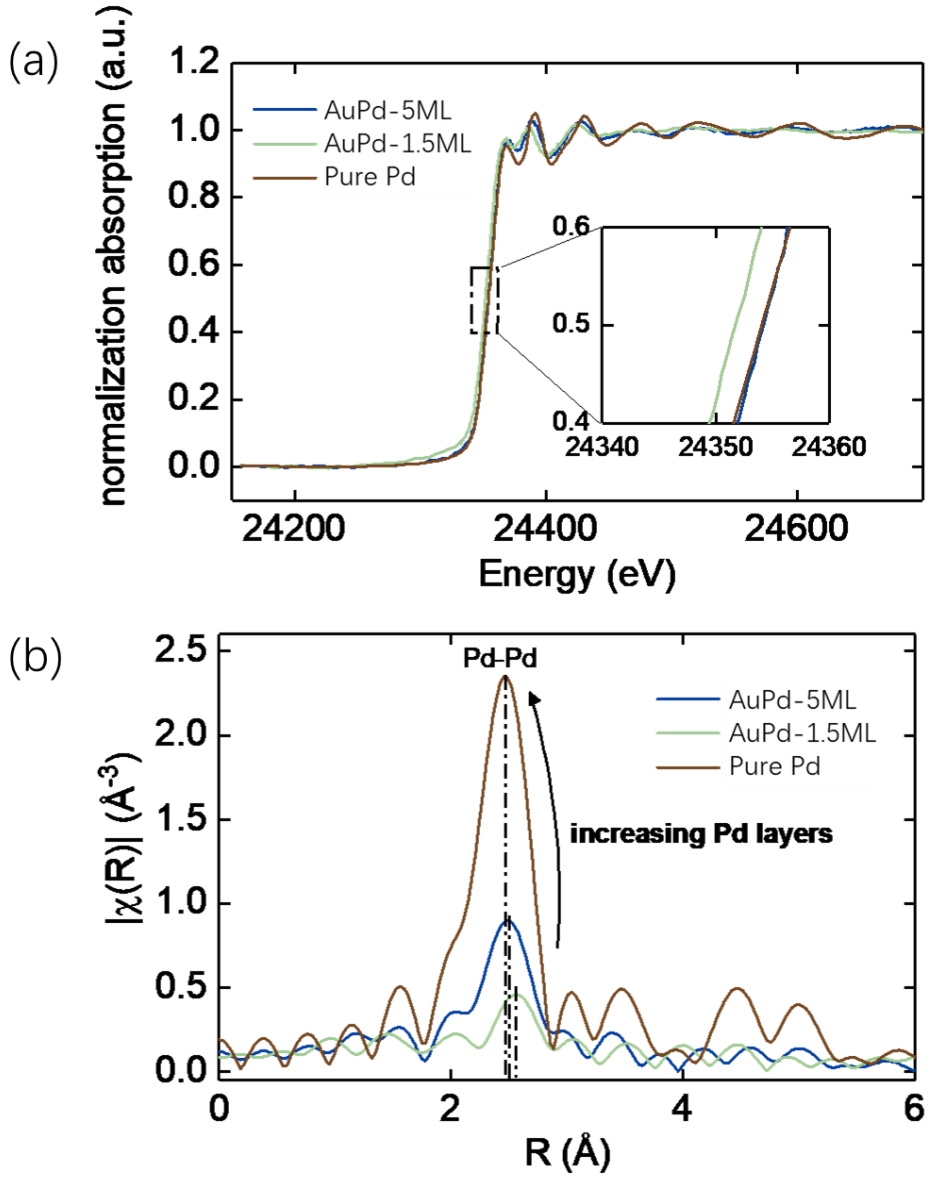

Figure 4-3-9. XAFS analysis of pure Pd (brown line), 5 monolayers of Pd on Au (blue line), and 1.5 monolayers of Pd on Au (green line) on (a) Pd K edge and (b) metal-metal coordination numbers.

In short, the HAADF-STEM images clearly revealed that with more CV scans, the Pd overlayer would became thicker. The XAFS analysis indicated that thicker Pd overlayer would narrow the Pd-Pd distance, and thus strengthen the coordination ability

of the surface Pd atoms. The morphology and the structure property characterizations all fit in with our electrochemical results and our hypothesis. More CV scans would leads to thicker Pd shell, which would result in stronger binding affinity of OH^- intermediates, and thus influence the catalysis activity of ethanol oxidation reactions.

The comparison of layer-by-layer growth and island growth. Meanwhile, it should be figured out whether this layered growth mode could be realized by the typical constant potential deposition method. So the constant potential of -1.0 V is applied on AuNP/FTO for 5 minutes. The electrochemical properties cannot be real-time monitored and one more CV cycle is needed for property characterization. As shown in Figure 4-3-9a (red line), two Pd backward peaks can be observed in one CV cycle, indicating that two types of Pd simultaneously exist on the substrate. Compared with CV deposition method, the peak position of positive (ca. -0.3 V) and negative (ca. -0.4 V) backward peaks corresponds to that of strained (the 10^{th} CV scan) and pure Pd (the 40^{th} CV scan), respectively. With the constant potential deposition method, the deposition of strained Pd (layered growth mode, thermodynamically favored) and pure Pd (island growth mode, thermodynamically disfavored) simultaneously occurs, following the Stranski–Krastanov growth mode (layer-plus-island).[24]

During the kinetic controlled process, the deposition at thermodynamically favorable or unfavorable position is equally possible. The deposition process mainly depends on the specific pathway.[25] In the case of electrochemical deposition of Pd overlayer, the

charge distribution difference is the key pathway. The relatively sharp point (Pd island) obtains higher charge density than the flat point (Pd layer). So more Pd ions would be gathered and reduced at sharper point than relatively flat position, simultaneously forming island and layer Pd.

Typically, by limiting the mobility[26] or increasing the nucleation rate,[27] the thermodynamic deposition mode could be converted to the kinetic one. In CV deposition method, lower nucleation rate (milder reduction potential) and higher mobility (oxidation potential for dissolving unstable Pd atoms) is applied on the electrode. The reduced Pd atoms obtain the opportunity to choose the deposition position, at thermodynamically more stable point. While the relatively unstable atoms would be dissolved by the oxidation potential and have more chances to choose, until they were deposited at the stable point (Figure 4-3-9b). In contrast, the electrochemical environment for constant potential deposition method is higher nucleation rate (more negative reduction potential) and limited mobility (no oxidation potential). The freshly reduced Pd atoms have little chance to choose their deposition position. They were forced to be gathered and deposited on the higher charge density point and they could hardly leave the surface once deposited (Figure 4-3-9c).

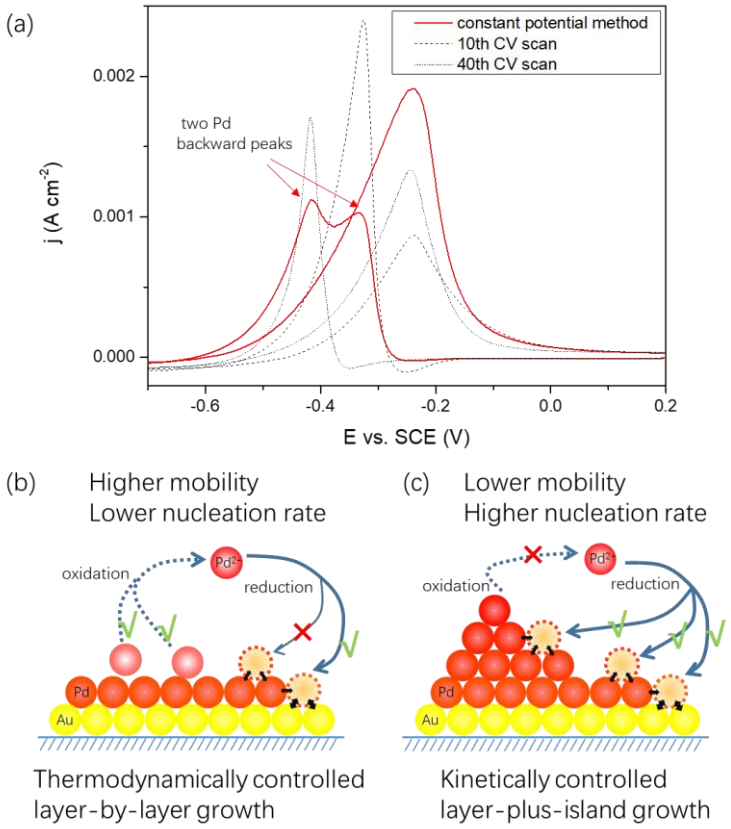

Figure 4-3-9. Cyclic voltammograms (a) of ethanol oxidation reactions catalyzed by Pd with layer-by-layer (black, b) and layer-plus-island (red, c) growth mode in 1.0 M NaOH and 1.0 M ethanol. Scan rate v=50 mV/s.

In order to characterize the morphologies of layered and island Pd shell, one-dimensional AuNW is the better Au substrate, rather than zero-dimensional AuNP. Since the structure of nanowire produces relatively large successive surface area for clear observation. The AuNW decorated FTO substrates were applied with CV and constant potential respectively for the deposition of Pd. The CV curves showed similar results with that of AuNP/FTO. Only one Pd backward peak can be observed with the CV deposition method (Figure 4-3-10a), while two Pd backward peaks simultaneously

exist during the constant potential deposition process (Figure 4-3-10b). With CV deposition method, the Pd overlayer on AuNW is smooth and flat, without any clearly observed island or branch (Figure 4-3-10c). While for the constant potential deposition method, the Pd shell is rough with lots of Pd islands deposited on the surface (Figure 4-3-10d, blue rectangles). Both the electrochemical signals and TEM images verify that the CV deposition method follows the layered growth mode (thermodynamically favorable structure) and the constant potential would lead to the growth of Pd islands (kinetically favorable structure).

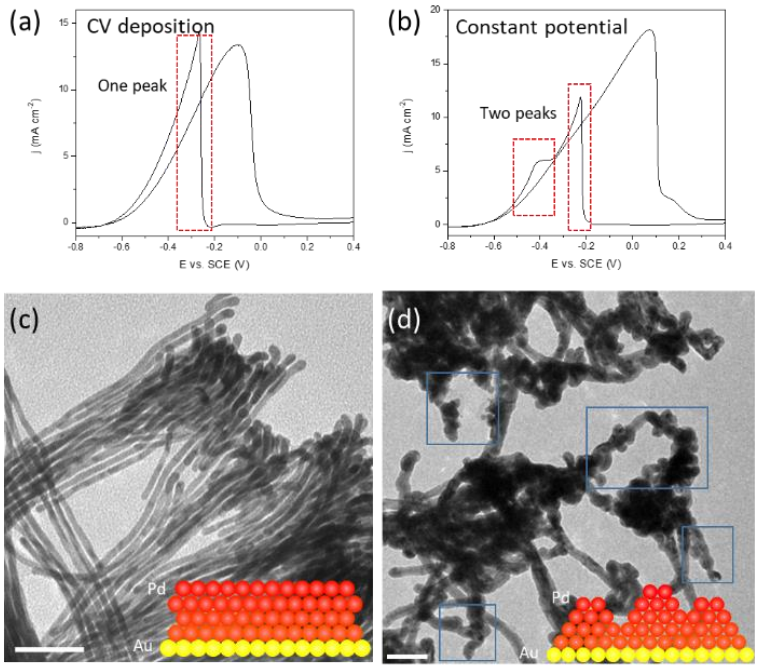

Figure 4-3-10. (a, b) Cyclic voltammograms and (c, d) TEM images of Pd deposited AuNW/FTO substrate with (a, c) CV and (b, d) constant potential deposition method. (Scale bar: 50 nm)

Fine-tuning the deposition rate by $PdCl_2$ concentration. If there was further requirement for fine-tuning of the electrochemical properties, the deposition rate can be reduced by decreasing the $PdCl_2$ concentration in the electrolyte. When the concentration is decreased to 8 μM, the onset potential would not shift until the 9th cycle (Figure 4-3-11, black line). This broaden plateau section (the 1st to the 9th cycle) indicates that more CV cycles are needed for the full coverage of the first Pd atomic monolayer and more possible sub-atomic Pd monolayer can be achieved before the 9th CV cycle. The declined shifting rate of onset potential can be observed after the 9th cycle and the tuning accuracy could be enhanced for more desired Pd shell thickness, resulting in more possible electrochemical properties. When the concentration is increased to 32 μM, the plateau section was cut to five cycles, faster to cover the first monolayer (Figure 4-3-11, blue line). If the $PdCl_2$ concentration was further increased to 64 μM, the plateau section is disappeared and the potential shift occurred at the second CV cycle. In addition, the pure Pd state would occur much earlier at the 12th cycle. This could largely reduce the deposition time to acquire the targeted Pd state (Figure 4-3-11, purple line).

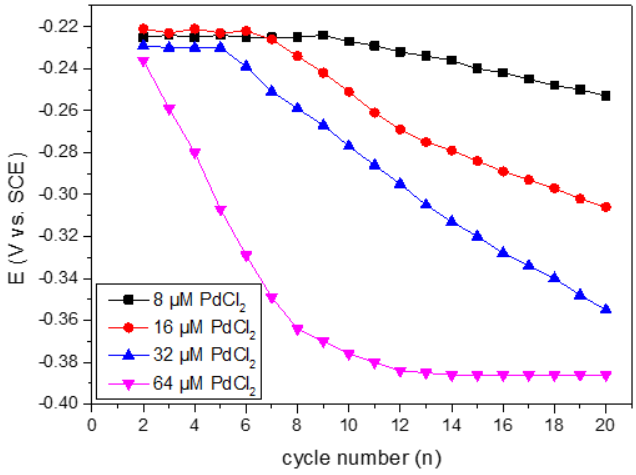

Figure 4-3-11. Cycle number dependence of Pd backward onset potential with different concentration of $PdCl_2$ in 1.0 M NaOH and 1.0 M ethanol.

This thickness-property correlation could be explained by d-band theory proposed by Nørskov.[28] The electronic state of strained Pd overlayers on Au surface is different from that of pure Pd, due to the expanded distance of surface Pd atoms on Au. This would lead to the up-shift of d-band center owing to the band narrowing and thus be responsible for the changing of binding affinity and catalytic activity.[9] With the increasing thickness of Pd overlayer, the electronic influence of inner Au core on surface Pd atom would gradually be weakened. In CV deposition experiment, the negative shifting of onset potential is in agreements with d-band theory and the binding affinity of different intermediates could be real-time monitored. With various binding affinities, fine-tuning catalytic activities of different reactions can be realized during the CV deposition process.

4.4. Conclusion

In summary, we demonstrate the synthetic method for the deposition of Pd shells on Au with successively changing thickness through CV scans. The binding affinity of different intermediates can be fine-tuned by real-time monitoring the negative shift of onset potentials. The catalytic activity of ethanol oxidation is correlated with -OH binding affinity. Based on the backward peak current density, the most optimized catalytic activity point can be identified at the 7^{th} CV scan. To our interest, the layer-by-layer and the layer-plus-island growth mode, can be achieved by CV scan and constant potential deposition method, respectively, leading to drastically different electrochemical characteristics.

4.5. Reference

1. Chaturvedi, S.; Dave, P. N.; Shah, N. K., Applications of nano-catalyst in new era. *Journal of Saudi Chemical Society* **2012,** *16* (3), 307-325.
2. Croy, J. R.; Mostafa, S.; Hickman, L.; Heinrich, H.; Cuenya, B. R., Bimetallic Pt-Metal catalysts for the decomposition of methanol: Effect of secondary metal on the oxidation state, activity, and selectivity of Pt. *Applied Catalysis A: General* **2008,** *350* (2), 207-216.
3. (a) Park, J.; Zhang, L.; Choi, S. I.; Roling, L. T.; Lu, N.; Herron, J. A.; Xie, S.; Wang, J.; Kim, M. J.; Mavrikakis, M., Atomic Layer-by-Layer Deposition of Pt on Pd Octahedra for Enhanced Catalysts toward the Oxygen Reduction Reaction. *Acs Nano* **2015,** *9* (3), 2635-47; (b) Zheng, Y.; Chen, C.; Zhan, Y.; Lin, X.; Zheng, Q.; Wei, K.; Zhu, J., Photocatalytic Activity of Ag/ZnO Heterostructure Nanocatalyst: Correlation between Structure and Property. *Journal of Physical Chemistry C* **2008,** *112* (29), 10773-10777.
4. Xu, R.; Wang, D.; Zhang, J.; Li, Y., Shape-dependent catalytic activity of silver nanoparticles for the oxidation of styrene. *Chemistry, an Asian journal* **2006,** *1* (6), 888-93.
5. Koper, M. T., Hydrogen electrocatalysis: a basic solution. *Nature chemistry* **2013,** *5* (4), 255-6.

6. Cuenya, B. R., Synthesis and catalytic properties of metal nanoparticles: Size, shape, support, composition, and oxidation state effects. *Thin Solid Films* **2010,** *518* (12), 3127-3150.
7. Fang, H.; Yang, J.; Wen, M.; Wu, Q., Nanoalloy Materials for Chemical Catalysis. *Advanced materials* **2018,** *30* (17), e1705698.
8. Tan, R. L.; Song, X.; Chen, B.; Chong, W. H.; Fang, Y.; Zhang, H.; Wei, J.; Chen, H., Levelling the playing field: screening for synergistic effects in coalesced bimetallic nanoparticles. *Nanoscale* **2016,** *8* (6), 3447.
9. Kibler, L. A.; Elaziz, A. M.; Hoyer, R.; Kolb, D. M., Tuning reaction rates by lateral strain in a palladium monolayer. *Angewandte Chemie* **2005,** *44* (14), 2080-2084.
10. (a) Previdello, B. A.; Sibert, E.; Maret, M.; Soldo-Olivier, Y., Palladium Electrodeposition onto Pt(100): Two-Layer Underpotential Deposition. *Langmuir : the ACS journal of surfaces and colloids* **2017,** *33* (9), 2087-2095; (b) Peter, M.; Flores Camacho, J. M.; Adamovski, S.; Ono, L. K.; Dostert, K. H.; O'Brien, C. P.; Roldan, C. B.; Schauermann, S.; Freund, H. J., Trends in the binding strength of surface species on nanoparticles: how does the adsorption energy scale with the particle size? *Angewandte Chemie* **2013,** *52* (19), 5175.
11. George, S. M., Atomic layer deposition: an overview. *Chemical Reviews* **2010,** *110* (1), 111-131.
12. Choy, K. L., Chemical vapour deposition of coatings. *Progress in Materials Science* **2003,** *48* (2), 57-170.
13. Herrero, E.; Buller, L. J.; Abruña, H. D., Underpotential deposition at single crystal surfaces of Au, Pt, Ag and other materials. *Chemical Reviews* **2001,** *32* (39), 1897-930.
14. Zhang, Q.; Lee, I.; Ji, B. J.; Zaera, F.; Yin, Y., Core–Shell Nanostructured Catalysts. *Accounts of Chemical Research* **2013,** *46* (8), 1816-24.
15. He, J.; Wang, Y.; Feng, Y.; Qi, X.; Zeng, Z.; Liu, Q.; Teo, W. S.; Gan, C. L.; Zhang, H.; Chen, H., Forest of Gold Nanowires: A New Type of Nanocrystal Growth. *Acs Nano* **2013,** *7* (3), 2733-40.
16. He, J.; Wang, Y.; Feng, Y.; Qi, X.; Zeng, Z.; Liu, Q.; Wei, S. T.; Gan, C. L.; Zhang, H.; Chen, H., Forest of Gold Nanowires: A New Type of Nanocrystal Growth. *Acs Nano* **2013,** *7* (3), 2733-40.
17. Youngkook, K.; Lai, S. C. S.; Paramaconi, R.; Koper, M. T. M., Electrocatalytic oxidation of alcohols on gold in alkaline media: base or gold catalysis? *Journal of the American Chemical Society* **2011,** *133* (18), 6914.
18. Shen, P. K.; Xu, C., Alcohol oxidation on nanocrystalline oxide Pd/C promoted electrocatalysts. *Electrochemistry Communications* **2006,** *8* (1), 184-188.
19. (a) Lee, Y. W.; Kim, M.; Kim, Y.; Kang, S. W.; Lee, J. H.; Han, S. W., Synthesis and Electrocatalytic Activity of Au−Pd Alloy Nanodendrites for Ethanol Oxidation. *Journal of Physical Chemistry C* **2010,** *114* (17), 7689-7693; (b) Lima, R. B. D.; Varela, H., Catalytic oxidation of ethanol on gold electrode in alkaline media. *Gold Bulletin* **2008,** *41* (1), 15-22.
20. Bianchini, C.; Shen, P. K., Palladium-based electrocatalysts for alcohol oxidation

in half cells and in direct alcohol fuel cells. *Chemical Reviews* **2009,** *109* (9), 4183-4206.
21. (a) Luo, Y.-R., *Comprehensive handbook of chemical bond energies*. CRC press: 2007; (b) Fan, F. R.; Liu, D. Y.; Wu, Y. F.; Duan, S.; Xie, Z. X.; Jiang, Z. Y.; Tian, Z. Q., Epitaxial Growth of Heterogeneous Metal Nanocrystals: From Gold Nano-octahedra to Palladium and Silver Nanocubes. *Journal of the American Chemical Society* **2008,** *130* (22), 6949-51.
22. Huang, X.; Shumski, A. J.; Zhang, X.; Li, C. W., Systematic Control of Redox Properties and Oxygen Reduction Reactivity through Colloidal Ligand-Exchange Deposition of Pd on Au. *Journal of the American Chemical Society* **2018,** *140* (28), 8918-8923.
23. Kibler, L. A.; Elaziz, A. M.; Hoyer, R.; Kolb, D. M., Tuning reaction rates by lateral strain in a palladium monolayer. *Angewandte Chemie International Edition* **2010,** *44* (14), 2080-2084.
24. Bauer, E.; Jh, V. D. M., Structure and growth of crystalline superlattices: From monolayer to superlattice. *Physical Review B Condensed Matter* **1986,** *33* (6), 3657.
25. Wang, Y.; He, J.; Liu, C.; Chong, W. H.; Chen, H., Thermodynamics versus kinetics in nanosynthesis. *Angewandte Chemie International Edition* **2015,** *54* (7), 2022-2051.
26. (a) Xie, S.; Choi, S. I.; Lu, N.; Roling, L. T.; Herron, J. A.; Zhang, L.; Park, J.; Wang, J.; Kim, M. J.; Xie, Z., Atomic layer-by-layer deposition of Pt on Pd nanocubes for catalysts with enhanced activity and durability toward oxygen reduction. *Nano Letters* **2014,** *14* (6), 3570-3576; (b) Wang, X.; Vara, M.; Luo, M.; Huang, H.; Ruditskiy, A.; Park, J.; Bao, S.; Liu, J.; Howe, J.; Chi, M., Pd@Pt Core-Shell Concave Decahedra: A Class of Catalysts for the Oxygen Reduction Reaction with Enhanced Activity and Durability. *Journal of the American Chemical Society* **2016,** *137* (47), 15036-42.
27. (a) He, G.; Zeng, J.; Jin, M.; Zhang, H.; Lu, N.; Wang, J.; Kim, M. J.; Xia, Y., A Mechanistic Study on the Nucleation and Growth of Au on Pd Seeds with a Cubic or Octahedral Shape. *ChemCatChem* **2012,** *4* (10), 1668-1674; (b) Lee, Y. W.; Kim, D.; Hong, J. W.; Kang, S. W.; Lee, S. B.; Han, S. W., Kinetically controlled growth of polyhedral bimetallic alloy nanocrystals exclusively bound by high-index facets: Au-Pd hexoctahedra. *Small* **2013,** *9* (5), 646-646.
28. Hammer, B.; Nørskov, J., Electronic factors determining the reactivity of metal surfaces. *Surface Science* **1995,** *343* (3), 211-220.

5. Conclusion and Future Work

5.1. Conclusion

In order to relief and solve the energy crisis problem around the world, two major methods would be thoroughly studied and carried out. One is to replace the usage of fossil fuels (coal, oil and natural gas) with more renewable energies (solar, wind, hydro energy, etc.), and the other is to enhance the energy conversion efficiency. This dissertation is mainly focused on these two topics. In Chapter Two and Three, it mainly discussed the fabrication method of high-efficiency anodes for direct ethanol fuel cell, one of the most promising alternatives for non-renewable resources and their performances for electro-oxidation of ethanol. In Chapter Four, the layer-by-layer deposition of Pd on Au surface was demonstrated with the help of cyclic voltammetry (CV) scans, where the binding affinity and the catalytic activity could be fine-tuned during the deposition process. This dissertation, focusing on the electro-oxidation of ethanol, was investigated in the anode fabrication method to enhance its catalytic activity as well as stability and the establishment of structure-property correlation to raise the catalysis efficiency.

The direct ethanol fuel cell has attracted more and more attentions, as the new generation of portable fuel cell, because of its high volumetric energy density, low toxic, easy storage and transport. Some practical ethanol fuel cells have been produced and used in daily lives, but the drawback is obvious that the power density is still not high enough for further higher efficiency applications, only for demonstrations of low

power density devices.

So here we proposed a synthetic method of the high surface area Pd-based flexible electrode with high catalytic activity for the catalysis of ethanol oxidation reaction, with high tolerance to intermediate poisoning. The ultrathin Au nanowire (AuNW) forest was successfully grown on the three dimensional substrate, nickel foam. Then the Au surface was coated with uniform Pd shell by electrochemical deposition method to alter the surface active atoms from Au to Pd, which was more active than Au on catalyzing ethanol oxidation reactions. The peak current density increased 3.3, 11.2 and 48.1 times, with enhanced stable current of 27,17 and over 140 times, compared with Pd coated bare nickel foam, Pd coated AuNW on fluorine doped tin oxide (FTO) and the state-of-the-art catalyst, Pd on activated carbon (Pd/C), respectively. The peak current could still remain 98.4 % after the nickel foam was bended 30 degree for 15 times. Both the peak current density and the stability of the AuNW nickel foam substrate was better than that of most published presentative electrodes in recent years. This electrode could be served as one promising potential alternative anode, catalyzing ethanol oxidation reactions for practical direct ethanol fuel cells in the future.

The AuNW nickel foam could be served as the primary cell system, nickel foam as the anode and AuNW as the cathode. So the Pd shell can be conveniently and effectively deposited on the Au surface, after the AuNW nickel foam substrate was dropped into the Pd solution. The catalytic activity and the stability of the Pd coated AuNW nickel foam by primary cell coating method was almost the same as that of the electrochemical

deposition method coated one. These results clearly demonstrated one potential quick method for the deposition of medium active metal on most active and least active two metal system.

When the amount of Pd precursors in the solution was reduced, the Pd shell was found out to be unstable and it could move to cover the exposed Au surface with the help of CV scans at room temperature in ethanol electro-oxidation system. This would remain similar catalytic activity and stability with the previous methods, while the deposited amount of Pd was much less, leading to the unparalleled specific current up to 6464 A/g. The combination of primary cell deposition method and CV scans formed one convenient and effective deposition method. After detailed investigation of different reaction conditions, serval necessary conditions were discovered, CV scans within Pd redox region, sodium hydroxide in the solution and the appearance of Au surface, for the repining of the Pd nanomaterials. On the basis of the necessary and unnecessary conditions, reasonable mechanism was proposed that the Pd nanomaterial was first oxidized to the Pd ion into the electrolyte and then it was reduced back onto the Au surface with the help of reduction CV scans.

With the understanding of previous experiment result, the Pd ions were found out to be the key factor of deposition on the Au surface. Some amount of the Pd ions was added into the ethanol aqueous solution under CV scanning. With lower concentration of $PdCl_2$ (16 μM, 50 mL), three steps of the growth of Pd shell could be clearly observed on Au surface, covering Au surface, growing strained Pd and growing pure Pd. With

this coating method, fine-tuning of the Pd thickness on Au core would be easily realized, leading to the tuning of -OH group binding energy on Pd surface. It is well known that the onset of the backward peaks of Pd ethanol oxidation reactions corresponded to the -OH binding affinity on the Pd shell. In this experiment, the onset potential can be fine-tuned with different CV cycle numbers or Pd concentration. By tuning the -OH binding affinity, the catalytic activity of ethanol oxidation would also be altered and this onset potential difference could be monitored during the deposition process. This would make this deposition method, not only accurate, but also easily controlled.

5.2. Future Work

On the basis of the successful preparation of Pd coated Au nanowire forest on nickel foam and the method to layered grown Pd layers on Au surface by CV coating method to fine tune the -OH binding energy on Pd, several interesting future works were proposed below.

First, the direct ethanol fuel cell could be fabricated by our prepared electrode. The high surface area Pd coated Au nanowire on nickel foam electrode has been successfully prepared as the anode of the ethanol fuel cell. One suitable cathode and a suitable system could be formed to study the fuel cell system to see whether our electrode was efficient and stable enough to be served as the practical fuel cell. The estimated current density and the power density of the electrodes should be high due to

the large active surface area provided. If the combination of the anode and cathode was effective enough, the production could be expanded to larger scale. Since the fabrication methods of growing Au nanowires and coating Pd shell were quite easier to be expanded.

The electrons move from anode to cathode in the direct ethanol fuel cells and in most cases, the cathode reaction is oxygen reduction reaction.[1] Antolini and Gonzalez summarized that the suitable cathode catalyst was Pt/C, Ag/W_2C, Pd, Pt/Ru, Pt-Co/C and Pt-Pd/C.[2] These were all good catalysts for oxygen reduction reaction. Meanwhile, the surface area of cathode should also be comparable with the anode, so the cathode should also be some high surface area substrate, like nickel foam and carbon cloth. The fabrication of multi-functional nickel foam substrate with highly dispersed active nanomaterial layers as cathode catalysts had been researched well and these cathodes have already helped demonstrate a bright future for the development of direct ethanol fuel cells. So the fabrication of cathode section would not hinder much.[3]

Second, some other active types of nanomaterials could also be deposited on the Au nanowire forest nickel foam platform to investigate some other electrochemical reactions. The most outstanding advantage of this Au nanowire nickel foam system was the high surface area provided by the combination of nanowire forest and nickel foam. For other electrochemical reactions, high catalytic activity and good stability might still be obtained. Since the large active surface area provided much higher possibilities for the reactants to reach to surface, the catalytic activities of most of the reactions should

be increased a lot.

Different noble metals are suitable for different electrochemical reactions. For example, it is well known that the platinum was one of most favorable catalysts for oxygen reduction reaction,[4] hydrogen evolution reaction,[5] etc. The Au-based electrode was usually used for the oxidation of glucose,[6] formic acid,[7] carbon monoxide,[8] hydrazine,[9] etc.[10] Besides the ethanol oxidation reaction, the Pd-based electrode was also suitable for methanol oxidation reaction,[11] oxygen reduction reaction,[12] hydrogen oxidation reaction,[13] etc.[14] With high surface area platform, AuNW nickel foam, theoretically, the catalytic activity of these reactions could all be enhanced when the shell metal was altered to the desired one.

Third, the primary cell deposition method could be further refined to obtain more applications and the precise construability. For the primary cell coating method, one of the most obvious advantages is time-saving and simple operation, only serval minutes to fully cover the large surface area, and the convenience of large scale. However, the controllability was not good enough since there were not enough parameters to change. There are still some other things that we could work on to further refine this coating method, such as applying high temperature, applying stirred condition, combination of two or more metal salts in solution and applying assistance, like current to help the growing. And after we complete the refining steps, this could be a more effective and simple method to coat metal on metal surface.

Fourth, we could test other metal salts in solution to be coated on metal surface by

our monitored CV coating method. For CV coating method, we only test the successful coating Pd on Au surface, but there were lots of other combinations such as, coated silver on gold, platinum on gold and so on. Lots of other possible coating combination we could test in the future to see whether this is a common coating method or it could only work on Pd-Au system. If we could find out many other possible coating combinations, we could also test many other reactions besides the ethanol oxidation reaction.

Fifth, we could test other reactions with the different thickness of Pd on Au surface by CV coating method to see the different effects of ultrathin layer. We knew that with different thickness of Pd on Au, the binding energy of OH on Pd could be precisely controlled. However, we did not know how to utilize this fine tuning method in other reactions. We could test other reactions which would linked with the adsorption of OH on surface, such as the oxygen reduction reaction, the stability test of ethanol oxidation reaction, and the hydrogen evolution reaction. With different binding energy, we could see at which point, we could obtain the best catalytic activities, which could help us further understand the mechanism of the reactions.

5.3. Reference

1. Kamarudin, M. Z. F.; Kamarudin, S. K.; Masdar, M. S.; Daud, W. R. W., Review: Direct ethanol fuel cells. *International Journal of Hydrogen Energy* **2013,** *38* (22), 9438-9453.
2. Antolini, E.; Gonzalez, E. R., Alkaline direct alcohol fuel cells. *Journal of Power Sources* **2010,** *195* (11), 3431-3450.
3. An, L.; Zhao, T. S.; Xu, J. B., A bi-functional cathode structure for alkaline-acid

direct ethanol fuel cells. *International Journal of Hydrogen Energy* **2011,** *36* (20), 13089-13095.
4. Katsounaros, I.; Schneider, W. B.; Meier, J. C.; Benedikt, U.; Biedermann, P. U.; Auer, A. A.; Mayrhofer, K. J. J., Hydrogen peroxide electrochemistry on platinum: towards understanding the oxygen reduction reaction mechanism. *Physical Chemistry Chemical Physics Pccp* **2012,** *14* (20), 7384-7391.
5. Yin, H.; Zhao, S.; Zhao, K.; Muqsit, A.; Tang, H.; Chang, L.; Zhao, H.; Gao, Y.; Tang, Z., Ultrathin platinum nanowires grown on single-layered nickel hydroxide with high hydrogen evolution activity. *Nature Communications* **2015,** *6*, 6430.
6. Chaudhuri, S. K.; Lovley, D. R., Electricity generation by direct oxidation of glucose in mediatorless microbial fuel cells. *Nature Biotechnology* **2003,** *21* (10), 1229-1232.
7. Beltramo, G. L.; Shubina, T. E.; Koper, M. T., Oxidation of formic acid and carbon monoxide on gold electrodes studied by surface-enhanced Raman spectroscopy and DFT. *Chemphyschem* **2010,** *6* (12), 2445-2445.
8. Herzing, A. A.; Kiely, C. J.; Carley, A. F.; Landon, P.; Hutchings, G. J., Identification of active gold nanoclusters on iron oxide supports for CO oxidation. *Science* **2008,** *321* (5894), 1331-1335.
9. Ozoemena, K. I.; Nyokong, T., Electrocatalytic oxidation and detection of hydrazine at gold electrode modified with iron phthalocyanine complex linked to mercaptopyridine self-assembled monolayer. *Talanta* **2005,** *67* (1), 162-168.
10. Burke, L. D.; Nugent, P. F., The electrochemistry of gold: II the electrocatalytic behaviour of the metal in aqueous media. *Gold Bulletin* **1998,** *31* (2), 39-50.
11. Zhen, Y.; Zheng, H.; Ding, M.; Bao, X., Porous Palladium Nanoflowers that Have Enhanced Methanol Electro-Oxidation Activity. *Journal of Physical Chemistry C* **2009,** *113* (3), 1001-1005.
12. Lim, B.; Jiang, M.; Camargo, P. H.; Cho, E. C.; Tao, J.; Lu, X.; Zhu, Y.; Xia, Y., Pd-Pt bimetallic nanodendrites with high activity for oxygen reduction. *Science* **2010,** *40* (33), 1302-1305.
13. Shao, M., Palladium-based electrocatalysts for hydrogen oxidation and oxygen reduction reactions. *Journal of Power Sources* **2011,** *196* (5), 2433-2444.
14. Antolini, E., Palladium in fuel cell catalysis. *Energy & Environmental Science* **2009,** *2* (9), 915-931.